A STUDY ON DEVELOPING HIGH PERFORMANCE NON-SHRINKING GROUT (HPNSG) UTILIZING LOCAL MATERIALS

BY

MOHAMMED ABDELRAHMAN SALIH ABDELRAHMAN

A Thesis Presented to the
DEANSHIP OF GRADUATE STUDIES

KING FAHD UNIVERSITY OF PETROLEUM & MINERALS

DHAHRAN, SAUDI ARABIA

In Partial Fulfillment of the
Requirements for the Degree of

MASTER OF SCIENCE

In

CIVIL ENGINEERING

JUNE. 2015

KING FAHD UNIVERSITY OF PETROLEUM & MINERALS
DHAHRAN 31261, SAUDI ARABIA

DEANSHIP OF GRADUATE STUDIES

This thesis, written by **MOHAMMED ABDELRAHMAN** under the direction of his thesis adviser and approved by his thesis committee, has been presented to and accepted by the Dean of Graduate Studies, in partial fulfillment of the requirements for the degree of **MASTER OF SCIENCE IN CIVIL ENGINEERING**.

Thesis Committee

Prof. Omar S. Baghabra Al-Amoudi
(Adviser)

Prof. Mohammed Maslehuddin
(Member)

Prof. Shamshad Ahmad
(Member)

Dr. Omar A. Al-Swailem
Department Chairman (A)

Prof. Salam A. Zummo
Dean of Graduate Studies

7/16/15
Date

To my lovely family

and friends

and Khalid Abu-Sin

ACKNOWLEDGEMENTS

All praise is due to Allaah, SubhaanaHu wata'aala, for guiding and granting me knowledge, courage and health, to complete this study with success. May His peace and blessings be upon the best of mankind, Mohammad Ibn 'Abdillaah (sallallahu 'alayhi wa sallam), his household, his companions and those who follow his golden path of guidance.

I would like to thank my parents (Najwa & Abdelrahman), sisters and brother for their constant prayers, encouragement and support throughout my live. They are the source of power, inspiration and confidence in me.

I am in great debts to the Kingdom of Saudi Arabia, represented by King Fahd University of Petroleum and Minerals, for providing me the financial support and world class facilities which made my life smoother and easier to devote myself fully to academic and research works.

With deep and indebted sense of gratitude, I would like to express my sincere thanks to my thesis advisor, Prof. Omar S. Baghabra Al-Amoudi, for his invaluable support, guidance, continuous encouragement and all possible cooperation and patience throughout the period of my research and preparation of thesis documentation. Work-

ing with him was a wonderful and learning experience, which I thoroughly enjoyed.

My sincere thanks and appreciation are due to the thesis committee members Prof. Mohammad Maslehuddin and Prof. Shamsad Ahmad for investing their time and their support, critical reviews and suggestions to improve this work.

I am grateful to all the faculty and staff of the Civil and Environmental Engineering (CEE) Department, the Center for Engineering Research, and the Center for Environment & Water at KFUPM, particularly my boss, Dr. Abdallah S. Elamin, for his guidance, support, and motivation.

I have to thank all professors in the CEE Department, specially, Prof. M. H. Baluch, for the significant contribution to my knowledge directly or indirectly. The courses I took with Prof. Baluch redefined to me the meaning of solid mechanics, analysis and structures.

Finally, I have to thank the entire Sudanese community at the KFUPM subcontinent for their company and good influence during the course of my MS degree. Also, thanks are extended to all friends and cousins overseas; in Sudan, Saudi Arabia, and United States, for their unlimited moral support.

TABLE OF CONTENTS

LIST OF TABLES

LIST OF FIGURES

LIST OF ABBREVIATIONS

ρ_g	density of a grout (Kg/m^3)
ρ_c	density of the cement grains (Kg/m^3)
ρ_w	density of the water (Kg/m^3)
D_a	apparent chloride diffusion coefficient (m^2/seconds)
ACI	American Concrete Institute
ASCE	American Society of Civil Engineers
ASTM	American Society of Testing Materials
BS	British Standards
C	chloride concentration (%)
C_i	initial chloride-ion concentration of the specimen mass (%)
C_s	chloride ion concentration at the surface of a concrete specimen mass (%)
CEB	Comité Euro-International du Béton

CSA	Canadian Standards Association
CSE	copper/copper sulfate electrode
EXP	Expansive agent
FA/TA	ratio of the weight of fine aggregate to the weight of total aggregate
FIB	fédération internationale du béton
HCP	half-cell potential
HPNSG	High Performance Non Shrinking Grout
I_{corr}	Corrosion current density
J	flux of chloride ions, $(\frac{mol}{m^2.sec})$
LPRM	Linear Polarization Resistance Method
LSP	Limestone powder
MK	Metakaolin Clay
NP	Natural Pozzolan
PCA	Portland Cement Association
R_p	Resistance to polarization
SCE	saturated calomel electrode
SF	Silica Fume
SP	Superplasticizer
t	exposure time (seconds)
TA/p	ratio of the weight of total aggregate to the weight of powder

w/c	ratio of the weight of water to the weight of cement
w/p	ratio of the weight of water to the weight of powder
x	depth below the exposed surface (m)

THESIS ABSTRACT

NAME: Mohammed Abdelrahman

TITLE OF STUDY: A STUDY ON DEVELOPING HIGH PERFORMANCE NON-SHRINKING GROUT (HPNSG) UTILIZING LOCAL MATERIALS

MAJOR FIELD: Civil Engineering

DATE OF DEGREE: June 2015

Grouting technique started two centuries ago. Grout is a construction material used to fill cracks and voids. It is a self-consolidating material that can be placed without mechanical vibration. It consists of cementitious materials like Portland cement, filler, aggregate and limestone powder. Superplasticizer may be used to reduce the amount of water in order to increase the strength and reduce the shrinkage of a grout. To produce non-shrinking grout needs to use expansive agent in order to control the shrinkage.

This research aimed to developing high performance non-shrinking grout utilizing local materials, such as silica fume, metakaolin, natural pozzolan and limestone powder. The fresh and hardened properties and shrinkage and durability characteristics as well as the cost of these grouts were evaluated and compared with the commercial

ones.

The mechanical properties (compressive strength, splitting tensil strength and modulus of elasticity) of the developed grouts were comparable with that of the commercial grouts. While the drying shrinkage of the developed grouts was less than that of the commercial grouts, the durability characteristics (chloride diffusion coefficient, corrosion potential and corrosion current density) of the developed grouts were better than those of the commercial grouts. Therefore, the expected life for the developed grouts was proven to be longer than that of commercial ones, with much lower initial and overall cost.

MASTER OF SCIENCE

KING FAHD UNIVERSITY OF PETROLEUM AND MINERALS

Dhahran 31261, Saudi Arabia

مستخلص الرسالة

الاسم	محمد عبدالرحمن
عنوان الرسالة	دراسة عن تطوير مادة الحقن بالأسمنت (Grout) عالي التحمل والمقاوم للإنكماش بإستخدام المواد المحلية
التخصص	الهندسة المدنية
تاريخ التخرج	يونيو 2015

بدأت تقنية الحقن العلاجي بالأسمنت منذ قرنين تقريباً، وهي مادة إنشائية ذاتية الدمك تستخدم لملئ التشققات والفجوات بصبها دون إستخدام اي نوع من الهزازات الميكانيكية. تتكون هذه المادة (Grout) من الأسمنت، الحصى كمادة مالئة، الملدنات لتقليل نسبة الماء وزيادة المقاومة، كما يمكن إستخدام مضافات الإستطالة؛ لتقليل الأنكماش.

يهدف هذا البحث لتطوير مادة للحقن لها مقدرة عالية على التحمل ومقاومة للإنكماش، ولها خصائص ديمومة كبيرة، وذلك بإستخدام مواد صناعية ومحلية مثل؛ الصلصال (metakaolin)، البوزولان الطبيعي (natural pozzolan)، بودرة كسارات الحصى (limestone powder)، غبار السيليكا (silica fume). وتم فحص الخواص الميكانيكية، والإنكماش ومميزات الديمومة بالإضافة لمناقشة شاملة للنتائج. كما تم

تقييم تكلفة مواد الحقن التي تم تطويرها ومقارنة كل تلك النتائج مع المنتجات التجارية.

تدل نتائج الخواص الميكانيكية للمواد المطورة في هذه الدراسة أنها قريبة من المنتجات التجارية، بينما الأنكماش أقل للمواد المطورة في هذه الدراسة. وتدل نتائج الديمومة أن المنتجات المطورة أفضل من المنتجات التجارية. كما إن تكلفة إنتاج وصيانة المنتجات المطورة أقل بكثير من المنتجات التجارية المتوفرة في السوق المحلية.

ماجستير العلوم

جامعة الملك فهد للبترول والمعادن

الظهران ٣١٢٦١، المملكة العربية السعودية

CHAPTER 1

INTRODUCTION

1.1 INTRODUCTION TO GROUT AND GROUTING

After water, concrete is the most widely used material in the world. It is used in many applications, such as building frames, tanks, bridges and pavements. Annually, more than 10 billion tons of concretes is consumed annually all over the world [1]. However, One of the main problems assocoated with concrete is its inferior durability. Deteriorating concrete structures needs to be repaired to extend their life to keep them continue in their functioning.

Cement grout is generally utilized to repair deteriorated structures [2]. There are many causes for cracks in concrete. One of them is the heat development during hardening [3]. Second is attributed to drying shrinkage due to water evaporation, especially in hot-dry environments [4]. Shrinkage causes serious problems, like cracking, warping (or curling) [5], and debonding [6]. Expansion of grout due to thermal change is relatively high because of the high coefficient of thermal expansion of Portland cement, which is approximately 18 to 20 $\times$ 10^{-6} mm/mm/°C compared with 7.4 to 13.0 $\times$ 10^{-6} mm/mm/°C for concrete [7, 8].

It is believed that the word "grout" was derived from the middle English word "grùt" meaning coarsely ground meal, which was later applied to porridge [9]. Grouting is an established technique that was first used to fill cracks in rock strata to stop leakage of water. Most grouts used for this application contain a mixture of clay, lime, or cement with water [10].

Grouting may be categorized according to general criteria, such as; purpose of the structure, depth of the structure, temporary or permanent works, among other categories [11]. There are different applications of grouts concrete, such as repairing cracks and holes in concrete structures [12], strengthening historical masonry buildings [3], repairing hydropower structures (like dams, power station, etc.) [8], and for anchoring bolts, cables, or rods not designed to sustain high tensile loads [13]. Also, grout can be used for underground soil construction, such as the sealing of self-supporting underground constructions [14], grouting of soil and rock [15] to improve the soft marine clays present within the excavation [16]. Grout is also used in post-tensioning ducts to transfer stress between wires and concrete and to prevent corrosion [17].

The pioneer in grouting technique was a French engineer called Charles Berrgny [18]. In 1802, he invented a percussion pump to repair a damaged structure in the harbor of Dieppe, a small town in France. Later in 1883, during the construction of Thames Tunnel - an underwater tunnel - passing under the river Thames in London, Engineer Marc Isambard Brunel became the first one to use Portland cement as a cement grout [19]. In 1955, epoxy grout, made from epoxy resin and a filler powder, was invented by Robert L. Rowan Sr. to be used in structures that exhibited damage due to impact loading and chemical reactions [20].

Grouts are generally prepared utilizing sand, cement and other additives while several commercial grouts, such as those produced by Sika, Fosroc, FoundOcean, and others, are available in the market, which are costly. Therefore, there is a need to develop high performance and cheap grouts utilizing local materials.

1.2 NEED FOR THIS RESEARCH WORK

As mentioned earlier, cracks are the major causes of durability problems of reinforced concrete structures in Saudi Arabia. The cracked components need to be repaired to utilize their useful service life. Grouts are utilized to repair these deteriorated structures. The commercial grouts available in the local market are expensive and all may not satisfy the performance criteria in the local exposure conditions. Thus, there is a need to develop high performance non-shrinking grout utilizing indigenous materials available locally.

1.3 OBJECTIVES OF THE RESEARCH

The overall objective of the proposed study was to develop high performance non-shrinking grout (HPNSG) utilizing indigenous raw materials. The specific objectives were as the following:

1. To develop optimum non-shrinking grout mixtures utilizing indigenous materials,

2. To evaluate the shrinkage characteristics and mechanical properties of the developed non-shrinking grouts,

3. To compare the properties of the developed grout mixtures with those of few commercial grouts in the local market, and

4. To provide recommendations on the use of the developed grouts.

1.4 RESEARCH PLAN

The work was executed in the following five phases:

First: Gathered information about the subject through comprehensive and extensive literature review.

Second: Prepared testing equipment and weighing scales, specimens moulds and experimental accessories. Also imported all the materials used in this study.

Third: Got optimum dosages of superplasticizer by running trial mixtures with small volumes.

Four: Cast HPNSG specimens that were cured in water, thereafter, proposed tests were carried out.

Five: Data were analyzed, and report covering the whole process was finally prepared in which conclusions were drawn from the experimental results and recommendations were provided.

CHAPTER 2

LITERATURE REVIEW

2.1 HIGH PERFORMANCE GROUT

The demand for grouting increased with time; hence, researchers developed several grouts and grouting techniques and applied these to various fields. Various researchers developed high-performance grouts using different types of mineral or chemical admixtures [21–23] and these high-performance grouts are being used in the field for grouting ducts.

2.2 SPECIFICATIONS AND REQUIRMENTS OF GROUT

The basic characteristics of a grout are its required strength, durability, and above all its injectability [24]. The most important features in grouting manufacturing are: adequate fluidity, self-compacting behaviour [25], and penetrability [3].

The flowability properties are affected by a wide different factors, to say some of them are: ingredients content, properties and dosage of superplasticizer type. Also, the water to cement or binder ratio, fine and coarse aggregates used, condition of weather (mainly moisture content and temperature), the method of mixing (manual

or in automatic mixer) and the time taken to mix [26, 27].

The injectability (penetration) of fresh grout may be considered as the most important property to get good working grouting [8]. It is required to insure that grout can fill all voids and cracks and to keep continuity of the old materials with grout materials and keep all material compatible [27].

The workability behaviour was characterized by the rheological parameters such as yield stress and plastic viscosity [27]. To get self-compacting grout, the grout must be viscous and its deformation is high [28]. The rheology is affected by the ingredients of the mixture and particle grout size [29]. The properties that effect injectability can be summarized as follows [30]:

i. Satisfactory penetrability characteristics: Penetrability is governed by the minimum width of cracks against the maximum grain size of solids (usually aggregates).

ii. Sufficient fluidity: The possibility of flow without the need to external pressure or vibrations.

iii. Satisfactory stability of the suspension: It occurs when there is minimum possible bleeding and avoidance of segregations.

2.3 CONSTITUENT MATERIALS

The materials used in cementitious grouts may include [24]: Portland cements, fillers such as fine and coarse aggregate. Additives like silica fume, metakaolin, limestone powder or natural pozzolan, can be added separately or by mixing of two materials. Further, it can contain superplasticizers and expansive agents.

2.3.1 Cement

The hydration process of Portland cement is a complex process, whereby a series of chemical reactions take place instantaneously, or in a sequence manner [31]. According to ASTM C 150, five Portland cement types can be used to produce grout concrete [32]. To choose a certain type of cement is to rely on the required properties and time to achieve the required strength. The following paragraphs summarize the properties of the five types of Portland cement and their applications [32]:

Type I: Can be used for all grout jobs when special properties of the rest of four other types are not required.

Type II: Can resist sulfate attack, so can used for underground work. Also, the heat of hydration is less than Type I, so it can be used when the heat of hydration is an issue.

Type III: The rate of hydration is faster than Type I and Type II, and can be used if the structure has to be put in service in 10 days. Also, the surface area is finer than the other types thereby improving the workability and pumpability (injectability).

Type IV: This type has the least heat generation in hydration process, and is rarely used in grouting.

Type V: It can resist high sulfates, seldom used in grout concrete. However, it can be used for underground work for soils and wells when there is high sulfate content.

2.3.2 Silica Fume (SF)

Silica fume is a by-product of the manufacture of silicon and ferrosilicon alloys. Silica fume particles consist of very fine particles. They are spherical in shape with a mean diameter of approximately 100 times finer than cement. Silica fume is a very reactive pozzolan. Its use is expected to produce dense and impermeable concrete [33].

Silica fume can be used as a filler, although it is often used in applications such as bridges and parking garages to minimize chloride penetration into concrete [34].

Silica fume gives high compressive strength [35–42]. Also, silica fume reduces bleed and permeability, and improves workability and stability [16, 43]. The addition of silica fume results in an increased water demand because of its extreme particle's fineness. Thus, to maintain workability, a superplasticizer must be added to the grout, sometimes with dosage higher than the limits recommended by the superplasticizer manufacturer [40].

Research with varying amounts of silica fume addition has shown that silica fume addition is optimized at around 5-7% cement weight replacement [40, 44]. Silica fume grouts have also been found to be thixotropic in nature; that is, they remain sticky and cohesive at rest, but retains their fluidity when agitated [37, 45].

It is to be noticed that the increasing dosages of silica fume may lead to increase plastic shrinkage. It is found that the fineness of silica fume has good correlations with the possibility of getting plastic shrinkage cracking, specially in hot weather [46]. Further, if the grout has a temperature greater than $35\,^{\circ}C$, there will be loss in workability, below that temperature the grout presented self-leveling [47].

Silica fume grouts tend to have a lower pH than plain grouts and, therefore, the concentration of chlorides necessary to breakdown the passive layer on the steel may be reduced. However, this effect is considered small in comparison to the reduced chloride diffusivity rates found in silica fume grouts [38].

2.3.3 Limestone Powder (LSP)

Limestone is a sedimentary rock composed largely of the minerals calcite and aragonite, which are different crystal forms of calcium carbonate ($CaCO_3$). Most limestone is composed of skeletal fragments of marine organisms such as coral or foraminifera. It is made up of about 10% of the total volume of all sedimentary rocks [48].

Replacement of cement by LSP up to 20% can improve workability, strength, and can resist corrosion [49]. LSP enhances fluidity and reduces yield stress of highly

flowable mortar [50]. Through pore-filling effect, LSP reduces permeability that can increase strength and improves durability and produce compact structure [51].

LSP enhances properties physically because of their small particle sizes, which enhances the packing density of powder and reduce the gaps, thus resulting in less entrapped water [52]. Chemically; LSP supplies ions into the solution, thus modifying the kinetics of hydration and the morphology of hydration products [53].

2.3.4 Natural Pozzolan (NP)

Natural pozzolans one of the oldest materials used by people. The term "pozzolan" comes from a volcanic ash mined at Pozzuoli, Italy [34]. Pozzolans are natural rocks of volcanic origin and composed of silica and alumina oxides with little lime [54]. Pozzolans can be categorized as both supplementary cementitious materials as well as mineral admixtures [55].

Using of NP as replacement of cement by ratio 15% to 35% can improve the resistance of cement against sulfate attack, alkali-silica reactivity, and reduce permeability. Due to the absence of lime, the hardening rate is very slow and takes long time, so the compressive strength, splitting and flexural strengths at early age will be relatively low and will improve within longer curing periods [56–59].

In Kingdom of Saudi Arabia, natural pozzolanic material is available from the basalt fields (harrat) spread within the "Edge of Arabian Shield". It has almost the same chemical analysis despite the fact that they came from different locations [60].

2.3.5 Metakaolin (MK)

Metakaolin is a replacement cementitious material with pozzolanic properties [61]. MK is a poorly crystallized pozzolan obtained by calcining high purity kaolin clay at temperatures of $700 - 800\,^{\circ}C$ [62], and grounded to particle sizes between 1 to 2 micrometers [34].

MK improves permeability [34] thereby leading to higher durable concrete [63]. Accordingly, MK is usually used in bridges and parking garages to minimize chloride penetration [34]. The strength increases when MK is used as replacement of cement in dosages of 10 to 20% [62]. However, there will be large reduction in workability, which requires more dosage of superplasticiser.

2.3.6 Fine Aggregates (FA)

The sand, used in cement grout, acts as a filler material. Sand can be used in grout if it passes ASTM Sieve No.16 [32]. The increasing percentage of sand can cause segregation, which can be avoided by using finer sand or adding a mineral admixture.

2.3.7 Coarse Aggregates (CA)

The coarse aggregate (particle size greater than 4.75 mm) can be used in grout up to a size of 12 mm (1/2") [64]. The coarse aggregate should not contain clay because that may produce excessive creep and shrinkage [65].

2.3.8 Superplasticizer (SP)

To get high performance grout concrete, usage of superplasticizer is necessity. It can reduce water demand significantly that increases initial and final strength [15], the viscosity also gets to increase, making the grout more workable and easy to handle and to pump [66]. Reducing water will improve water impermeability, durability and reduce bleeding and segregation. One of the most important advantage of superplasticizer is to reduce shrinkage, thereby making the cracks less and the creep declines [15].

2.3.9 Expansive Agent (EXP)

To produce non-shrinkage grout concrete, shrinkage-compensating agents should be added to mix. The expansive agents have the ability to increase volume chemically through certain reactions [67].

The main mechanism of expansive concrete is the growth of the expansive hydration products right after setting under moist conditions, such as etringite (AFt) and monosulfoaluminate (AFm). These hydration products have a good crystal structure and large volume expansion with a high crystal growth pressure. They can increase the volume of concrete through the growth of the crystals [68].

The hydration rate of shrinkage-compensating concrete is usually higher than that of normal Portland cement concrete. The microstructure of shrinkage-compensating concrete at an early age contains a large number of AFt crystals. With the process of hydration, C–S–H can fill in the spaces occupied by water and surround the AFt crystals. Hence, a much denser microstructure can be produced [69]. Also, the shrinkage-compensating concrete has a denser microstructure and a higher gel-to-space ratio, therefore, its resistance to water penetration and ion diffusion is greatly improved. As a result, the migration rate of water, and the diffusion rate of chloride ions, oxygen, and carbon dioxide into the concrete are reduced [70]. Generally speaking, shrinkage-compensating concrete has better durability than normal concrete in respect of carbonation, corrosion of steel bar, freezing–thawing, chemical resistance and leaching [71].

2.3.10 Water

Mixing water:

Drinking water is suitable for grout concrete [72, 73]. Any water can be used if it does not affect the hydration process. Local water sources, up to several thousand parts

per million of mineral acids and dissolved solids, can be used. If there is sugar or its derivative in water, or large amounts of dissolved sodium or potassium, that water should be avoided [73].

Water to cement ratio (w/c) has significant influence on all grout properties [74]. Reducing the (w/c) ratio makes the microstructure dense, with smaller pore size, thereby decreasing the permeability and increasing the durability [75].

Curing water:

Curing water should be free from any material that can negatively affect the hydration reaction process in Portland cement, such as dissolved sodium and potassium salts [72, 76].

2.4 BATCHING

The fresh properties of the grout, such as its rheology or the tendency of the solids to settle, will be strongly influenced by its water/cement ratio. The hardened strength will also be critically dependent on the water/cement ratio of the grout. It is, therefore, very important that grout mixes are accurately batched. The density of a grout (ρ_g) is related to the water/cement ratio as follows [24]:

$$\rho_g = \frac{(1 + w/c)}{(\frac{w/c}{\rho_w} + \frac{1}{\rho_c})} \tag{2.1}$$

For most applications, the useful range of water/cement ratio for structural grouts (as opposed to those used in geotechnical engineering or for bulk void filling) will be about 0.3 to 0.45. For a cement with a density of 3150 kg/m^3, this will give a range of grout densities from 2105 to 1889 kg/m^3 [24].

2.5 HARDENED PROPERTIES OF GROUT

Compressive strength is perhaps the most important property of hardened concrete. Not only is it vital in itself in most structural applications, but also it can be related to many other properties, such as elastic modulus and durability, which are more difficult to measure directly [77]. Compressive strength is usually measured on either cubes or cylinders. UK practice is to use cubes, sometimes as small as 10 mm for neat cement grouts, but more commonly 50, 75 or 100 mm [78].

In general, for concrete as specimens size go large, the average strength will reduce [79]. However, tests on neat cement grouts have shown generally insignificant differences between results from cube sizes varying from 50 to 100 mm [80]. The exception was strength measured at one day old, which increased with specimen size, probably due to increased temperature from heat of hydration effects.

For cementitious mixes, the principal factors influencing the compressive strength and the rate of gain of strength are [24]:

i. age

ii. water/cement ratio (or, more strictly, when using partial cement replacement materials, the water/binder ratio)

iii. curing conditions

iv. composition, fineness and type of the cement

v. proportions of cement replacement materials

vi. the presence of admixtures.

The tensile strength of grouts, being typically 10% of the compressive strength, has less importance, and it is not often measured [24].

2.6 DURABILITY OF GROUT

Durability can be defined as the ability of a material to remain serviceable for at least the required lifetime of the structure of which it forms a part. However, many structures do not have a well-defined lifetime and, in such cases, the durability should ideally be such that the structure remains serviceable more or less indefinitely, given reasonable maintenance. Degradation of a grout can result from either the environment to which it is exposed to (for example, saline environment) or from internal causes within the grout (as in alkali-aggregate reaction) [81]. However, it is perhaps more useful to divide the degradation processes into two broad groups:

i. Those that initially involve chemical reactions which subsequently lead to loss of physical integrity; these include attack by sulfates, sea water and other saline water, acids and alkali-silica reaction;

ii. Those which directly lead to physical effects, such as attack by fire.

2.6.1 Mechanisms of Chloride Ion Transport

The rate of most of the degradation processes is controlled by the rate at which moisture, air or other aggressive agents can penetrate the grout [82]. The most important transport means include capillary absorption, hydrostatic pressure, and diffusion. The most familiar method is diffusion (i.e, the movement of chloride ions under a concentration gradient). For this to occur, the concrete must have a continuous liquid phase and there must be a chloride ion concentration gradient [83].

2.6.2 Chloride Diffusion

Chloride diffusion into concrete, like any diffusion process, is controlled by Fick's First Law, which, in the one-dimensional situation normally considered, states [24]:

$$J = -D_a \frac{dC}{dx} \tag{2.2}$$

where:

J = flux of chloride ions, $\frac{mol}{m^2.sec}$

D_a = a pparent chloride diffusion coefficient, m^2/seconds,

C = chloride concentration, concrete mass %,

x = depth below the exposed surface, m.

In practical terms, this equation is only useful after steady-state conditions have been reached, i.e. there is no change in concentration with time. It can be used, however, to derive the relevant equation for non-steady conditions (when concentrations are changing), often referred to as Fick's Second Law [84]:

$$\frac{\partial C}{\partial t} = D_a \frac{\partial^2 C}{\partial x^2} \tag{2.3}$$

The chloride concentration at any depth and any time can be obtained by solving this differential equation. The solution is:

$$C(x,t) = C_s - (C_s - C_i) \,.\, \mathrm{erf}(\frac{x}{\sqrt{4\, D_a\, t}}) \tag{2.4}$$

where:

C_s = chloride ion concentration at the surface of a concrete specimen, concrete mass %,

C_i = initial chloride-ion concentration of the specimen, concrete mass %,

t = exposure time, seconds,

erf = error function described in Equation 2.5 below.

$$\mathrm{erf}\, z = \frac{2}{\sqrt{\pi}} \int_0^x e^{-u^2}\, du \tag{2.5}$$

where z refers to the expression $\frac{x}{\sqrt{4\,D_a\,t}}$ and u is a regression variable. The value of this error function corresponding to the specific depth x and time t can be obtained from standard mathematical reference books [85].

By referring to Equation.2.4, which includes the effect of changing concentration with time (t), this equation has been solved using the boundary condition $C_{(x=0,t>0)}$ = C_s (the surface concentration is constant at C_s), the initial condition $C_(x > 0, t = 0) = 0$ (the initial concentration in the concrete is 0) and the infinite point condition $C_(x = \infty, t > 0) = 0$ (far enough away from the surface, the concentration will always be 0).

Diffusivity measurements on cement grouts have generally been carried out on relatively mature specimens. As might be expected, higher water/cement ratios lead to higher diffusivities; for example, Page et al. [86] have found values for chloride ion diffusivity through saturated grout at 25°C of 2.6, 4.4 and 12.4×10^{-12} m^2/s for water/cement ratios of 0.4, 0.5 and 0.6, respectively.

2.7 DEFORMATION

Deformation of cement grouts results both from environmental effects, such as moisture movement or change in temperature, and from applied stress, either short or long term [87].

2.7.1 Types of Shrinkage

Volume changes accompany the loss of moisture from fresh or hardened cementitious materials. The term "*drying shrinkage*" is generally used for hardened material. The term "*plastic shrinkage*" is used for unhardened "plastic" concrete prior to time of setting, since its response to loss of moisture is quite different. "*Carbonation shrinkage*", which occurs when hydrated cement reacts with carbon dioxide from the atmosphere,

can be regarded as a special case of drying shrinkage [24, 88]. The drying shrinkage and factors influenced it will be illustrated with little details in next section

2.7.2 Drying Shrinkage

In case of no moisture exchange with the environment, i.e. in sealed conditions, there will be a small decrease in volume while the grout is still plastic resulting from reactions of the Portland cement. During the hardening process, the internal relative humidity keeps decreasing thereby leading to further net overall volume reduction, called autogenous shrinkage [89]. If water is continuously available from the environment, e.g. the grout is immersed, then some of this is absorbed and there is a small progressive increase in volume. Expressed in linear strain terms, this expansion may reach 0.2% after several years. Of much greater significance for the structural performance of grouts is the shrinkage and swelling associated with loss or gain of moisture with a changing environment. Movements of 1% strain or more can be obtained, in timescales of days or weeks. That action is drying shrinkage [90]. The behaviour is repeated with successive cycles of drying and wetting, as illustrated schematically in Figure 2.1 maximum shrinkage occurs on the first drying, and a considerable part of this is irreversible and must be distinguished from the reversible portion resulting from alternating wet and dry conditions [91]. Further drying and wetting cycles result in progressively smaller amounts of irreversible shrinkage. Also shown in Figure 2.1 is the relatively small, continuous swelling on permanent immersion.

2.7.3 Factors Influencing Shrinkage

The water to cement ratio affects the shrinkage [92]. Powers [93] has concluded that for smaller the water to cement ratio at the beginning, the less the proportion of capillary pores in the mature cement. According to Ishai [94], an increase in w/c ratio would intensify the shrinkage of cement paste and would accelerate the volume

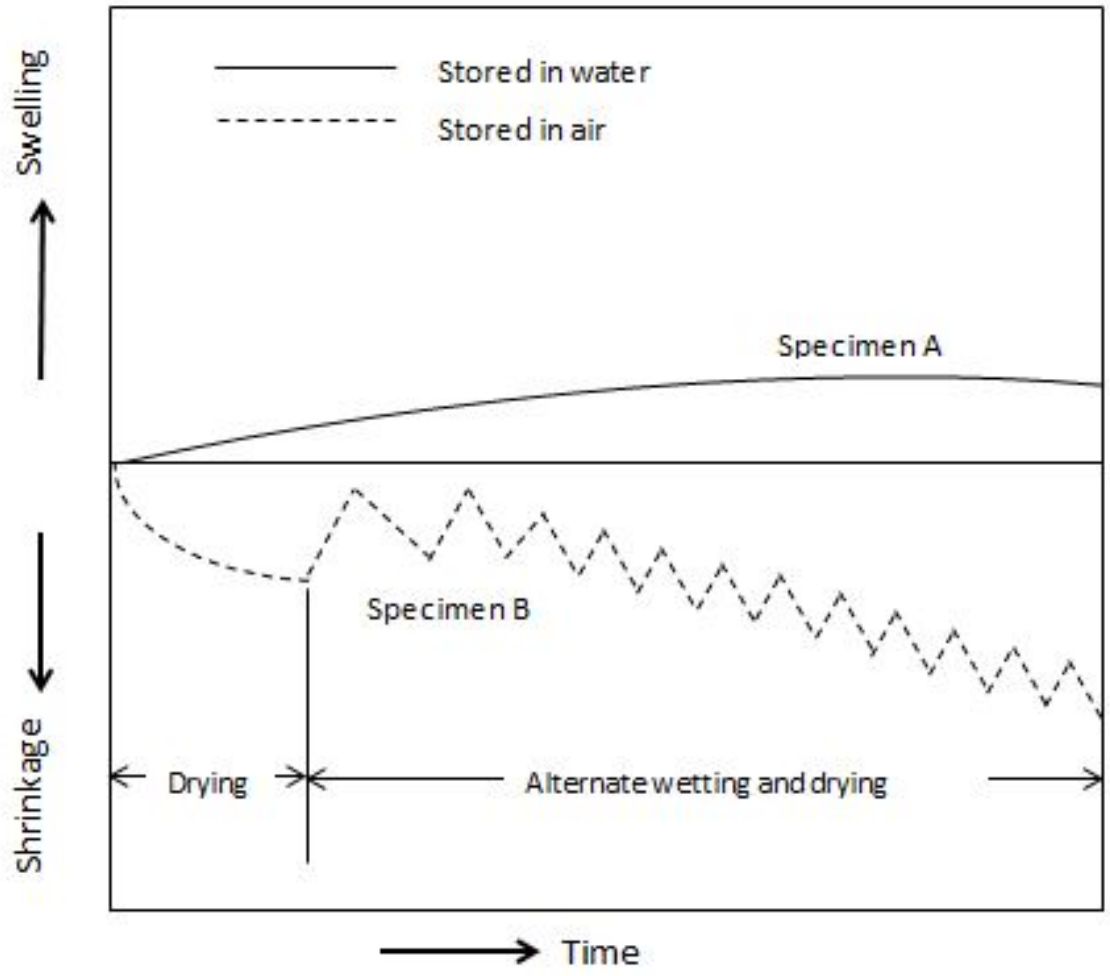

Figure 2.1: Schematic illustration of moisture movements in concrete (PCA 1967).

contraction process by providing more space for free-water diffusion. Further, the higher the percentage of capillaries and voids in the concrete system due to an increase in w/c ratio would reduce the rigidity of the solid matrix and its capacity to resist deformation. It is, therefore, expected that the shrinkage of cement paste will be greater if the w/c ratio is higher.

The nature and type of cement has a considerable influence on shrinkage [95]. For four different cement types (ordinary Portland, aluminous cement, slag, and portland with high early strength) [96], an ordinary portland cement gave 0.22 percent shrinkage in a neat paste at 1,000 days and a Portland having a high early strength gave 0.35

percent shrinkage. Dutron [97] indicated for ordinary Portland a figure of the same order of magnitude, for aluminous cement, 0.25 percent. The same author showed that in Portland and slag mixtures, the shrinkage increased with the proportion of the latter. The higher shrinkage of high-strength concrete can likely be attributed to the greater cement content, which is accompanied by a considerably greater amount of heat and, thus, rate of hydration. Graf [98] noticed the influence of the grain size of the cement on shrinkage due to the increase of surface area. Haller [99] has shown that shrinkage increased from 0.117 percent to 0.169 percent in 90 days when the specific surface increased from 1,355 to 2,280 cm^2/g for the same Portland cement. However, the influence of the degree of hydration on drying shrinkage was not so simple, for two reasons [24]:

i. Unhydrated cement grains act as a restraint against movement, thereby reducing the shrinkage at low degrees of hydration.

ii. With a high degree of hydration, there is less water in capillary pores, and the earlier loss of water from the gel pores results in greater shrinkage.

The proportion of aggregate has an influence on the shrinkage of concrete since aggregates are stiffer than the cement paste and, therefore, restrain its moisture movement [96]. But a few aggregates undergo excessive volume changes themselves on wetting and drying and aggregate that is shrinking fails to restrain the shrinking of the paste [100].

Powers [93] as well as Tremper and Spellman [101] emphasized the cumulative effect on shrinkage in making poor choices in the selection of materials. Powers assumed a constant w/c ratio and concluded: "Wrong choices of alternatives (with respect to volume change) can result in about seven times as much shrinkage as would result from the best choices." Meininger [102] concluded that due to the source of coarse aggregate alone, concrete shrinkage can vary up to 100 percent.

2.8 THERMAL EXPANSION

The linear coefficient of thermal expansion of a neat cement grout varies between about 10 and 20 $\times 10^{-6}$ per °C [24]. The value varies with moisture content, reaching a maximum at about 70% relative humidity. The thermal expansion is affected by moisture movement within the grout. However, it is time dependent, for that, the increase in expansion when the temperature increases, after while tends to decrease with constant temperature. For these reasons, estimates of movements in structural situations from tests on laboratory specimens should be treated with caution. Most aggregates have thermal expansion coefficients lower than that of neat cement grouts and, therefore, the presence of aggregate leads to a reduced coefficient for the composite grout, and to a reduced dependence on relative humidity [24].

2.9 INFLUENCE OF MIXING PROCEDURE

Not much information on the influence of mixing time is available from the literature review. Mixing time of 5, 6-12, 1-10 and 10-15 minutes were adopted by Banfill [103], Paoli et al. [104], Schwarz [105] and Sio-Keong [106], respectively, but the volume of mix was not known for the first three researchers.

Grout mixers are often classed as high shear or low shear mixers though there is no clear dividing line between the two types. Indeed, it may be easier to judge the type of mixer by the grout it produces. Jefferis [24] gave Table 2.1 to find comparative properties to be expected of high and low shear mixed grouts. He mentioned that the table should be taken as merely a guideline and not definitive.

Some factor also play role in differentiating between high and low shear mixers that include [107]: mixer shaft rotational speed, mix head peripheral speed and the clearance between mix head and adjacent fixed surfaces and the energy input during mixing (mixer power per unit volume of mix multiplied by mixing time). But the

author believed that for small mixture, low shear mixer can handle the mix without problem of bleeding or cohesion issue.

Table 2.1: Comparative properties of high and low shear mixed grouts.

property	Mixer	
	Low Shear	High Shear
Bleed	High	Low
Yield Stress	Low	High
Plastic Viscosity	High	Low
Internal cohesion	Low	High

CHAPTER 3

EXPERIMENTAL PROGRAM

3.1 INTRODUCTION

In this chapter, the materials used in the experimental program were stated along with their characteristics and sources. In accordance with the theme of this research, most of the materials employed in the research program were procured from local sources within the Kingdom. Further, the experimental procedures followed in the investigation were clearly laid out. Four different waste materials that are available locally were employed as filler materials for developing the grout.

The research work was carried out in three major stages. The first stage involved selection of the materials, and designing the trial mixtures. In the second phase, preparation of specimens was carried out and in the third phase, testing of specimens was done to ascertain the mechanical, and durability. In this chapter, all these three phases are discussed thoroughly.

3.2 MATERIALS USED IN THE STUDY

3.2.1 Cement

The cement type used was ASTM C 150 Type I, having a specific gravity of 3.15. This is the most commonly used cement type in the Kingdom. Its chemical composition is shown in Table 3.1

Table 3.1: Chemical composition of Type I cement, (OPC).

Component	**Weight (%)**
CaO	64.7
SiO_2	22
Al_2O_3	5.64
Fe_2O_3	3.80
K_2O	0.36
MgO	2.11
Na_2O	0.19
Equivalent alkalis	0.33
SO_3	2.10
Loss on ignition	0.70
C_3S	55.9
C_2S	19
C_3A	7.5
C_4AF	9.8

3.2.2 Silica Fume (SF)

The SF employed in this study was sourced from a local ready-mixed company. Its specific gravity is 2.25. Its chemical properties are shown in Table 3.2

Table 3.2: Chemical composition of the silica fume used in this study.

Component	Weight (%)
SiO_2	92.5
Al_2O_3	0.72
Fe_2O_3	0.96
CaO	0.48
MgO	1.78
SO_3	-
K_2O	0.84
Na2O	0.5
Loss on ignition	1.55

3.2.3 Natural Pozzolan (NP)

The natural pozzolan used this study was obtained locally from volcanic rocks in the Western Province of Saudi Arabia. Its specific gravity is 3.00, and its chemical composition is shown in Table 3.3

Table 3.3: Chemical composition of the natural pozzolan used in this study.

Component	Weight (%)
SiO_2	42.13
Al_2O_3	15.33
Fe_2O_3	12.21
MgO	8.50
CaO	8.06
K2O	0.84
Na2O	2.99
$Na_2O+(0.658K_2O)$	3.54
Loss on Ignition	-
Moisture	0.17

3.2.4 Limestone Powder (LSP)

The LSP used in the research was sourced from a limestone rock quarry in Abu Hadriyah, Eastern Province of Saudi Arabia. It has a specific gravity of 1.60 and its chemical composition is shown in Table 3.4

Table 3.4: Chemical composition of the limestone powder used in this study.

Component	**Weight (%)**
SiO_2	11.79
CaO	45.7
Al_2O_3	2.17
Fe_2O_3	0.68
MgO	1.8
K_2O	0.84
Na_2O	1.72
$Na_2O+(0.658K_2O)$	2.27
Loss on Ignition	35.1
Moisture	0.2

3.2.5 Metakaolin(MK)

The MK used in the research was sourced from Qatif, Eastern Province of Saudi Arabia. It has a specific gravity of 2.0 and its chemical composition is shown in Table 3.5.

Table 3.5: Chemical composition of the calcined clay (MK) used in this study.

Component	**Weight (%)**
SiO_2	46.37
Al_2O_3	35.37
Fe_2O_3	6.66
MgO	4.58
K_2O	1.76
Na_2O	0.95

3.2.6 Aggregates

Sand, an abundantly available material in the Kingdom, was used as the fine aggregate in this study. The specific gravity of fine aggregate was 2.53. Table 3.6 shows the grading of the sand used in the study.

Table 3.6: Grading of the fine aggregates used in this study.

ASTM Sieve #	Size (mm)	% passing
4	4.75 mm	100
8	2.36 mm	100
16	1.18 mm	100
30	600 μm	76
50	300 μm	10
100	150 μm	4

In addition to sand, aggregates used in this study were crushed limestone sourced from a local quarry in Abu Hadriah, Eastern Province of Saudi Arabia. The coarse aggregate had only one aggregate size of 2.36 mm (ASTM Sieve No.8), and a specific gravity of 2.60. Table 3.7 shows the coarse aggregate grading.

Table 3.7: Grading of the aggregates used in this study.

ASTM Sieve #	Sieve size (mm)	% passing
4	4.75	100
8	2.36	0

3.2.7 Expansive Agent (EXP)

Fosroc® Cebex 100 was used as an expansive material to give mixture positive expansion. Cebex 100 also works as a superplasticizer. Its technical data are shown in Table 3.8, as obtained from the manufacturer. In spite of the recommended dosage by the

manufacturer was 0.908% by cement weight, the dosage was optimized for a water to cement ratio between 0.44 to 0.48%.

Table 3.8: Technical data for Cebex 100.

Chloride content:	Nil to BS 5075
Compressive Strength:	The plasticising action of Cebex 100 allows reduction of the water/cement ratio of cementitious grouts whilst maintaining flow properties. This gives improvement in strength and long term durability when cured under restraint.
Setting times:	Cebex 100 does not significantly affect the setting times of cement based grouts.
Expansion Character:	The controlled positive expansion in unset grouts incorporating Cebex 100 overcomes plastic settlement when measured in accordance with ASTM C 827. An unrestrained expansion of up to 4% is typical.
Time for expansion:	15 minutes to 2 hours. Temperatures over 20 °C may slightly reduce these times.
Compatibility:	Cebex 100 is compatible with all types of Portland cements.

3.2.8 Superplasticizer (SP)

The superplasticizer employed in all the trial mixes in this investigation was Nafores 801 P. Nafores 801 P is a sodium salt of polynaphthalene sulphonic acid. It was sourced from a local supplier in the Kingdom. Its technical data are shown in Table 3.9, as obtained from the manufacturer. As recommended by manufacturer, field trials should be conducted to determine the optimum dose for particular application. Generally 0.2 to 1% of Nafores 801 P was used based on weight of cement.

Table 3.9: Technical data for Nafores 801 P.

Chemical classification	Sodium salt of polynaphthalene sulphonic acid
Appearance and form	Beige to brownish free flowing powder
Solid content	93 ± 1%
pH of 10% solution	7 – 9
Bulk density g/cc	0.7 ± 0.02
Ionic nature	Anionic
Solubility	Soluble in water in all proportions

3.2.9 Mixing Water

The normal sweet water available in the laboratory tap was used throughout the trial mixing and preparation of test specimens for evaluation of hardened properties of successful mixes.

3.2.10 Commercial Grouts

In this study, for the purpose of comparison, two commercial grouts from two different manufacturers were used. The products were SikaGrout®-214 and Fosroc® Conbextra GP which were manufactured by Sika and Fosroc companies, respectively. Table 3.10 gives some properties for both commercial grouts used in the study, as obtained from the manufacturer.

Table 3.10: Properties of commercial grouts used in this study.

Property	**SikaGrout®-214**		**Fosroc® Conbextra GP**	
Density	2200 kg/m^3		2080 kg/m^3	
Compressive Strength	@ 1 day	30 MPa	@ 1 day	15 MPa
	@ 7 day	-	@ 7 day	45 MPa
	@ 28 day	65	@ 28 day	65 MPa
Expansion	0.025 - 0.10% after 28 days		1% plastic state	
Mixing ratio Water/Powder Ratio	Plastic consistency	0.11–0.12	Flowable	0.16–0.18
	Flowable (max. strength)	0.12–0.13	Trowellable	0.136–0.144
	Highly flowable (max. flow)	0.14–0.15		

3.3 HPNSG TRIAL MIXES

Twenty seven (27) mixes were tried in the study. Twenty five (25) of the mixes were binary mixtures of waste materials with cement, while two (2) mixes were commercial grout.

3.3.1 Mix Parameters of the Trial Mixes

Table 3.11 shows the parameters used in the trial mixes. As can be seen from the Table, all design parameters were fixed for all the mixes, except the quantities of superplasticizer required for each trial mix to achieve self compatibility. These dosages were obtained by trials on the grout mixes until the flow attained satisfactory levels.

Table 3.11: Mix parameters used in the trial mixes.

w/p ratio	0.32 (Constant)
TA/p ratio	1.75 (Constant)
FA/TA ratio	0.40 (Constant)
Expansion material/p	0%, 0.25%, 0.5%
Superplasticizer (SP) dosage	Variable
% of replacement of SF	5%, 10%, 15%
% of replacement of NP	20%
% of replacement of LSP	10%, 20%
% of replacement of MK	10%, 15%

The codes for trial mixes, percentage of material's replacement, and percentage of expansion material were given in Table 3.12. The code has three segments, the first is the name of replacement material, the second is the percentage of replacement, and the third is the percentage of expansive material. For example "SF-10-0.25" means the replacement material is Silica Fume, with 10% replacement of cement and 0.25% of expansion material to total powder.

Table 3.12: Combinations and proportions of waste materials and cement for each of the mixes for detailed evaluation.

S/N	Trial ID	Rep. Mat.	% of Rep.	% Exp. Mat.
M1	Ctrl-0-0	-	-	0
M2	SF-5-0	SF	5	0
M3	SF-5-0.25		5	0.25
M4	SF-5-0.5		5	0.5
M5	SF-10-0		10	0
M6	SF-10-0.25		10	0.25
M7	SF-10-0.5		10	0.5
M8	SF-15-0		15	0
M9	SF-15-0.25		15	0.25
M10	SF-15-0.5		15	0.5
M11	LSP-10-0	LSP	10	0
M12	LSP-10-0.25		10	0.25
M13	LSP-10-0.5		10	0.5
M14	LSP-20-0		20	0
M15	LSP-20-0.25		20	0.25
M16	LSP-20-0.5		20	0.5
M17	NP-20-0	NP	20	0
M18	NP-20-0.25		20	0.25
M19	NP-20-0.5		20	0.5
M20	MK-10-0	MK	10	0
M21	MK-10-0.25		10	0.25
M22	MK-10-0.5		10	0.5
M23	MK-15-0		15	0
M24	MK-15-0.25		15	0.25
M25	MK-15-0.5		15	0.5
M26	Sika® - 214			
M27	Fosroc® Conbextra GP			

3.3.2 Mix Design for the Trial Mixtures

The idea of design mixture is to keep the same volume for all trials for purpose of comparing. At the beginning, the control volume was calculated considering the whole powder was cement. The volume was found by summing the volume of each component which is the weight divided by its specific gravity. For each other mix, the volume of aggregate was unknown, it was substituted to keep the mix volume the same as the control mixture [108]. The analytical derivation of the masses of fine and coarse aggregates was calculated as follows:

The total weight of Powder (W_p) is the weight of cement (W_c) plus the weight of replacement (W_r), then the weight of total aggregate (W_{TA}) can be found by:

$$W_{TA} = 1.75 \times W_p \tag{3.1}$$

Then, the weight of fine aggregate (W_{FA}) is given by:

$$W_{FA} = 0.4 \times W_{TA} \tag{3.2}$$

While the weight of crushed limestone aggregate (W_{CA}) is:

$$W_{CA} = 0.6 \times W_{TA} \tag{3.3}$$

The weight of water (W_w) can be calculated from (W/p) ratio which was 0.32:

$$W_w = 0.32 \times W_p \tag{3.4}$$

The volume for the control mix (V_1), where there was no any replacement is the summation of weight of ingredients by its specific gravity:

$$V_1 = \frac{W_c}{SG_c} + \frac{W_{FA}}{SG_{FA}} + \frac{W_{CA}}{SG_{CA}} + \frac{W_w}{SG_w} \tag{3.5}$$

When there was replacement of cement by any weight (W_r), the volume of mix without aggregate (V_2) is given by:

$$V_2 = \frac{W_c}{SG_c} + \frac{W_r}{SG_r} + \frac{W_w}{SG_w} \tag{3.6}$$

The difference between control volume V_1 and V_2 should be substituted by aggregate, the volume of total aggregate (V_3):

$$V_3 = V_2 - V_1 \tag{3.7}$$

Finally, the weight of fine and crushed aggregate will be proportional to its specific gravity and can be calculated by using Equation 3.7 and Equation 3.8, respectively

$$W_{FA} = \frac{V_3}{\frac{1}{SG_{FA}} + \frac{1.5}{SG_{CA}}} \tag{3.8}$$

3.3.3 Weights of Constituent Materials in Trial Mixtures

The weights of constituent materials for the trial mixtures, obtained by applying the equations in the previous section, are shown in Table 3.13. In this table, the last column shows the flow by centimeters, that result from the flow table test for each trial. All the weights in the table are by grams. For the last two mixes, which are for commercial grouts, the water/powder ratio was taken from the data sheet provided by manufacturers, in this case, w/p was 0.14 for Sika® 214 and, 0.17 for Fosroc® Conbextra GP.

Table 3.13: Weights (in grams) of the constituent materials for the trial mixtures.

S/N	Cement	Additive Material		FA	CA	water	EXP	SP	Flow (cm)
TM1	6000	-		4200	6300	1920	0.0	79	24.3
TM2	5225	**SF 5%**	275	3814.1	5721.1	1760	0.0	146.3	24.3
TM3	5225		275	3814.1	5721.1	1760	13.8	146.3	23.7
TM4	5225		275	3814.1	5721.1	1760	27.5	146.3	24.1
TM5	4950	**SF 10%**	550	3778.2	5667.2	1760	0.0	154.0	23
TM6	4950		550	3778.2	5667.2	1760	13.8	154.0	24.7
TM7	4950		550	3778.2	5667.2	1760	27.5	154.0	24.5
TM8	4675	**SF 15%**	825	3742.2	5613.4	1760	0.0	165.0	24.8
TM9	4675		825	3742.2	5613.4	1760	13.8	165.0	24.5
TM10	4675		825	3742.2	5613.4	1760	27.5	165.0	23
TM11	4950	**LSP 10%**	550	3676.0	5514.0	1760	0.0	75	25
TM12	4950		550	3676.0	5514.0	1760	13.8	62	23.5
TM13	4950		550	3676.0	5514.0	1760	27.5	50	23.6
TM14	4400	**LSP 20%**	1100	3502.0	5253.0	1760	0.0	75	24.9
TM15	4400		1100	3502.0	5253.0	1760	13.8	62	18.2
TM16	4400		1100	3502.0	5253.0	1760	27.5	50	21
TM17	4400	**NP 20%**	1100	3832.0	5748.1	1760	0.0	100	25.1
TM18	4400		1100	3832.0	5748.1	1760	13.8	87	24.9
TM19	4400		1100	3832.0	5748.1	1760	27.5	75	21.3
TM20	4950	**MK 10%**	550	3746.7	5620.1	1760	0.0	78	24.8
TM21	4950		550	3746.7	5620.1	1760	13.8	65	18.6
TM22	4950		550	3746.7	5620.1	1760	27.5	52	18.9
TM23	4675	**MK 15%**	825	3695.1	5542.6	1760	0.0	78	24.9
TM24	4675		825	3695.1	5542.6	1760	13.8	65	25
TM25	4675		825	3695.1	5542.6	1760	27.5	52	24.8
TM26	**Sika® 214**		17000			2380			24.9
TM27	**Fosroc® Conbextra GP**		17000			2890			18.9

3.3.4 Preparation and Curing of Specimens

Concrete specimens were prepared and cured to carry out various tests planned in this study. Batching of each mix was proportioned by weight. The dry components were mixed for seven minutes in a mixer with capacity 0.2 m^3 (see Figure 3.1). Then, the water was gradually added to the mixer while it was running. The period of adding water continued for eight to ten minutes. After that, the mixture became ready to discharge, thereafter, the flow table test was carried out according to ASTM C 230 [109] (see Figure 3.2), then the mix was poured into the molds. After casting, the specimens were covered with plastic sheet for 24 hours in the laboratory environment (22 $\pm$ 3 °C) to minimize loss of mix water. After 24 hours, the specimens were demoulded and placed in a curing tank till the time of test. Table 3.14 shows the type and number of specimens used in this study.

Figure 3.1: Mixer used in this study.

Figure 3.2: Flow table test.

3.4 TESTS ON TRIAL MIXES

In this sections, brief description to the tests carried out in this study was presented:

3.4.1 Compressive Strength

Compressive strength specimens were 50×50×50 mm concrete cubes. The compressive strength was determined according to ASTM C 942 [110] after 3, 7, 14 and 28 days of water curing. The specimens were tested using an automatic compression machine of hydraulic type of Matest® brand, shown in Figure 3.3. The compressive load was applied at a constant rate of 0.8 kN/s until the specimen failed and the maximum load (kN) was noted. The compressive strength was calculated by dividing the failure load by the cube cross-sectional area.

Figure 3.3: Matest® hydraulic type compressive strength testing machine.

Table 3.14: Type and number of specimens prepared and tested.

No.	Tests	Specimen Type	Dimensions (mm)	Test Standard	Specimen Tested
1	Compressive strength	Cube	50×50	ASTM C 942	324
2	Tensile strength (Split)	Cylinder	75×150	ASTM C 496	81
3	Modulus of elasticity	Cylinder	75×150	ASTM C 469	81
4	Drying shrinkage	Prism	25×25×285	ASTM C 157	81
5	Corrosion potentials	Cylinder	75×150	ASTM C 876	81
6	Corrosion current density	Cylinder	75×150	LPRM	
7	Chloride Diffusion	Cylinder	75×150	ASTM C 1556	81
Total Number of Specimens					738

3.4.2 Splitting Tensile Strength

Splitting tensile strength specimens were 75 mm by 150 mm concrete cylinders. The test was conducted according to ASTM C 496 on 28-day cured specimens. The specimens were tested using an automatic compressive testing machine of hydraulic type, shown in Figure 3.4. Compressive loading was applied at a constant rate of 0.4 kN/s through narrow bearing strips, complying with the provisions of ASTM C 496, until the specimen failed by splitting. The splitting load (kN) was recorded for each of 3 samples representing each mix.

The splitting tensile strength was determined using the formula in the Section 8.1 of ASTM C 496M – 04, given by:

$$T = \frac{2P}{\pi l d} \tag{3.9}$$

where:

T = splitting tensile strength, MPa,

P = maximum applied load indicated by the testing machine, N,

l = specimen length, mm, and

d = specimen diameter, mm.

Figure 3.4: Test arrangement for splitting tensile strength.

For each mix, the average of 3 specimens was recorded as the splitting tensile strength of that concrete mix.

3.4.3 Modulus of Elasticity

The modulus of elasticity or Young's modulus of a material is an important mechanical property that affects the deformation characteristics under a given state of stress. A material with a low Young's modulus shows more deformation than the one with a higher modulus, even if they have the same strength.

For the determination of Young's (chord) modulus for the HPNSG specimens, 75 mm $\times$ 100 mm concrete cylinder specimens were used. The test was conducted according to ASTM C 469 on 28-day cured specimens. The specimens were tested using the same automatic testing machine used in compressive and tensile strength

tests. Compressive loading was applied at a constant rate of 0.5 kN/s at the ends of the specimen, via a load cell, until it failed.

Figure 3.5 shows the test arrangement. The arrangement consisted of a cylindrical sample clamped in 2 circular steel frames, perfectly aligned and bearing 2 LVDTs on opposite sides, such that any compressive strain applied at the ends of the test specimen is picked up by the LVDTs. The linear deformations captured by the LVDTs and the load sensed by the load cell are recorded by a data logger. The load and linear deformation data were copied from the logger for stress-strain curves plotting and calculation of chord modulus, using the formula in the Section 7.1 of ASTM C 469M – 04, given by:

$$E = \frac{S_2 - S_1}{\epsilon_2 - 0.000050} \tag{3.10}$$

where:

E = Chord modulus of elasticity, MPa,

S_2= Stress corresponding to 40% of ultimate load,

S_1= Stress corresponding to a longitudinal strain, ϵ_1, of 50 millionths, MPa, and

ϵ_2= Longitudinal strain produced by stress S_2.

For each mix, the average of three specimens' modulus of elasticity was recorded as the modulus of elasticity of that grout mixture.

3.4.4 Drying Shrinkage

Shrinkage is the reduction in the volume of concrete caused mainly by the loss of water due to evaporation from a freshly-hardened concrete exposed to air. Shrinkage may result in cracking of restrained concrete members. A total of three HPNSG prismatic specimens of 25×25×285 mm were prepared for each mix for determining the drying

Figure 3.5: Test arrangement for determining the modulus of elasticity.

shrinkage according to ASTM C 157 [111]. Three specimens were tested and their average values were reported. A setup consisting of a stand fitted with an LVDT connected to a data logger was used, as shown in Figure 3.6.

3.4.5 Corrosion Measurement

The corrosion resistance of specimens was evaluated by exposing them to a 5% sodium chloride solution. Reinforced grout specimens, measuring 75 mm in diameter and 150 mm high, were prepared with a 12 mm diameter steel bar placed at the center. A cover of 25 mm was provided at the bottom. The reinforcing steel bars were coated with cement paste followed by an epoxy coating at the bottom of the bar and at the concrete-air interface to avoid crevice corrosion. Figure 3.7 shows the schematic view of the reinforced HPNSG specimen.

Reinforcement corrosion was monitored by measuring the corrosion potentials, according to ASTM C 876 [112] and the corrosion current density by the linear polarization

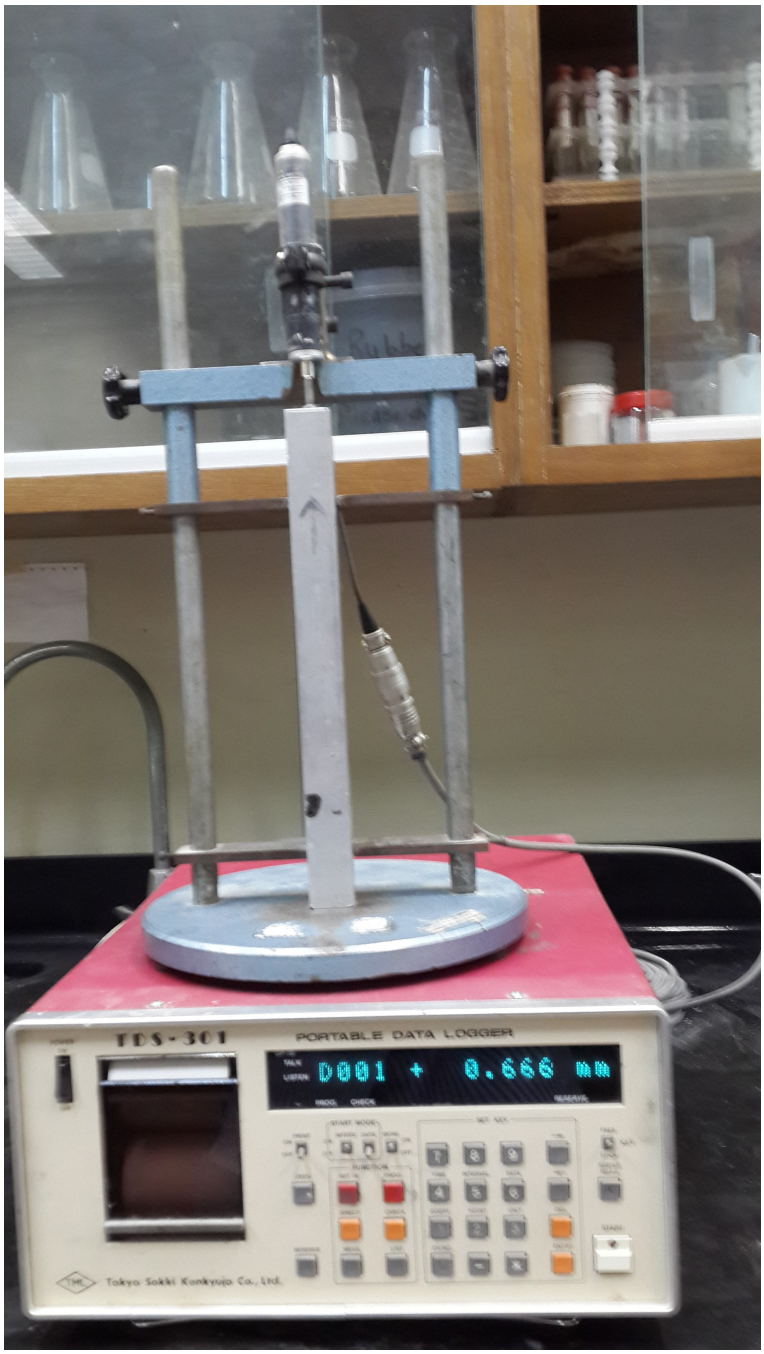

Figure 3.6: Setup for measuring drying shrinkage.

resistance method (LRPM) [113]. The corrosion potential measurements were conducted at regular intervals.

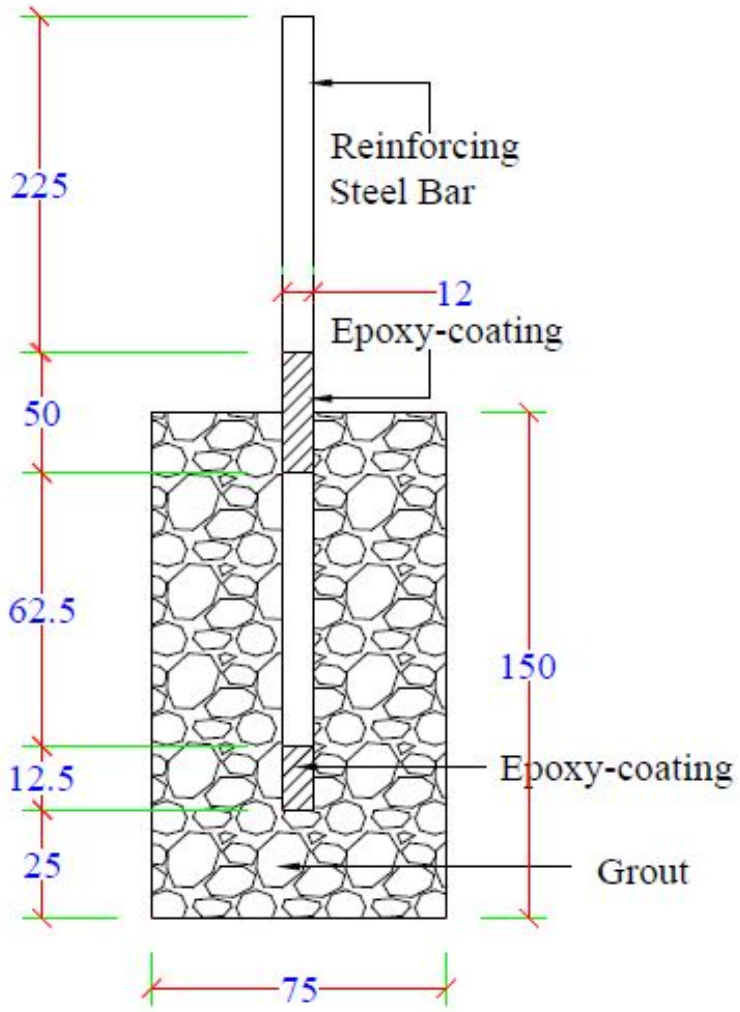

Figure 3.7: Schematic diagram of reinforced grout specimen used in corrosion measurement (Dimensions in mm).

Corrosion potentials

The corrosion potentials were measured using a saturated calomel reference electrode (SCE). The electrical lead from the reference electrode was connected to the positive

terminal of a high impedance digital voltmeter while the steel bar in the concrete specimen was connected to its negative terminal. Figure 3.8 shows a set of specimens for corrosion measurements.

Though it is generally accepted that corrosion potential measurements must be complemented by other methods [114], reliable relationships between potential and corrosion rate can be found in the laboratory for well established conditions [115]. These relationships can in no way be generalized, since wide variations in the corrosion rate are possible in a very narrow range of potentials [116]. The criteria for potential is presented in next chapter at Section 4.6.

Figure 3.8: Corrosion potential measurement setup.

Corrosion current density

The three electrode method was utilized to measure the resistance to polarization (R_p) using a Potentiostat/Galvanostat. The steel rod was connected to the working electrode terminal while a steel plate and a reference electrode were connected to the counter and reference electrode terminals of the Potentiostat/Galvanostat, respectively. The setup is shown in Figure 3.9 and Figure 3.10.

The steel was polarized to ± 10 mV of the corrosion potential at a rate of 3 mV/min and the resulting current between the counter and working electrode was measured. R_p was determined as the slope of the current-potential curve. Corrosion current density (I_{corr}) was evaluated using the following relationship [117]:

$$I_{corr} = \frac{B}{R_p} \tag{3.11}$$

where:

I_{corr} = Corrosion current density, $\mu A/cm^2$

R_p = Resistance to polarization, $\frac{\Delta E}{\Delta I}$, $\Omega.cm^2$

$$B = \frac{\beta_a \times \beta_c}{2.3(\beta_a + \beta_c)} \tag{3.12}$$

where:

β_a and β_c are the anodic and cathodic Tafel constants, mV/decade, respectively.

The Tafel constants are normally obtained by polarizing the steel to ± 250 mV of the corrosion potential (Tafel plot). However, in the absence of sufficient data on β_a and β_c, a value of B equal to 26 mV for steel in active condition and 52 mV for steel in passive condition is often used [118]. Lambert et al [119, 120] have reported a good correlation between the corrosion rates determined using these values and the

gravimetric weight loss method.

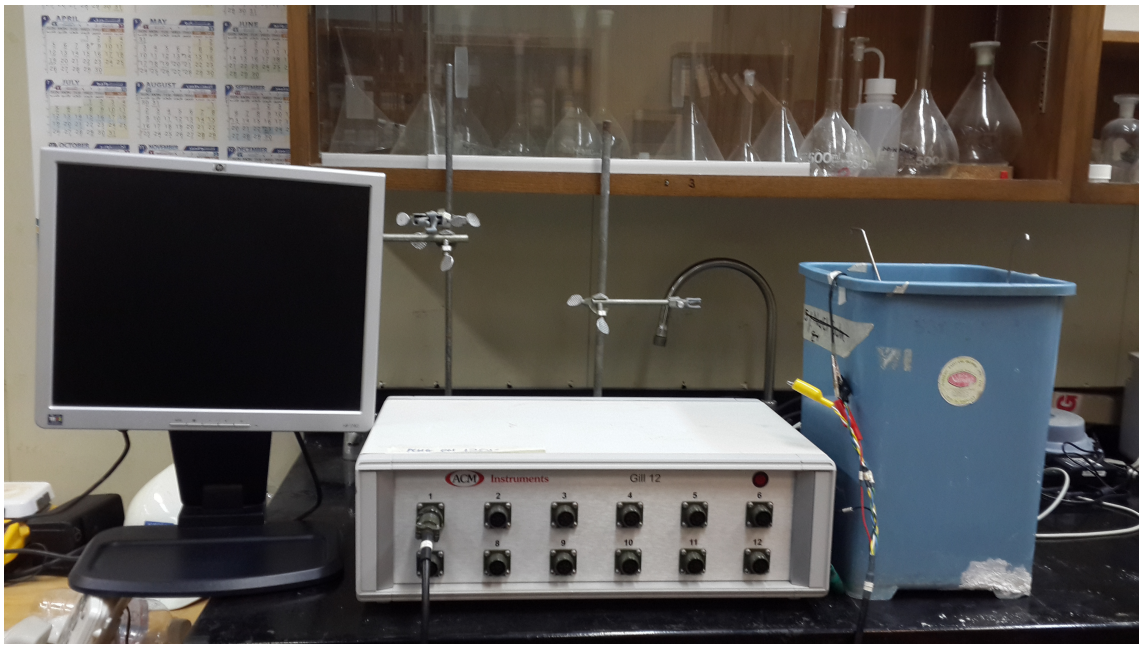

Figure 3.9: Corrosion potential measurement setup.

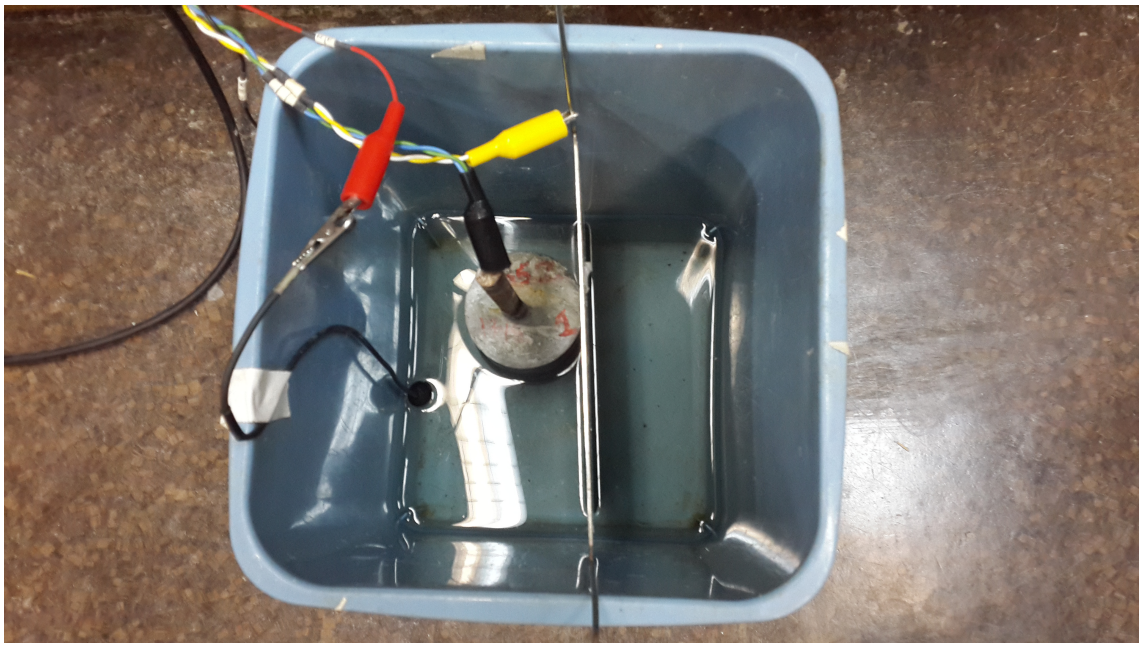

Figure 3.10: Pictorial view of the electrodes.

3.4.6 Chloride Diffusion

The chloride diffusion tests were performed following ASTM C1556 test method. The specimens were cured for 28 days, then coated with epoxy (except one side of the cylinder, as shown in Figure 3.11) and, thereafter, exposed to 5% sodium chloride solution for five months. Slices of 5 mm thickness (see Figure 3.12) were obtained at five (5) different depths (0-5, 10-15, 25-30, 75-80, and 95-100 mm) by cutting the cores using concrete cutting machine. The depths at which the cores were sliced to obtain chloride profile are given in Table 3.15.

Table 3.15: Depth of slices for chloride profile.

Slice No.	**Depth from surface (mm)**	**Average depth for analysis (mm)**
1	0-5	2.5
2	10-15	12.5
3	25-30	27.5
4	75-80	77.5
5	95-100	97.5

The procedure for finding the water soluble (free) chloride concentration is given below:

1. 5 g of powdered sample was taken into the beaker.
2. 50 ml of hot distilled water (105 °C) was added and the mixture was thoroughly stirred and left for 24 hours for the digestion of chloride.
3. The solution was filtered into the flask and the filtrate was made to 100 ml by adding distilled water, as shown in Figure 3.13.
4. 0.2 ml of the solution was taken through micro-pipette and 9.8 ml of distilled water was added into it for making it 10 ml.

5. After that, 2 ml each of 0.25 M ferric ammonium sulfate and mercuric thiocyanate was added into that 10 ml solution.

6. Solution was gently shaken and was taken into the a test tube.

7. The test tube was placed into the spectro-photometer (set at 460 nm wave length) and the absorbance value was measured.

8. Finally, the free chloride concentration was calculated using chloride calibration curve.

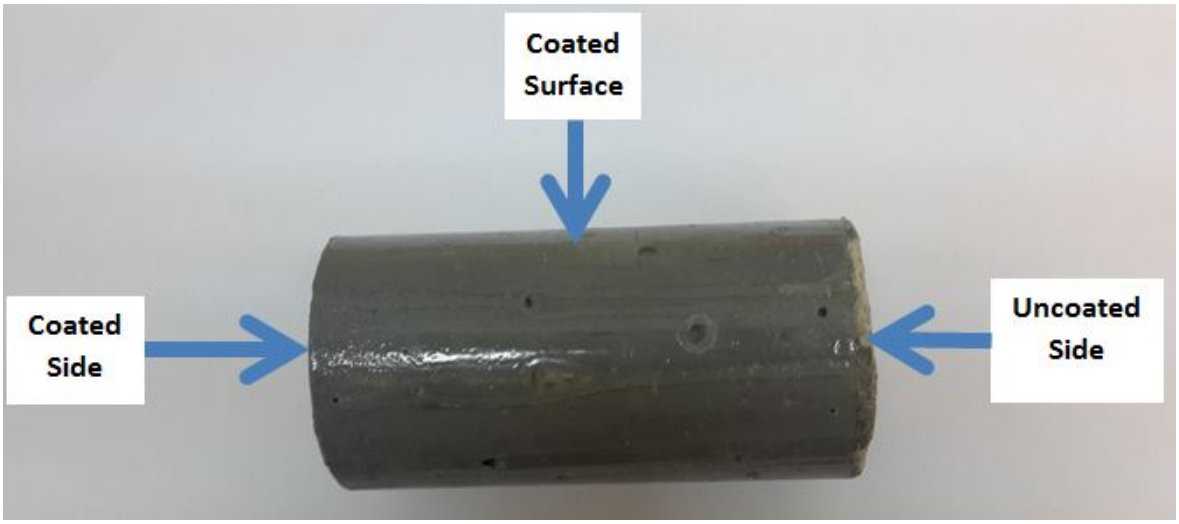

Figure 3.11: Specimen after coating.

Figure 3.12: Slice, 75 mm diameter and 5 mm thickness.

Figure 3.13: Samples left for filtration after digestion of chlorides.

CHAPTER 4

RESULTS AND DISCUSSION

In this chapter, the results of the experimental work were presented and discussed. For simplicity and clarity of presentation, the results are presented under individually devoted sections.

4.1 COMPRESSIVE STRENGTH FOR TRIAL MIXTURES

For each trial mix, the flow result from flow table test and the compressive strength at 3 and 7 days of curing will be reported as averages of three specimens prepared from each mix. For the codes used, the code has three segments, the first is the name of replacement material, the second is the percentage of replacement, and the third is the percentage of expansive material. For example, "SF-10-0.25" means the replacement material is silica fume, with 10% replacement of cement and 0.25% of expansive material to total powder.

Table 4.1 shows the summary of flow and compressive strengths for the trial mixes. For all the six mixes of silica fume, the compressive strength for 7 days was increased with increasing percentage of SF, and it was higher than that of the control mix, hence, all the three percentages of SF (5%, 10% and 15%) were selected for the final mixes for detailed evaluation.

Table 4.1: Flow and compressive strengths for the trial mixes.

Trial Mix ID	Flow (cm)	Compressive Strength (MPa)	
		3 days	7 days
TM1-Ctrl-0-0	24.6	33.9	39.3
TM2-SF-5-0	24.1	39.1	42.1
TM3-SF-5-0.3	23.2	33.8	38.5
TM4-SF-10-0	24.3	40.2	46.3
TM5-SF-10-0.3	24.0	39.6	43.6
TM6-SF-15-0	22.8	41.3	46.8
TM7-SF-15-0.3	23.4	39.9	44.8
TM8-LSP-10-0	23.7	31.8	36.7
TM9-LSP-10-0.3	23.5	30.4	35.6
TM10-LSP-20-0	24.1	31.3	35.2
TM11-LSP-20-0.3	22.9	30.9	35.0
TM12-LSP-30-0	22.7	23.8	27.5
TM13-LSP-30-0.3	23.4	20.5	22.3
TM14-NP-20-0	22.8	43.7	48.1
TM15-NP-20-0.3	23.1	38.2	44.3
TM16-NP-30-0	23.8	31.2	36.4
TM17-NP-30-0.3	22.7	25.7	28.5
TM18-MK-10-0	23.2	56.1	60.8
TM19-MK-10-0.3	22.1	47.5	52.3
TM20-MK-15-0	24.5	59.1	62.9
TM21-MK-15-0.3	23.8	49.8	55.7
TM22-MK-20-0	24.4	43.3	45.9
TM23-MK-20-0.3	23.6	37.9	39.9

For the mixes containing limestone powder, with 10% and 20%, the compressive strength for 7 days without any expansive agent was close to the control mix (36.7 and 35.0 compared to 39.3 MPa for the control mix). But, when the replacement percentage reached 30%, there was big drop in compressive strength (27.5 MPa). Hence, the mix with 30% LSP was ignored, and only 10% and 20% had been selected for detailed evaluation.

In the case of the mixes containing natural pozzolan, for 30% replacement by NP and 0.3% of expansive agent, the compressive strength was 28.5 MPa, while it was 44.3 MPa for same percentage of expansive agent and 20% of NP replacement. Therefore, only the 20% replacement had been selected for full investigation.

Finally, for the mixes containing metakaolin, the compressive strength kept increasing with more metakaolin as replacement, until it reached 20%, thereafter, the compressive strength dropped. Therefore, the 20% of metakaolin as replacement had been ignored, and both 10% and 20% had been chosen for detailed evaluation.

4.2 COMPRESSIVE STRENGTH

For each mix, the compressive strength at 3, 7, 14 and 28 days of curing are reported in this section.

4.2.1 Control Mix and Commercial Grouts

Table 4.2 summarizes the results of compressive strength for the control mix and commercial grouts. Figure 4.1 shows a schematic presentation of the compressive strength evolution with curing times, plotted from the values in Table 4.2.

Table 4.2 and Figure 4.1 show that both types of commercial grout used in this study reached nearly 94% of their strength in first week, while the control mix reached only 70.8% of strength at this early period (the rate of hydration was very high in both

commercial grouts at early stage). However, at 28 days, the control mix had a value nearly equal to 90% of Sika® grout-214 and 87% of Fosroc® GP grout. These data indicate that the two commercial grouts tend to develop their compressive strength at the early period (i.e., within 7 days), while the control mix continues to develop its compressive strength even after 28 days of curing.

Table 4.2: Compressive strength of the control mix and commercial grouts.

Mix ID	Compressive Strength (MPa)			
	3 days	**7 days**	**14 days**	**28 days**
M1-Ctrl-0-0	32.5	38.7	45.9	54.6
M26-Sika 214	52.0	56.5	58.2	60.1
M27-Fosroc Conbextra GP	53.0	59.4	61.3	63.1

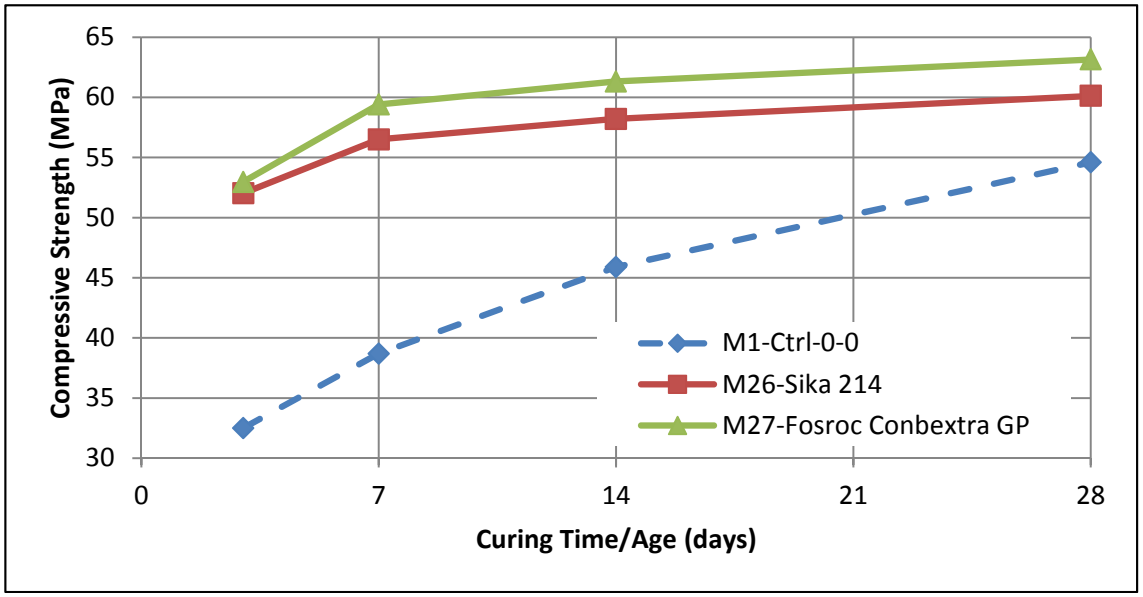

Figure 4.1: Compressive strength of control mix and commercial grouts.

4.2.2 Mixes Containing SF

Table 4.3 shows the summary of compressive strengths for the SF mixes. Figures 4.2, 4.3 and 4.4 display the compressive strength evolution with curing time, plotted from the values in Table 4.3 for the mixes containing SF.

Table 4.3: Compressive strength of HPNSG with SF.

Mix ID	Compressive Strength (MPa)			
	3 days	**7 days**	**14 days**	**28 days**
M1-Ctrl-0-0	32.5	38.7	45.9	54.6
M2-SF-5-0	38.8	41.8	50.7	59.1
M3-SF-5-0.25	34.5	39.7	48.2	56.4
M4-SF-5-0.5	33.2	35.4	45.7	53.7
M5-SF-10-0	39.9	45.6	52.4	60.4
M6-SF-10-0.25	40.6	43.6	49.7	56.5
M7-SF-10-0.5	37.2	41.2	46.8	54.1
M8-SF-15-0	38.1	45.9	61.2	64.5
M9-SF-15-0.25	37.9	44.8	53.1	60.5
M10-SF-15-0.5	35.5	39.4	50.2	58.7

From the data in these figures, almost all the mixes containing SF had strength greater than the control mix at almost all the curing periods. Generally, with increasing the percentage of replacement of SF, the strength slightly increased, which indicates that silica fume is not only highly pozzolanic, but its pozzolanic reaction is fast [121–124].

The concomitant addition of expansive material to SF seems to have a negative effect on strength because there was reduction in compressive strength that reached 10% with increase in expansive agent of 0.5% for M10.

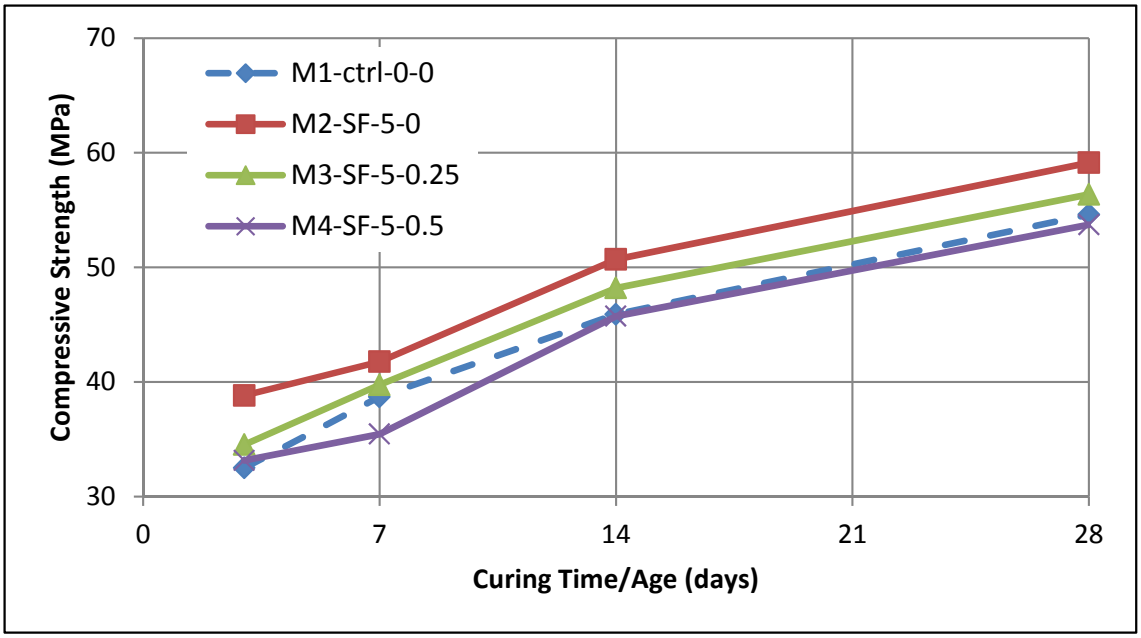

Figure 4.2: Compressive strength of HPNSG with 5% SF.

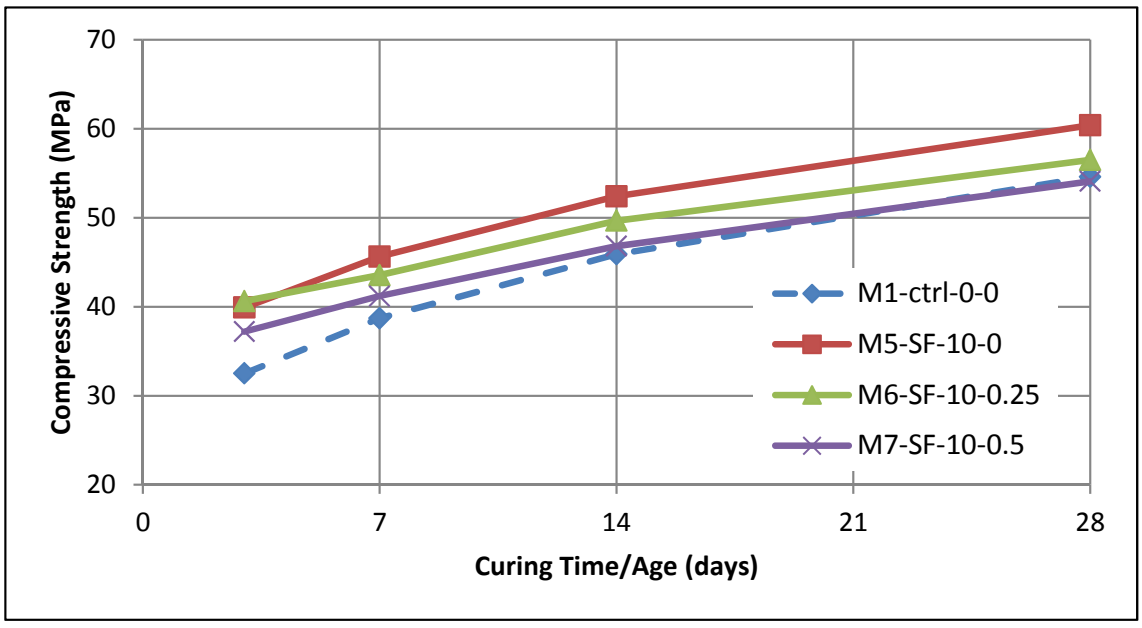

Figure 4.3: Compressive strength of HPNSG with 10% SF.

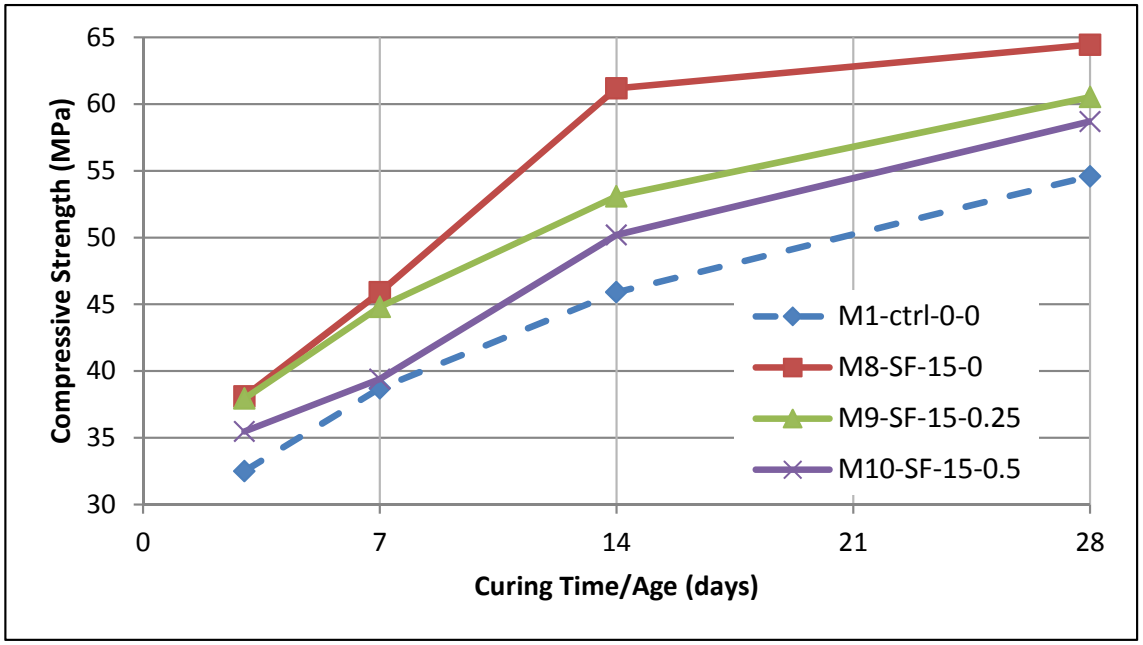

Figure 4.4: Compressive strength of HPNSG with 15% SF.

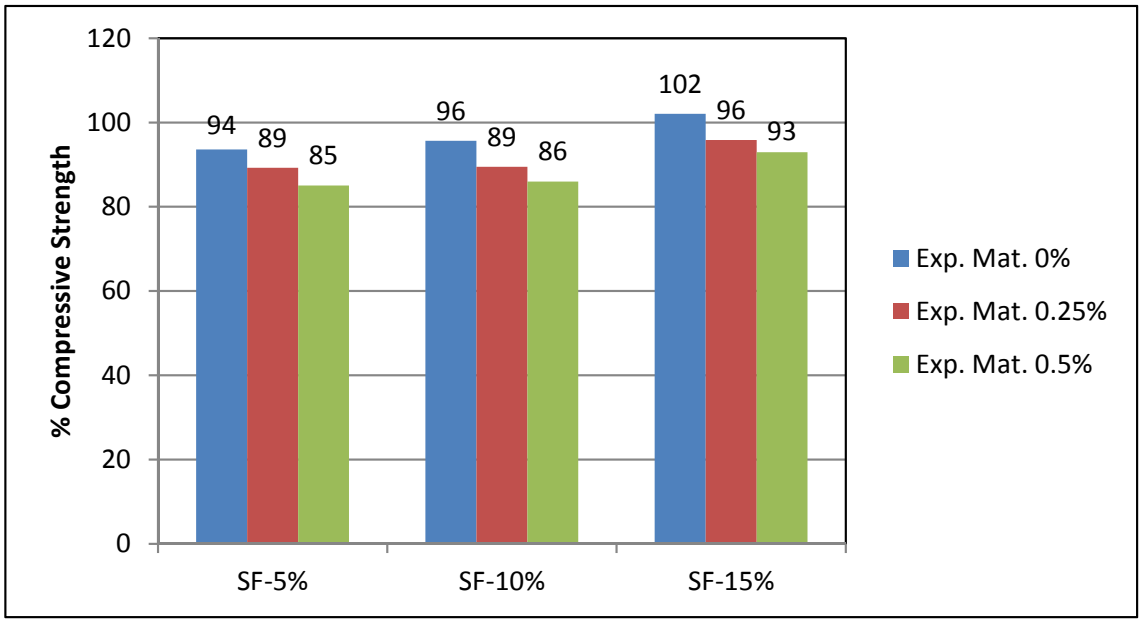

Figure 4.5: % Compressive Strength at age 28 days of SF to Fosroc Conbextra GP .

After a curing period of 28 days, the strength of SF mixes, as compared to the highest commercial grout compressive strength (which was Fosroc® Conbextra GP grout), is shown in Figure 4.5. It is clear from the data in this figure that the strength ratio at an age 28 days between SF mixes and Fosroc ranges from 85% to 102%.

Moreover, the strength of SF mixes was lower than Fosroc Conbextra GP grout except when SF replacement was 15% with 0% of expansive agent.

4.2.3 Mixes Containing LSP

Table 4.4 presents the summary of a compressive strength for the LSP mixes. Figures 4.6 and 4.7 show graphs of compressive strength evolution with curing time, plotted from the values in Table 4.4, for the mixes containing LSP. As can be seen from the data in Figures 4.6 and 4.7, all the mixes in this category had compressive strength at all ages lower than that of the control mix. Also the comressive strength went down with increasing the expansive agent, indicating that the negative influence of expansive material on compressive strength was noticeable. The compressive strength slightly decreased with increasing the percentage of LSP as replacement. Also, the rate of hardening was reduced with increasing the percentage of LSP from 10% to 20%. This can be attributed to the fact that LSP does not possess pozzolanic property [125,126], in addition to the negative dilution effect [127].

Table 4.4: Compressive strength of HPNSG with LSP.

Mix ID	**Compressive Strength (MPa)**			
	3 days	**7 days**	**14 days**	**28 days**
M1-Ctrl-0-0	32.5	38.7	45.9	54.6
M11-LSP-10-0	31.5	37.9	43.2	53.7
M12-LSP-10-0.25	30.3	36.4	41.6	51.5
M13-LSP-10-0.5	29.9	34.2	39.8	49.8
M14-LSP-20-0	31.1	36.8	41.6	51.3
M15-LSP-20-0.25	29.4	36.6	44.4	50.2
M16-LSP-20-0.5	30.2	33.2	38.6	48.3

The strength at 28 days for LSP mixes as compared to Fosroc Conbextra GP grout is presented in Figure 4.8. It is clear from the data in this figure that all LSP had

strength lower than Fosroc's grout, which was between 76% up to 85%.

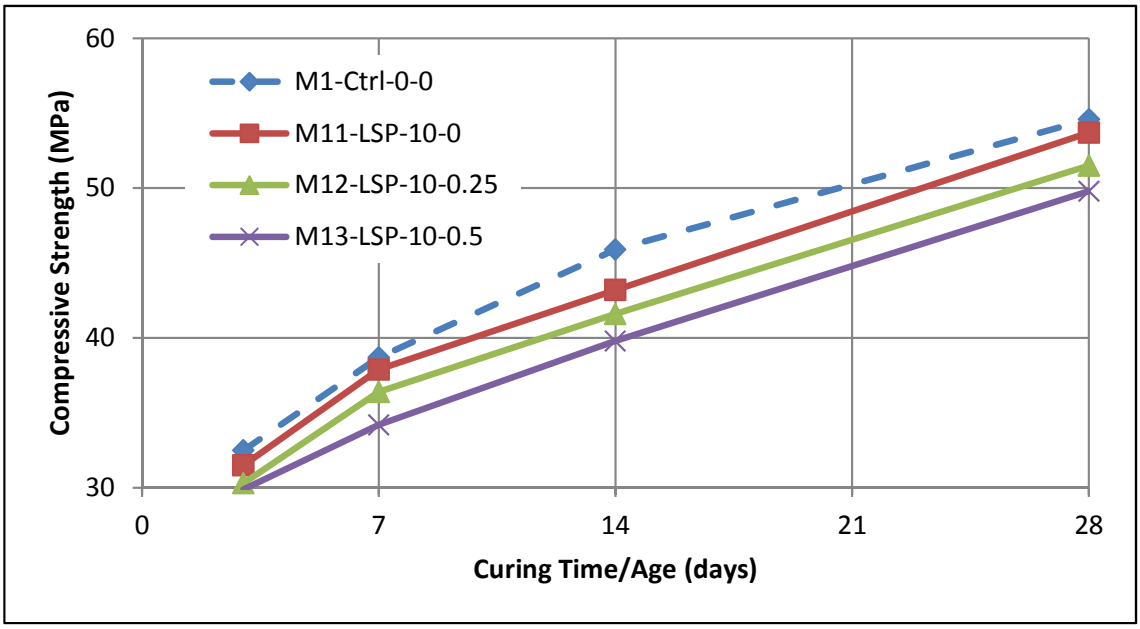

Figure 4.6: Compressive strength of HPNSG with 10% LSP.

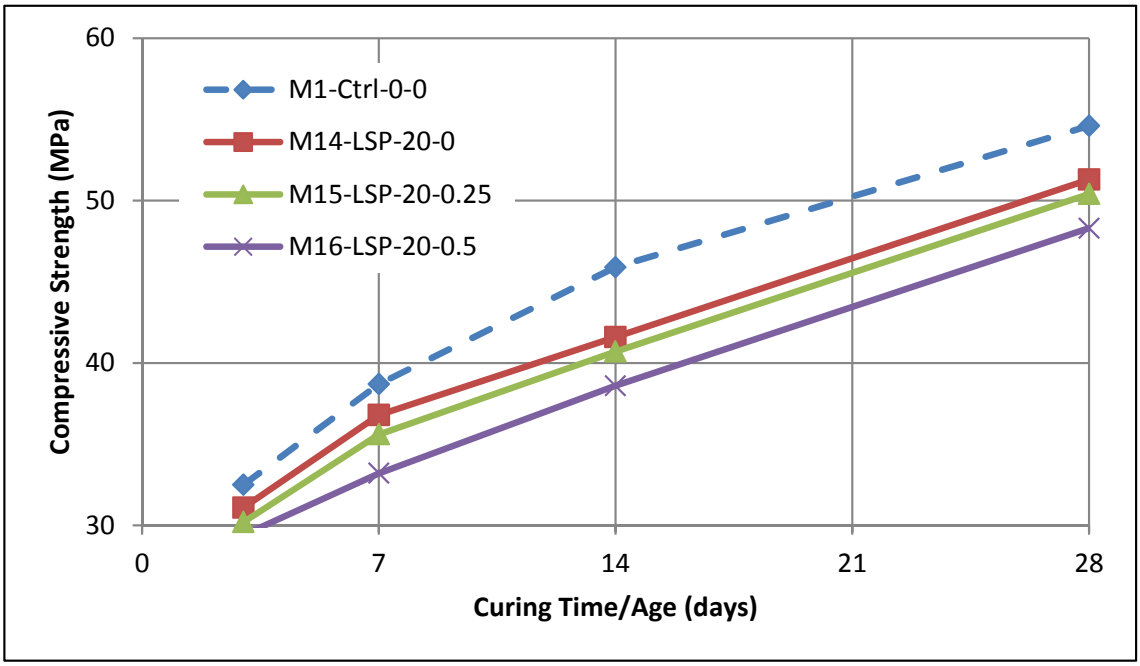

Figure 4.7: Compressive strength of HPNSG with 20% LSP.

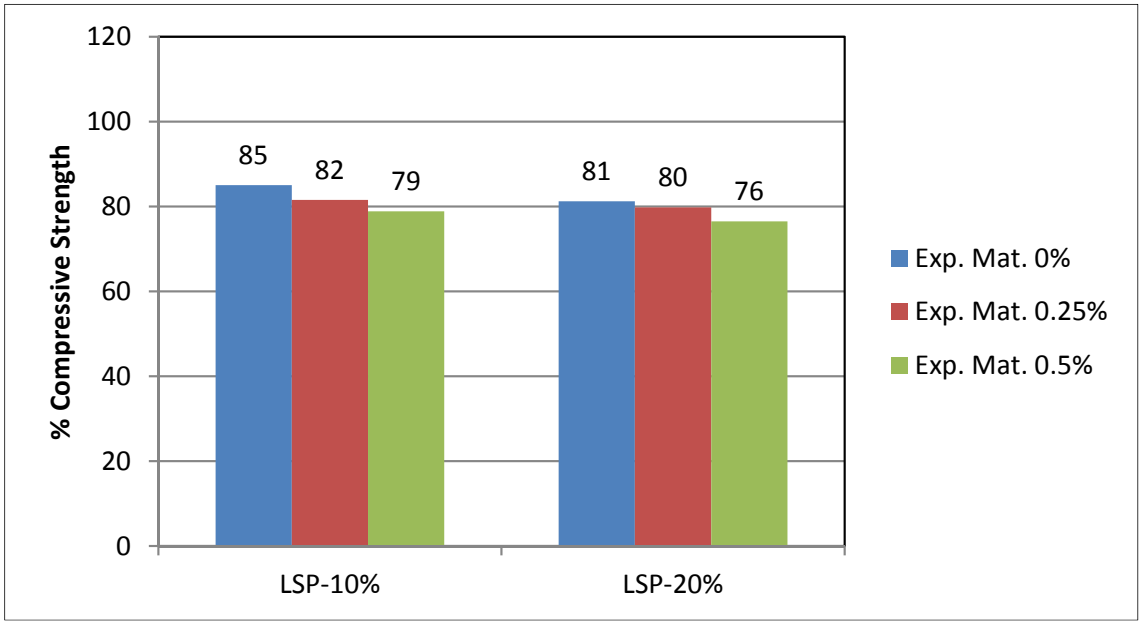

Figure 4.8: % Compressive Strength at age 28 days of LSP to Fosroc Conbextra GP.

4.2.4 Mixes Containing NP

Table 4.5 summarizes the result of compressive strengths for the NP mixes. Figure 4.9 shows the graph of compressive strength evolution with curing times, plotted from values in Table 4.5 for the mixes containing NP. As can be seen from the data in Figure 4.9, all the mixes that contained NP had strength below the control mix at all ages. There was a big gap at early age, but that gap got smaller at 28 days. For example, M17 and the control mix were almost equal to each other (54.6 and 51.2 MPa for the control mix and M17, respectively).

It can be noted that the strength went down with the increase in expansive material whereby the difference in strength between 0% and 0.5% of expansive material was about 11.3% at age of 28 days. Further, as previous reports indicated that NP has slow pozzolanic activity [128, 129], as was noted in this investigation. The ratio between the strength at 28 days and that at 3 days is 2.94, 2.95 and 2.89 for M17, M18 and M19, respectively.

The strength at 28 days for NP mixes as compared to Fosroc Conbextra GP grout

is reported in Fig. 4.10. All mixes had compresive strength lower than that of Fosroc grout, the ratio between NP mixes and Fosroc grout being 81%, 77% and 72% for M17, M18 and, M19, respectively.

Table 4.5: Compressive strength of HPNSG with NP.

Mix ID	Compressive Strength (MPa)			
	3 days	7 days	14 days	28 days
M1-Ctrl-0-0	32.5	38.7	45.9	54.6
M17-NP-20-0	17.4	28.8	39.9	51.2
M18-NP-20-0.25	16.5	27.4	37.5	48.6
M19-NP-20-0.5	15.7	25.3	35.6	45.4

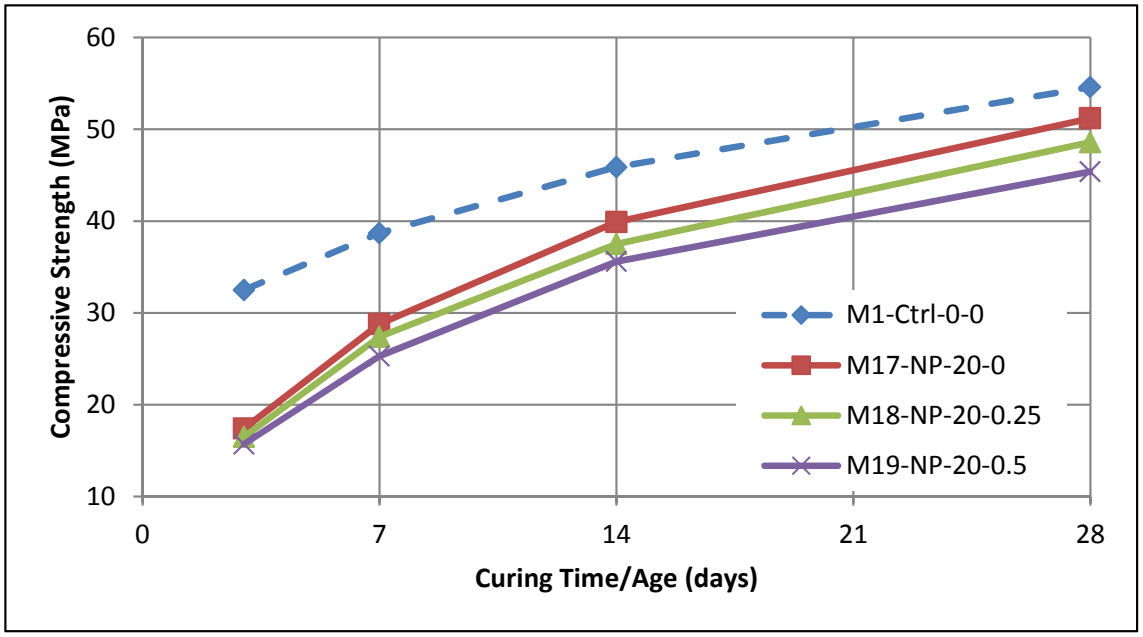

Figure 4.9: Compressive strength of HPNSG with 20% NP.

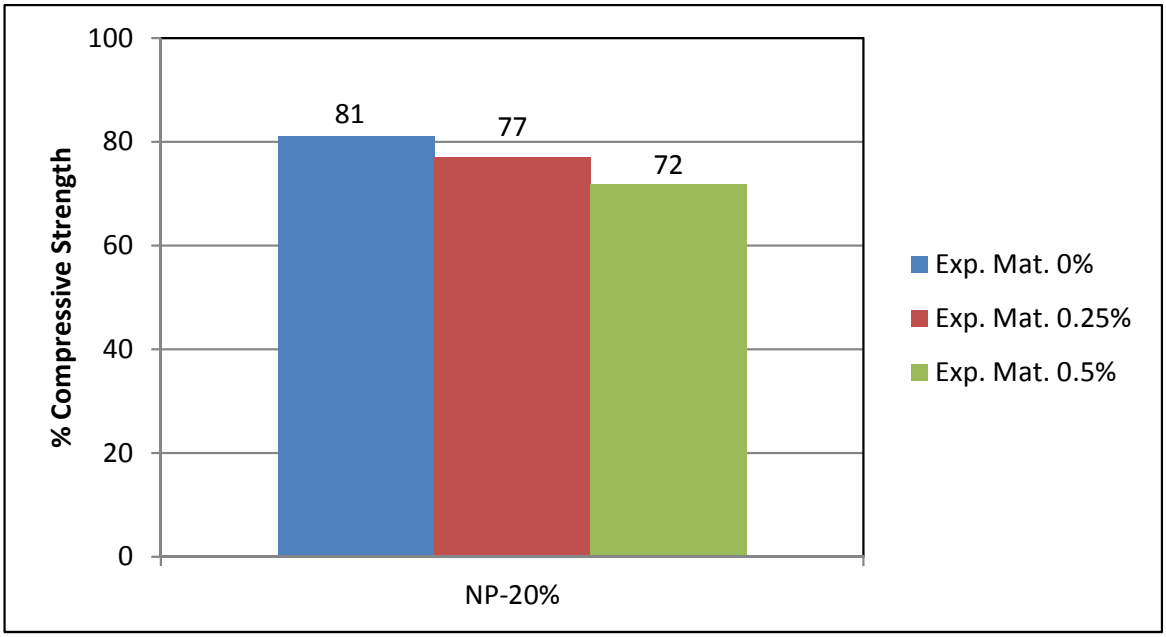

Figure 4.10: % Compressive Strength at age 28 days of NP to Fosroc Conbextra GP.

4.2.5 Mixes Containing MK

Table 4.6 shows the summary of compressive strength for the MK mixes. Figure 4.11 shows a schematic presentation of compressive strength evolution with curing time, plotted from values in Table 4.6 for the mixes containing MK.

Table 4.6: Compressive strength of HPNSG with MK.

Mix ID	Compressive Strength (MPa)			
	3 days	7 days	14 days	28 days
M1-Ctrl-0-0	32.5	38.7	45.9	54.6
M20-MK-10-0	55.9	60.2	63.3	67.5
M21-MK -10-0.25	44.0	49.8	55.7	63.2
M22-MK -10-0.5	41.3	45.5	52.6	58.5
M23-MK -15-0	59.9	63.2	69.5	73.5
M24-MK -15-0.25	49.2	54.3	62.5	67.9
M25-MK -15-0.5	42.5	46.7	53.4	59.5

It can be noticed that the mixes with MK achieved high strength; all six mixes had strength higher than the control mix. The highest strength was attained by the mix containing 20% MK and 0% of expansive material with a strength of 73.5 MPa. With increasing the expansive material, the strength declined. It is also clear that the strength went up when MK as replacement increased from 10% to 15%.

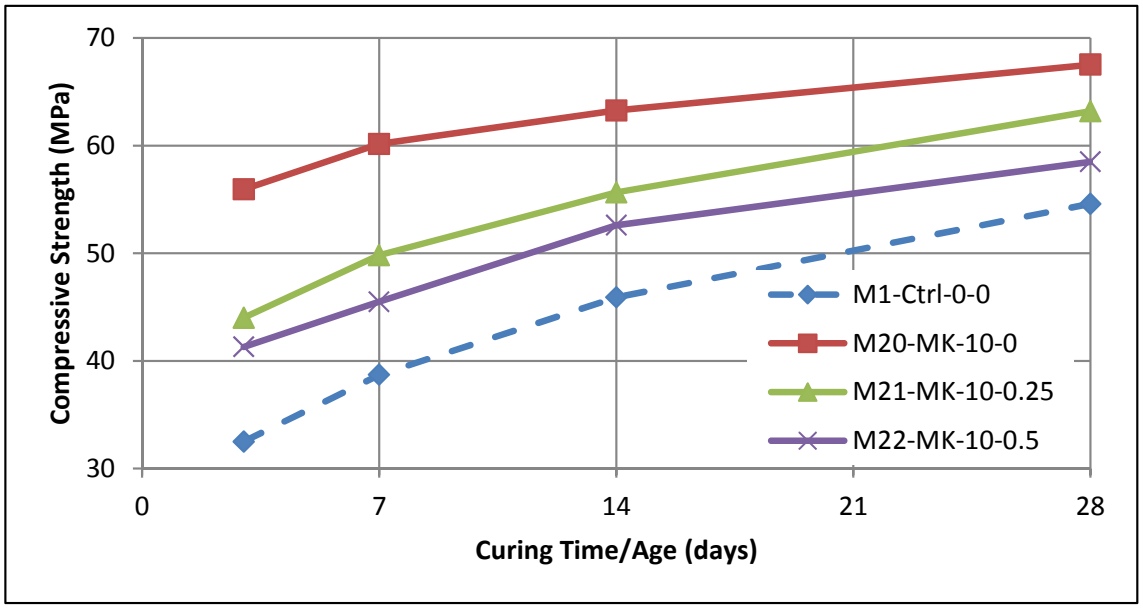

Figure 4.11: Compressive strength of HPNSG with 10% MK.

The strength at 28 days for MK mixes, as compared to Fosroc Conbextra GP grout, was reported in Figure 4.13. As shown in this figure, the four MK mixes had strength higher than Fosroc grout, the other two mixes containing high values of expansive material, M22 and M25, had slightly smaller strength compared to Fosroc® Conbextra grout. However, from the data in Figures 4.11 and 4.12, it can be shown that the strength was still developing with time, while for Fosroc the strength curve was almost flat at 28 days, as shown Figures 4.1.

The high pozzolanic activity of MK has been reported in the literature [63, 130–133]. It tends to improve both the mechanical and durability properties of concrete, though its performance is determined by the kaolinitic purity level of the source clay.

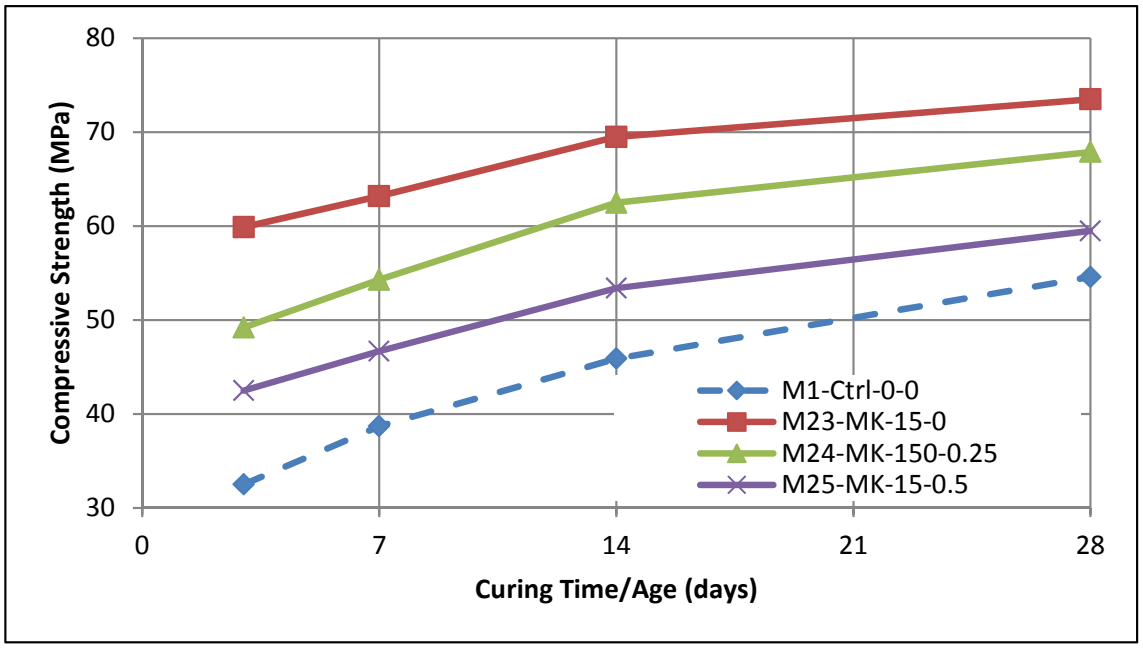

Figure 4.12: Compressive strength of HPNSG with 15% MK.

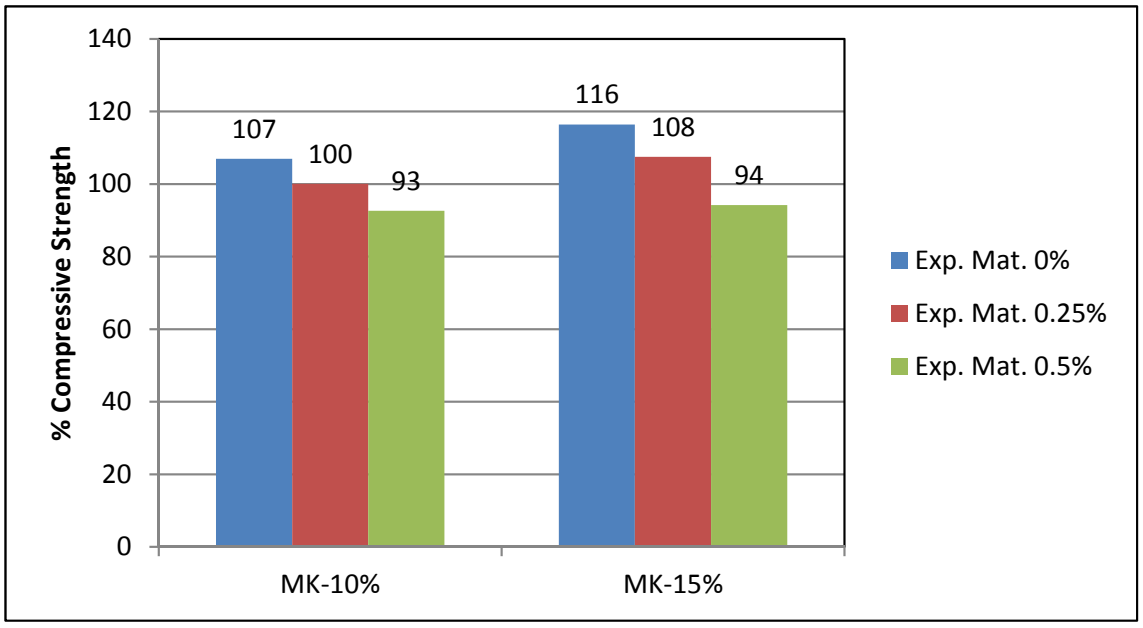

Figure 4.13: % Compressive Strength at age 28 days of MK to Fosroc Conbextra GP .

4.2.6 Summary of Compressive Strength for all Mixes

Table 4.7 summarizes the results of compressive strength for all mixes in this study. It can be noted that the commercial grouts and Mix No. 23 (M23-MK-15-0) had the highest early strength after 3 days of curing. Further, Mix No. 23 had also the highest compressive strength after 28 days of curing. Lastly, the data in this table clarifies the negative role of expansive agent for all the additives used in this investigation.

Table 4.7: Compressive strength of all mixes in this study.

Mix ID	Compressive Strength (MPa)			
	3 days	**7 days**	**14 days**	**28 days**
M1-Ctrl-0-0	32.5	38.7	45.9	54.6
M2-SF-5-0	38.8	41.8	50.7	59.1
M3-SF-5-0.25	34.5	39.7	48.2	56.4
M4-SF-5-0.5	33.2	35.4	45.7	53.7
M5-SF-10-0	39.9	45.6	52.4	60.4
M6-SF-10-0.25	40.6	43.6	49.7	56.5
M7-SF-10-0.5	37.2	41.2	46.8	54.1
M8-SF-15-0	38.1	45.9	61.2	64.5
M9-SF-15-0.25	37.9	44.8	53.1	60.5
M10-SF-15-0.5	35.5	39.4	50.2	58.7
M11-LSP-10-0	31.5	37.9	43.2	53.7
M12-LSP-10-0.25	30.3	36.4	41.6	51.5
M13-LSP-10-0.5	29.9	34.2	39.8	49.8
M14-LSP-20-0	31.1	36.8	41.6	51.3
M15-LSP-20-0.25	29.4	36.6	44.4	50.2
M16-LSP-20-0.5	30.2	33.2	38.6	48.3
M17-NP-20-0	17.4	28.8	39.9	51.2
M18-NP-20-0.25	16.5	27.4	37.5	48.6
M19-NP-20-0.5	15.7	25.3	35.6	45.4
M20-MK-10-0	55.9	60.2	63.3	67.5
M21-MK-10-0.25	44.0	49.8	55.7	63.2
M22-MK-10-0.5	41.3	45.5	52.6	58.5
M23-MK-15-0	59.9	63.2	69.5	73.5
M24-MK-15-0.25	49.2	54.3	62.5	67.9
M25-MK-15-0.5	42.5	46.7	53.4	59.5
M26-Sika® grout-214	52.0	56.5	58.2	60.1
M27-Fosroc® Conbextra GP	53.0	59.4	61.3	63.1

4.3 SPLITTING TENSILE STRENGTH

The tensile strength of concrete is usually assessed by the splitting cylinder test in accordance with ASTM C 496.

4.3.1 Control Mix and Commercial Grouts

Table 4.8 shows the average of 28-day splitting tensile strength values (f_{st}) for the control mix and the two commercial grouts used in the study. It is clear from the data in this table that both the control mix and the commercial grouts had very close tensile strength in a way similar to their compressive strength (see Figure 4.1).

Table 4.8: Split tensile strength of control mix and commercial grouts.

Mix ID	**Splitting Tensile Strength (MPa)**
M1-Ctrl-0-0	3.7
M26-Sika® 214	4.1
M27-Fosroc® Conbextra GP	3.9

4.3.2 Mixes Containing SF

Table 4.9 summarizes the average of 28-day splitting tensile strength values (f_{st}) for all SF mixtures. For all the nine SF mixes, the splitting tensile strength was higher than the control mix (except M4 and M7), because of their high compressive strength for silica fume mixes. M4 and M7 had slightly less tensile strength probably due to the high dosage of expansive material (0.5%).

Table 4.9: Split tensile strength of HPNSG with SF.

Mix ID	Splitting Tensile Strength (MPa)
M1-Ctrl-0-0	3.7
M2-SF-5-0	3.9
M3-SF-5-0.25	3.7
M4-SF-5-0.5	3.5
M5-SF-10-0	3.9
M6-SF-10-0.25	3.7
M7-SF-10-0.5	3.6
M8-SF-15-0	4.1
M9-SF-15-0.25	4.0
M10-SF-15-0.5	3.9

4.3.3 Mixes Containing LSP

Table 4.10 summarizes the average splitting tensile strength values (f_{st}) for all LSP mixtures. The values of splitting tensile strength for both the control mix and LSP mixes were very closed to each other and ranged between 3.4 to 3.7 MPa. Again, the mixes that contained the highest dosages of expansive agent exhibited the least tensile strength.

Table 4.10: Split tensile strength of HPNSG with LSP.

Mix ID	Splitting Tensile Strength (MPa)
M1-Ctrl-0-0	3.7
M11-LSP-10-0	3.7
M12-LSP-10-0.25	3.5
M13-LSP-10-0.5	3.4
M14-LSP-20-0	3.5
M15-LSP-20-0.25	3.5
M16-LSP-20-0.5	3.4

4.3.4 Mixes Containing NP

Table 4.11 shows the average of 28-day splitting tensile strength values (f_{st}) for all NP mixtures. The values of splitting tensile strength of all NP mixes were less than that of the control mix value. This inferior performance could be attributed to the low pozzolanic activity of NP.

Table 4.11: Split tensile strength of HPNSG with NP.

Mix ID	Splitting Tensile Strength (MPa)
M1-Ctrl-0-0	3.7
M17-NP-20-0	3.5
M18-NP-20-0.25	3.3
M19-NP-20-0.5	3.2

4.3.5 Mixes Containing MK

Table 4.12 shows the average of 28-day splitting tensile strength values (f_{st}) for all MK mixtures. The mixes containing MK had splitting tensile strength higher than the control mix in a way similar to the results of compressive strength. Again, the MK mixes containing high dosages of expansive agent had the lowest splitting tensile strength.

Table 4.12: Split tensile strength of HPNSG with MK.

Mix ID	Splitting Tensile Strength (MPa)
M1-Ctrl-0-0	3.7
M20-MK-10-0	4.4
M21-MK-10-0.25	4.3
M22-MK-10-0.5	3.9
M23-MK-15-0	4.8
M24-MK-15-0.25	4.3
M25-MK-15-0.5	4.0

4.3.6 Summary of Splitting Tensile Strength for all Mixes

Table 4.13 summarizes the results of splitting tensile strength for all mixes in this study. It can be noted that Mix No. 23 (M23-MK-15-0) had the highest splitting tensile strength after 28 days of curing (4.4 MPa), while the lowest value for splitting tensile strength was 3.2 MPa for the Mix No. 19 (M19-NP-20-0.5). Lastly, the data in this table clarifies the negative role of expansive agent for all the additives used in this investigation.

4.3.7 Model for the Splitting Tensile Strength

There are several empirical formulations for correlating the splitting tensile strength (f_{st}) with the compressive strength (f'_c); and most researchers achieved the expression of the type [134]:

$$f_{st} = k(f'_c)^n \tag{4.1}$$

where:

f_{st} = splitting tensile strength, MPa,

f'_c = compressive strengths, MPa,

k, n = coefficient can be obtained from the regression analysis.

The "n" value is generally within the range of 0.50 to 0.75 for *concrete* [134]. The existing expressions for estimating splitting tensile strength, as suggested by ACI [135], and CEB-FIB [136], are given below, respectively.

$$f_{st} = 0.59(f'_c)^{0.5} \tag{4.2}$$

$$f_{st} = 0.301(f'_c)^{0.67} \tag{4.3}$$

Table 4.13: Split tensile strength of all mixes in this study.

Mix ID	**Splitting Tensile Strength (MPa)**
M1-Ctrl-0-0	3.7
M2-SF-5-0	3.9
M3-SF-5-0.25	3.7
M4-SF-5-0.5	3.5
M5-SF-10-0	3.9
M6-SF-10-0.25	3.7
M7-SF-10-0.5	3.6
M8-SF-15-0	4.1
M9-SF-15-0.25	4.0
M10-SF-15-0.5	3.9
M11-LSP-10-0	3.7
M12-LSP-10-0.25	3.5
M13-LSP-10-0.5	3.4
M14-LSP-20-0	3.5
M15-LSP-20-0.25	3.5
M16-LSP-20-0.5	3.4
M17-NP-20-0	3.5
M18-NP-20-0.25	3.3
M19-NP-20-0.5	3.2
M20-MK-10-0	4.4
M21-MK-10-0.25	4.3
M22-MK-10-0.5	3.9
M23-MK-15-0	4.8
M24-MK-15-0.25	4.3
M25-MK-15-0.5	4.0
M26-Sika® 214	4.1
M27-Fosroc® Conbextra GP	3.9

Figure 4.14 shows the relationship between the splitting tensile and compressive strengths of all the grouts tested at 28 days. For comparison, Equations 4.2 and 4.3 are also included in the diagram. It was observed that there was a considerably high relationship between the splitting tensile and compressive strengths of the grout so that a regression analysis provided a correlation coefficient (R^2) of 0.95. Within the strength range of this study, both ACI and CEB-FIB models appeared to be well close to each other but provided relatively higher predictions. From the the regression analysis, the relationship between f_{st} and f'_c for the developed grout in this study can expressed as following:

$$f_{st} = 0.145(f'_c)^{0.81} \tag{4.4}$$

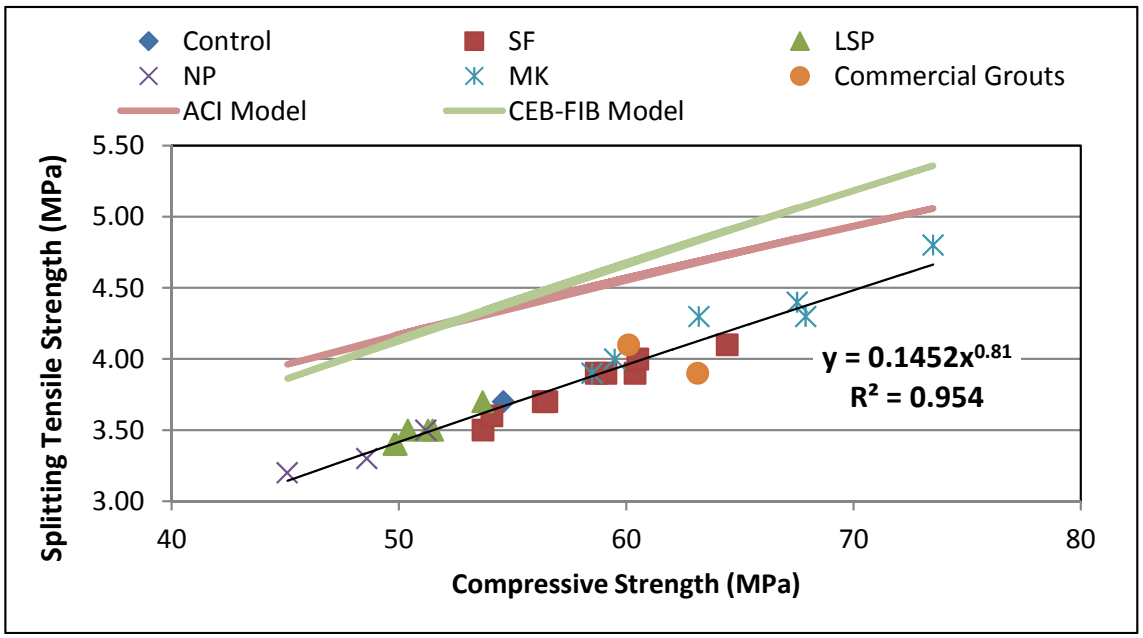

Figure 4.14: Relationship between compressive strength and splitting tensile strength.

4.4 MODULUS OF ELASTICITY

Tables 4.14 through 4.18 list the average values of modulus of elasticity after water-curing the grout specimens for 28 days.

4.4.1 Control Mix and Commercial Grouts

Table 4.14 shows the average of 28 day modulus of elasticity (E_c) for the control mix and the two commercial grouts. The modulus of elasticity for the control mix was higher than Fosroc® Conbextra GP (23.2 and 28.4 GPa for Fosroc® Conbextra grout and the control mix, respectively) and lower than Sika® grout-214 (33.9 GPa).

Table 4.14: Modulus of elasticity of control mix and commercial grouts.

Mix ID	**Modulus of Elasticity (GPa)**
M1-Ctrl-0-0	28.4
M26-Sika Grout®-214	33.9
M27-Fosroc® Conbextra GP	23.2

4.4.2 Mixes Containing SF

Table 4.15 shows the average 28-day modulus of elasticity (E_c) for SF mixtures. The table shows that all the mixes of silica fume had modulus of elasticity marginally higher than that of the control mix, which could be attributed to the fact that silica fume mixes had higher compressive strength than the control mix. Furthermore, it could be easily noted that the increase in the dosage of expansive agent tended to slightly decrease the modulus of elasticity of all SF mixes.

Table 4.15: Modulus of elasticity of HPNSG with SF.

Mix ID	Modulus of Elasticity (GPa)
M1-Ctrl-0-0	28.4
M2-SF-5-0	31.1
M3-SF-5-0.25	29.9
M4-SF-5-0.5	28.4
M5-SF-10-0	31.0
M6-SF-10-0.25	30.1
M7-SF-10-0.5	29.0
M8-SF-15-0	32.9
M9-SF-15-0.25	32.5
M10-SF-15-0.5	31.0

4.4.3 Mixes Containing LSP

Table 4.16 shows the average 28-day modulus of elasticity (E_c) for LSP mixtures. All the values of modulus of elasticity for LSP was lower than that of the control mix except mix M11, that was a little bit more than the control mix value because it had 0% of expansive material and 10% of LSP as replacement. However, when the percentage of LSP as replacement for the cement increased, the modulus of elasticity tended to decrease in a way similar to the compressive strength.

Table 4.16: Modulus of elasticity of HPNSG with LSP.

Mix ID	Modulus of Elasticity (GPa)
M1-Ctrl-0-0	28.4
M11-LSP-10-0	28.5
M12-LSP-10-0.25	27.8
M13-LSP-10-0.5	26.8
M14-LSP-20-0	27.6
M15-LSP-20-0.25	27.0
M16-LSP-20-0.5	26.6

4.4.4 Mixes Containing NP

Table 4.17 shows the average of 28-day modulus of elasticity (E_c) for NP mixtures. The modulus of elasticity for all NP mixes was less than that of the control mix value. Moreover, the modulus of elasticity tended to decrease with the increase of the expansive agent.

Table 4.17: Modulus of elasticity of HPNSG with NP.

Mix ID	Modulus of Elasticity (GPa)
M1-Ctrl-0-0	28.4
M17-NP-20-0	27.6
M18-NP-20-0.25	26.9
M19-NP-20-0.5	25.8

4.4.5 Mixes Containing MK

Table 4.18 summarizes the average of 28-day modulus of elasticity (E_c) for MK mixtures. All the six mixes cotaining MK had modulus of elasticity greater than the control mix. Further, the values of modulus of elasticity were declined with increasing the percentage of expansive agent. These finding are exactly similar to the results of the compressive and tensile strengths.

Table 4.18: Modulus of elasticity of HPNSG with MK.

Mix ID	Modulus of Elasticity (GPa)
M1-Ctrl-0-0	28.4
M20-MK-10-0	33.7
M21-MK-10-0.25	31.7
M22-MK-10-0.5	29.9
M23-MK-15-0	34.7
M24-MK-15-0.25	34.1
M25-MK-15-0.5	30.2

4.4.6 Summary of Modulus of Elasticity for all Mixes

Table 4.19 summarizes the results of modulus of elasticity for all mixes in this study. The data in this table do match with those in Tables 4.7 and 4.13 in terms of the role of the additive type (i.e., SF, LSP, NP or MK) and the role of expansive agent.

Table 4.19: Modulus of elasticity of HPNSG with MK.

Mix ID	**Modulus of Elasticity (GPa)**
M1-Ctrl-0-0	28.4
M2-SF-5-0	31.1
M3-SF-5-0.25	29.9
M4-SF-5-0.5	28.4
M5-SF-10-0	31.0
M6-SF-10-0.25	30.1
M7-SF-10-0.5	29.0
M8-SF-15-0	32.9
M9-SF-15-0.25	32.5
M10-SF-15-0.5	31.0
M11-LSP-10-0	28.5
M12-LSP-10-0.25	27.8
M13-LSP-10-0.5	26.8
M14-LSP-20-0	27.6
M15-LSP-20-0.25	27.0
M16-LSP-20-0.5	26.6
M17-NP-20-0	27.6
M18-NP-20-0.25	26.9
M19-NP-20-0.5	25.8
M20-MK-10-0	33.7
M21-MK-10-0.25	31.7
M22-MK-10-0.5	29.9
M23-MK-15-0	34.7
M24-MK-15-0.25	34.1
M25-MK-15-0.5	30.2
M26-Sika Grout®-214	33.9
M27-Fosroc® Conbextra GP	23.2

4.4.7 Model for the Modulus of Elasticity

There are several empirical formulations for evaluating modulus of elasticity (E_c) and compressive strength f'_c. For the *normal concrete*, Equations 4.5 and 4.6 proposed by ACI [137] and CEB-FIB [136], are given below, respectively.

$$E_c = 4.7(f'_c)^{0.5} \tag{4.5}$$

$$E_c = 21.5(\frac{f'_c}{10})^{\frac{1}{3}} \tag{4.6}$$

where:

E_c = Modulus of elasticity, GPa,

f'_c = compressive strengths, MPa.

Figure 4.15 shows the observed relationship between the modulus of elasticity and compressive strengths of the grouts tested at 28 days (the two commercial grouts was not included in regression). For comparison, Equations 4.5 and 4.6 are also included in the diagram.

It could be noted that there was a relationship between the modulus of elasticity and compressive strength of the grouts so that a regression analysis provided a high correlation coefficient (R^2) of 0.96. The prediction of ACI and CEB-FIB models were included in Figure 4.15 and they are in the higher side compared with the measured values. From the the regression analysis, the relationship between E_c and f'_c for the developed grouts in this study can expressed as follows:

$$E_c = 1.75(f'_c)^{0.702} \tag{4.7}$$

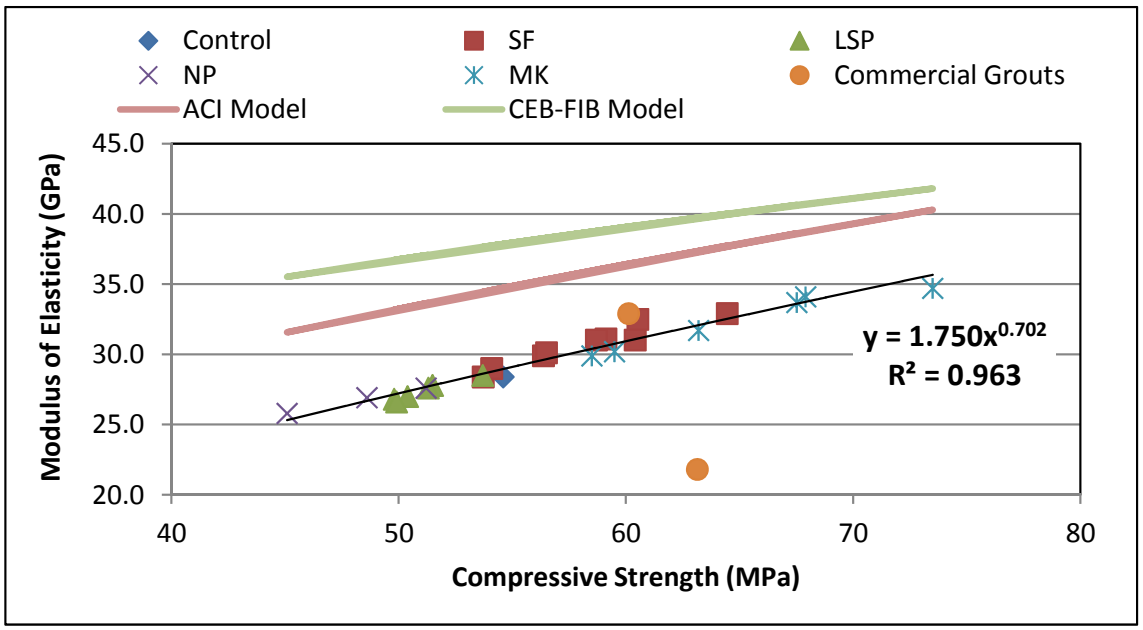

Figure 4.15: Relationship between compressive strength and modulus of elasticity.

4.5 DRYING SHRINKAGE

The drying shrinkage of all the grouts was measured over a period of about 260 days for all the mixtures using prism specimens of dimensions 25×25×285 mm after 28 days of water curing.

4.5.1 Control Mix and Commercial Grouts

Table 4.20 summarizes the average drying shrinkage values for both the commercial grouts and control mix, while Figure 4.16 shows the graph of drying shrinkage, taken at different times, and plotted from values in Table 4.20.

As can be seen in Figure 4.16, Fosroc grout exhibited the least shrinkage values at early stage, compared with Sika grout and control mix. After first week, Fosroc grout had only 27% of its final shrinkage (drying shrinkage at 259 days), whereas Sika and the control mix reached 51 and 48%, respectively, after the same period. However,

Table 4.20: Average drying shrinkage of control mix and commercial grouts.

Duration (days)	Drying Shrinkage (microns)		
	M1-Ctrl-0-0	**Sika® Grout-214**	**Fosroc® Conbextra GP**
0	0	0	0
1	116	85	45
3	280	253	154
7	240	303	174
14	265	339	339
28	376	412	442
42	387	446	504
56	400	499	553
70	419	515	577
84	432	525	592
105	463	556	611
126	485	577	623
147	488	588	632
203	491	592	635
259	497	596	637

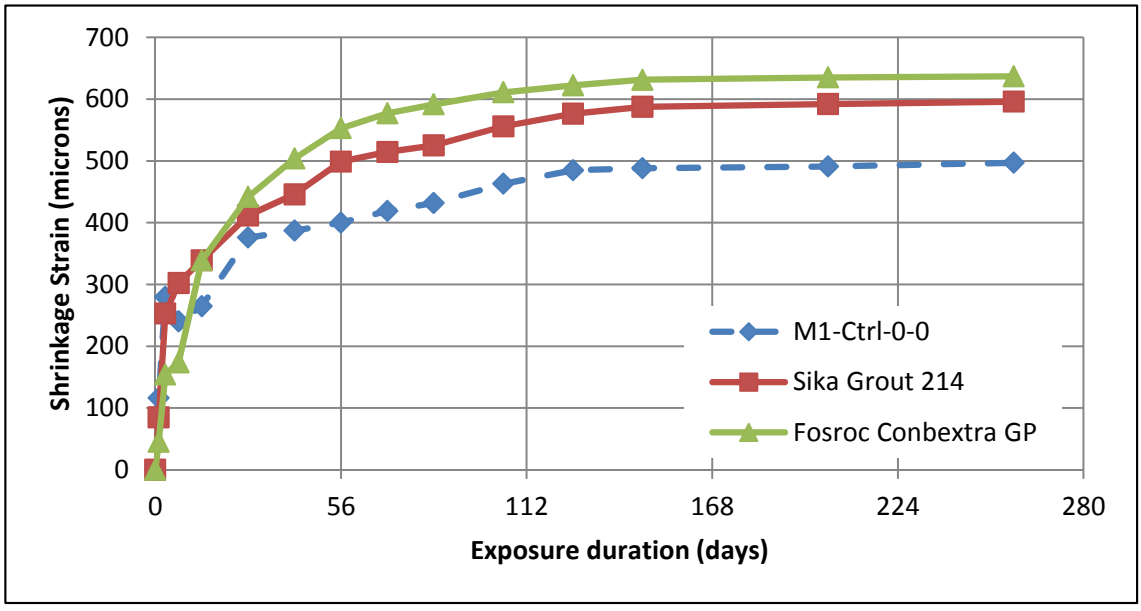

Figure 4.16: Drying shrinkage of the control mix and commercial grouts.

after 28 days, both commercial products had almost the same shrinkage percentage of 69%, while control mix reached 76% of their ultimate shrinkage.

The control mix had shrinkage much lower than both commercial grouts. As percentage from final shrinkage (shrinkage at 259 days), the control mix had shrinkage less by 20% from Sika® grout-214, and 28% from Fosroc® Conbextra GP. The drying shrinkage in the control mix was low compared with the commercial grouts which could be attributed to the presence of aggregate in the control mix. As it is well documented, aggregates tend to decrease the shrinkable volume in paste and work like internal support between paste [24, 88, 102, 138].

4.5.2 Mixes Containing SF

Table 4.21 summarizes the average numerical drying shrinkage values for all SF mixes. Figures 4.17 to 4.19 show the schematic presentation of drying shrinkage, taken at different times, plotted from the values in Table 4.21 for the mixes containing SF.

Table 4.21: Average drying shrinkage of HPNSG with SF and the control mix.

Duration	**Drying Shrinkage (microns)**									
(days)	**M1**	**M2**	**M3**	**M4**	**M5**	**M6**	**M7**	**M8**	**M9**	**M10**
0	0	0	0	0	0	0	0	0	0	0
1	116	75	22	41	103	20	17	57	143	60
3	280	200	67	62	130	230	121	250	192	113
7	240	250	82	145	236	178	166	336	235	119
14	265	266	182	183	336	192	180	387	281	136
28	376	378	246	226	367	300	280	430	293	219
42	387	416	274	233	447	312	312	431	303	261
56	400	425	279	247	449	328	320	438	329	330
70	419	442	282	254	476	340	336	467	364	364
84	432	452	293	259	497	345	339	502	383	365
105	463	462	307	289	521	363	355	526	387	380
126	485	487	312	299	537	374	367	542	391	384
147	488	489	316	307	545	378	372	550	393	388
203	491	494	320	312	551	386	378	557	398	391
259	497	503	323	315	554	390	380	560	399	392

Generally, in first week 40%, of the shrinkage occurred and more than 70% of shrinkage took place in first month. Even after about 8 months, all the mixes had shrinkage less than 500 microns, except for the three mixes having no expansive agent added to them; M2, M5 and, M8 with shrinkage values of about 503, 554 and 560 microns, respectively.

It is to be noted that the drying shrinkage increased with increasing the percentage of silica fume as replacement. Such high drying shrinkage is ascribable to the high pozzolanic reaction and pore size refinement mechanism of silica fume [138]. Furthermore, the drying shrinkage was almost equal with 0.25% and 0.5% of expansive agent for the same silica fume dosage. Hence, it seems that the role of silica fume on drying shrinkage to overshadow the effect of expansive agent.

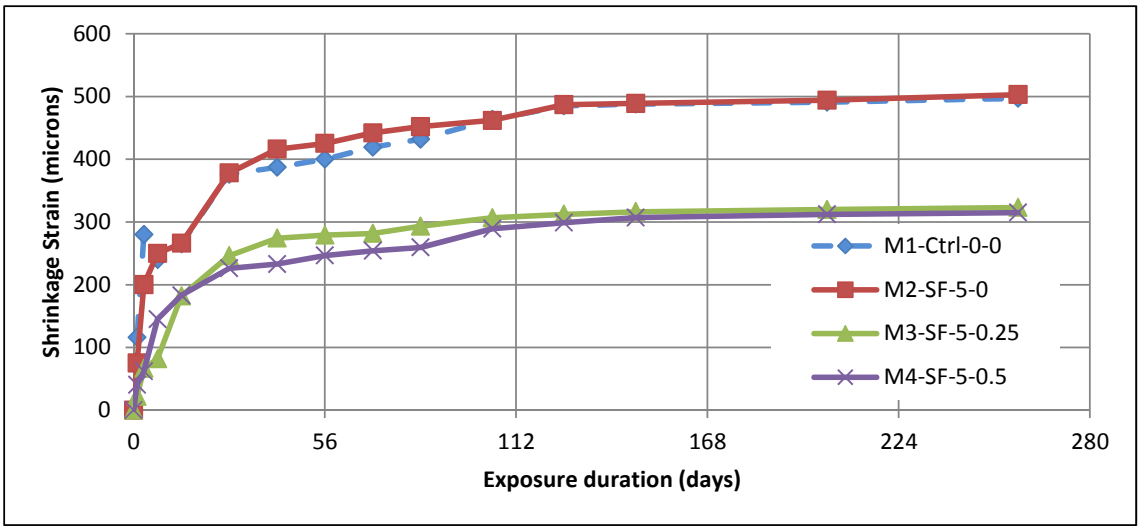

Figure 4.17: Drying shrinkage of HPNSG with 5% SF and the control mix.

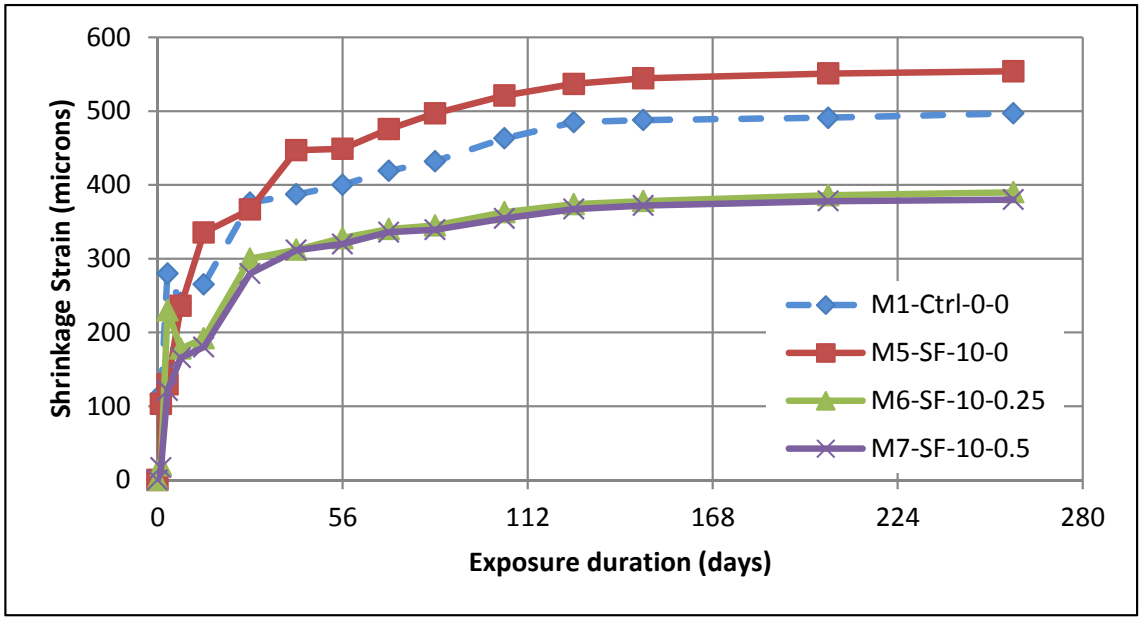

Figure 4.18: Drying shrinkage of HPNSG with 10% SF and the control mix.

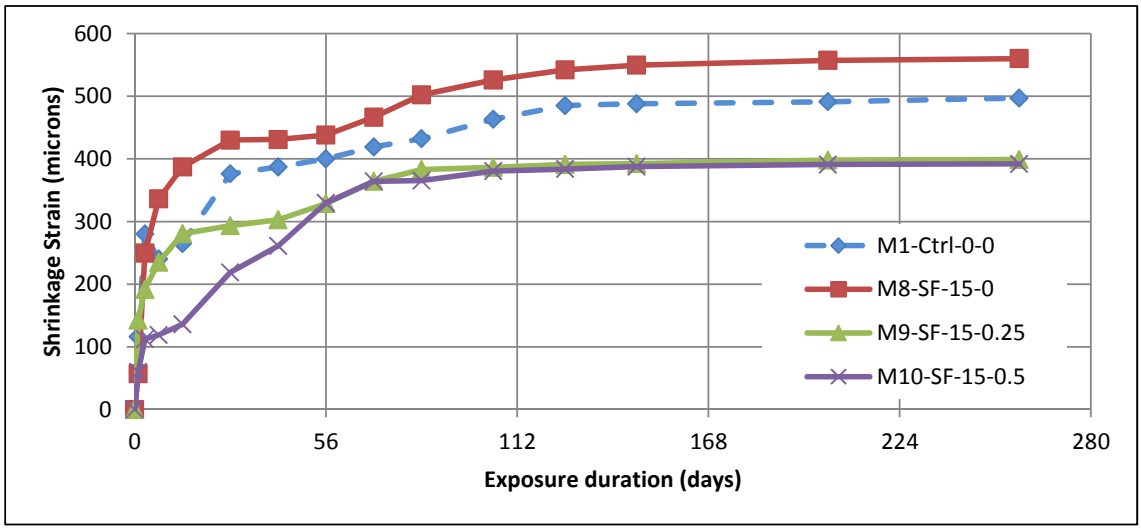

Figure 4.19: Drying shrinkage of HPNSG with 15% SF and the control mix.

4.5.3 Mixes Containing LSP

Table 4.22 shows the average numerical values of drying shrinkage for all LSP mixtures. Figures 4.20 and 4.21 display the graphs of drying shrinkage, taken at different times, and plotted from the data in Table 4.22 for the mixes containing LSP.

Figure 4.20 shows that only M11 had shrinkage slightly higher than the control mix, although in early age, all the mixes had almost the same shrinkage. With the increase in LSP to 20% by cement, it is obvious that the drying shrinkage declined with increasing the percentage of LSP, as shown in Figure 4.21> It is reported that limestone mortar paste seems to be less porous with more refined pores thus preventing desiccation [139] and LSP is also relatively an inert calcareous filler [140].

Table 4.22: Average drying shrinkage of HPNSG with LSP and the control mix.

Duration	**Drying Shrinkage (microns)**						
(days)	**M1**	**M11**	**M12**	**M13**	**M14**	**M15**	**M16**
0	0	0	0	0	0	0	0
1	116	66	54	91	94	53	59
3	280	144	157	165	137	143	147
7	240	188	198	215	201	158	169
14	265	206	219	229	277	177	179
28	376	187	270	224	364	200	180
42	387	244	274	269	383	245	254
56	400	267	313	301	382	262	292
70	419	384	361	311	393	314	302
84	432	421	371	313	400	338	311
105	463	471	391	328	421	340	324
126	485	492	400	336	435	342	333
147	488	503	410	346	447	343	338
203	491	505	415	352	452	345	340
259	497	506	418	353	454	345	341

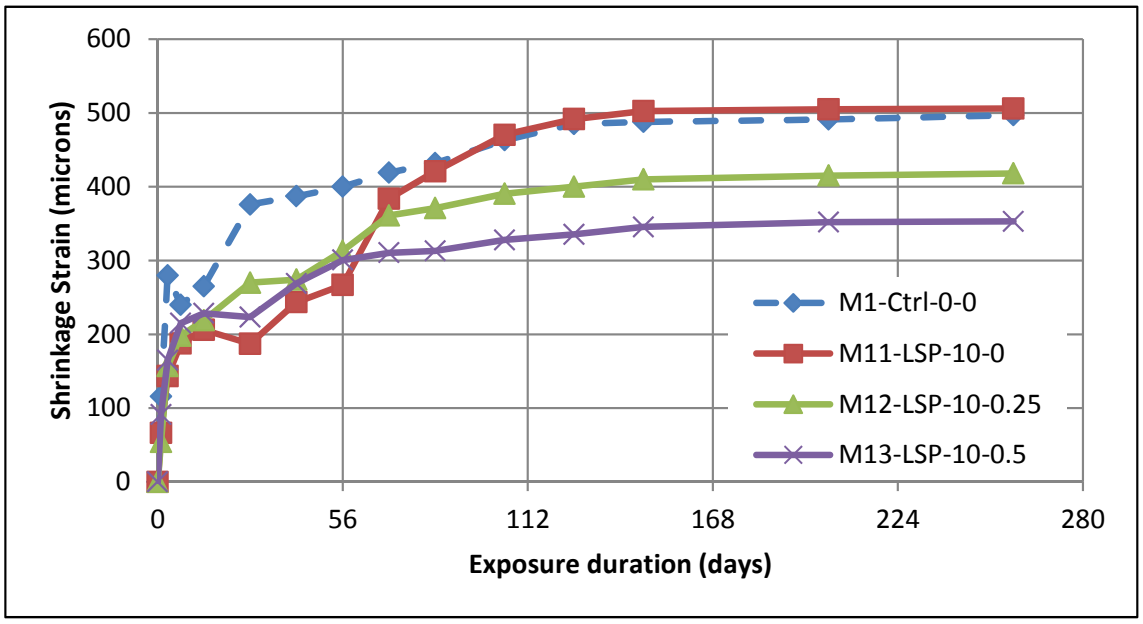

Figure 4.20: Drying shrinkage of HPNSG with 10% LSP and the control mix.

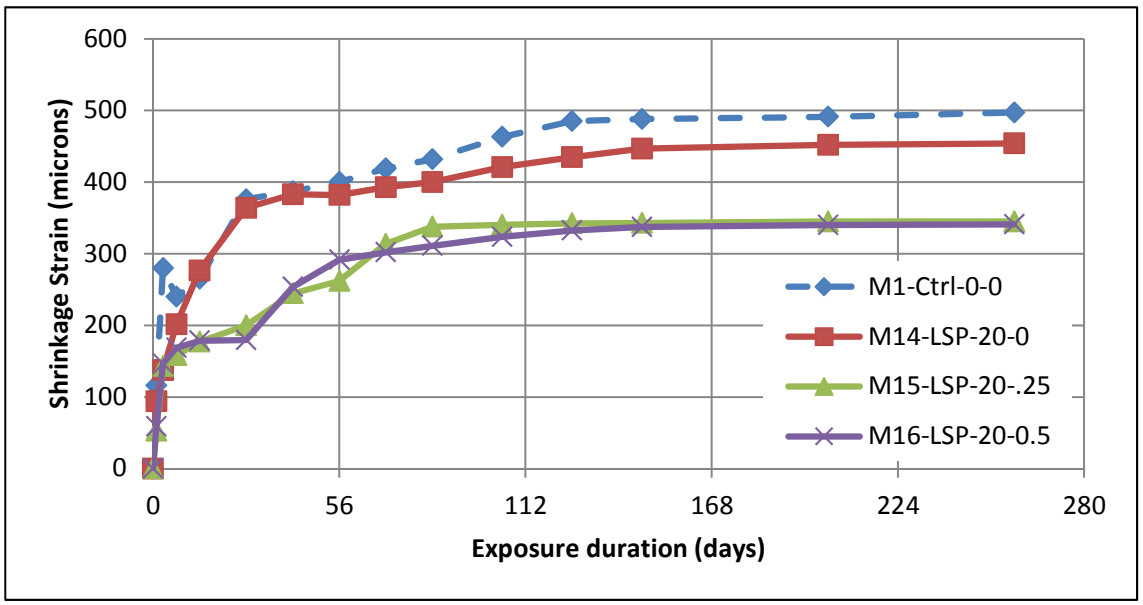

Figure 4.21: Drying shrinkage of HPNSG with 20% LSP and the control mix.

4.5.4 Mixes Containing NP

Table 4.23 summarizes the average drying shrinkage values for all NP mixtures. Figure 4.22 shows schematically the drying shrinkage data, taken at different times, plotted from the values in Table 4.23 for the mixes containing NP.

It is clear that all the three mixes with NP had shrinkage values lower than that of the control mix mostly at all ages (the total shrinkage for the control mix was 497 microns, while it was 396, 380 and 333 microns for M17, M18 and M19, respectively). Such low shrinkage could be ascribed to the quality of the microstructure of NP mixes and the pores refinement which prevent water evaporation [139]. The data in Table 4.23 and Figure 4.22 indicate that at early stage, M18 and M19 reached most of their shrinkage, after the first week, M18 reached 68% while M19 had 52% of their total shrinkage, that climbed up to 87% and 76% after 42 days, respectively. For M18 (the mix with no expansive material), it reached 40% after 7 days and 68% after 28 days. Hence, the role of the expansive agent seemed to mitigate drying shrinkage in NP mixes.

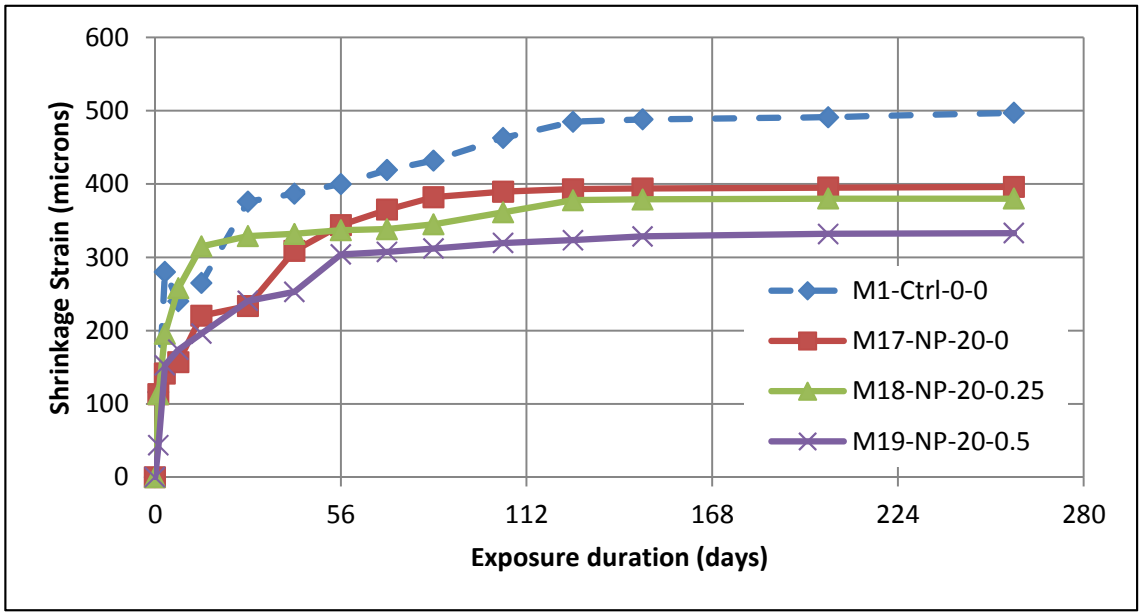

Figure 4.22: Drying shrinkage of HPNSG with 20% NP and the control mix.

Table 4.23: Average drying shrinkage of HPNSG with NP and the control mix.

Duration (days)	Drying Shrinkage (microns)			
	M1	**M17**	**M18**	**M19**
0	0	0	0	0
1	116	114	114	44
3	280	142	196	153
7	240	157	258	174
14	265	221	315	196
28	376	234	329	241
42	387	309	332	253
56	400	344	337	304
70	419	365	339	308
84	432	382	345	312
105	463	390	362	320
126	485	393	378	324
147	488	394	379	329
203	491	395	380	332
259	497	396	380	333

4.5.5 Mixes Containing MK

Table 4.24 shows the average drying shrinkage values for all MK mixtures. Figures 4.23 and 4.24 show the graphs of drying shrinkage, taken at different times, plotted from the values in Table 4.24 for all the mixes containing MK.

Figures 4.23 and 4.24 indicate that with increasing the percentage of MK, there was marginal decrease in shrinkage for the same expansive agent percentage. However, no any mix exceeded 500 microns, even after 259 days. All the six MK mixes had drying shrinkage lower than the control mix values, even with no any expansive agent added to the mixture because MK enhanced substantially the pore structure and reduced the content of the harmful large pores, thereby making the grout more impervious [134]. The difference in shrinkage between the control mix and MK mixes decreased with percentage of MK replacement went up, whereby the 10% of cement replaced with MK, those mixes had ultimate shrinkage close to that of the control mix (497 microns

Table 4.24: Average drying shrinkage of HPNSG with MK and the control mix.

Duration (days)	Drying Shrinkage (microns)						
	M1	**M20**	**M21**	**M22**	**M23**	**M24**	**M25**
0	0	0	0	0	0	0	0
1	116	106	73	60	60	101	58
3	280	260	222	181	201	190	67
7	240	280	227	206	251	236	91
14	265	307	251	285	318	277	122
28	376	327	285	328	329	285	153
42	387	350	357	338	341	312	167
56	400	418	403	367	367	337	230
70	419	451	411	382	421	345	263
84	432	472	414	368	448	352	283
105	463	479	437	378	459	358	299
126	485	485	454	382	465	362	310
147	488	491	469	387	473	367	315
203	491	493	472	390	477	370	316
259	497	495	472	391	480	371	317

for the control mix as compared to 495, 472 and 391 microns for M20, M21 and M22, respectively). When the MK dosage replaced reached 20% and the expansive material was used, the ultimate shrinkage for MK mixes was much lower compared to the control mix (497 microns for the control mix as compared to 480, 371 and 317 microns to M23, M24 and M25, respectively).

4.5.6 Summary of Drying Shrinkage for all Mixes

Table 4.25 summarizes the results of drying shrinkage for all mixes in this study. The data in this table indicate that the maximum drying shrinkage was noted in the mixes with SF (M2, M5 and M8) and the mix with the highest dosage of LSP (M11) in addition the commercial grouts. Though the high shrinkage in SF mixes is well documented in the literature [33, 42, 81, 138, 139, 141]; the high shrinkage of M11 could not be justified. However, all the developed grouts (including those with SF) had lower shrinkage than the two commercial grouts.

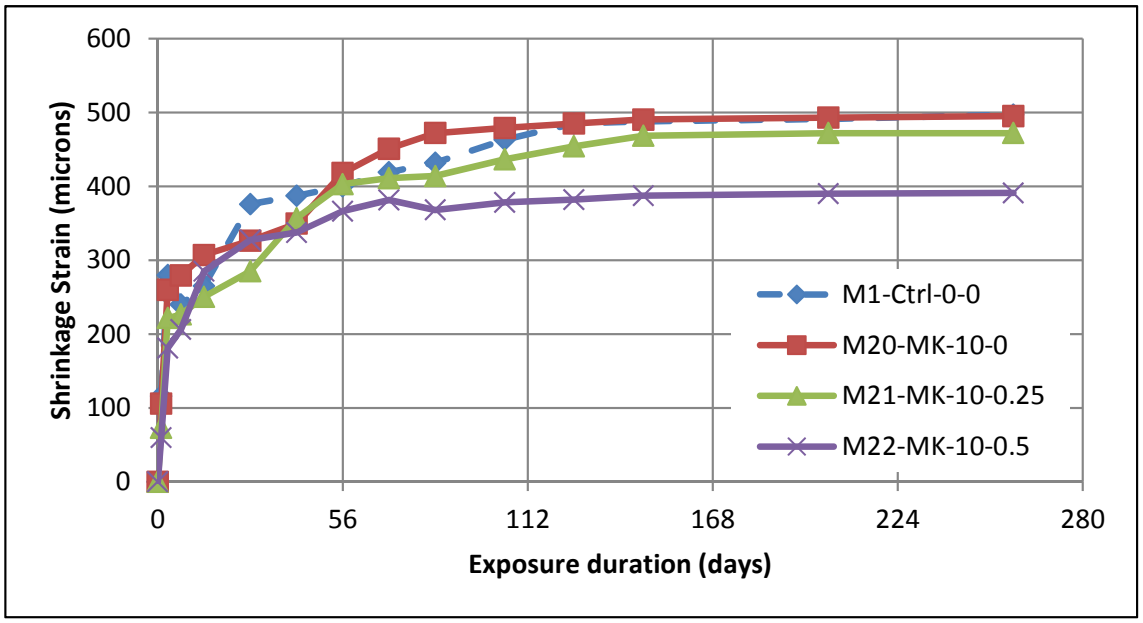

Figure 4.23: Drying shrinkage of HPNSG with 10% MK and the control mix.

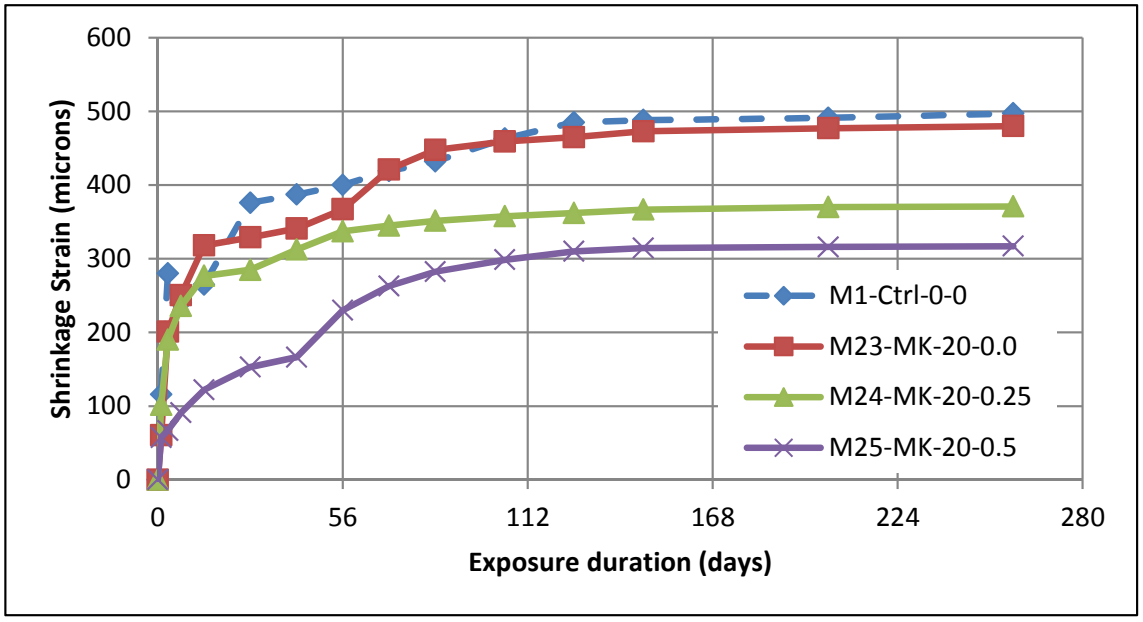

Figure 4.24: Drying shrinkage of HPNSG with 20% MK and the control mix.

As expected, with increasing the percentage of the expansive agent, the drying shrinkage declined. The shrinkage dropped by 37%, 30%, 16% and 34% with 0.5% of expansive agent for mixes with SF, LSP, NP and MK, respectively.

Table 4.25: Average drying shrinkage of all mixes in this study.

Mix ID	**Ultimate Drying Shrinkage (microns)**
M1-Ctrl-0-0	497
M2-SF-5-0	503
M3-SF-5-0.25	323
M4-SF-5-0.5	315
M5-SF-10-0	554
M6-SF-10-0.25	390
M7-SF-10-0.5	380
M8-SF-15-0	560
M9-SF-15-0.25	399
M10-SF-15-0.5	392
M11-LSP-10-0	506
M12-LSP-10-0.25	418
M13-LSP-10-0.5	353
M14-LSP-20-0	454
M15-LSP-20-.25	345
M16-LSP-20-0.5	341
M17-NP-20-0	396
M18-NP-20-0.25	380
M19-NP-20-0.5	333
M20-MK-10-0	495
M21-MK-10-0.25	472
M22-MK-10-0.5	391
M23-MK-15-0	480
M24-MK-15-0.25	371
M25-MK-15-0.5	317
M26-Sika® grout-214	596
M27-Fosroc® Conbextra GP	637

4.6 CORROSION POTENTIALS

Measurement of corrosion potential is one of the popular methods for monitoring reinforcement corrosion in concrete [142, 143]. It is conducted in accordance with the provisions of ASTM C 876 [112]. Figures 4.25 through 4.29 show the variation of

potential (E_{corr}) with time of exposure to the 5% NaCl solution for each group of specimens. As per ASTM C 876 standard, the probability of reinforcement corrosion is presented in Table 4.26. The threshold level of E_{corr} measured on a rebar at which corrosion is assumed to be active is shown in Figures 4.25 to 4.29. This threshold value of E_{corr} is -276 mV SCE for the standard Calomel electrode used for this monitoring process.

Table 4.26: Corrosion condition related with half-cell potential (HCP) measurements.

Open circuit potential (OCP) values		**Corrosion condition**
(mV vs. SCE)	**(mV vs. CSE)**	
<-426	<-500	Severe corrosion
<-276	<-350	High (<90% risk of corrosion)
-126 to -275	-350 to -200	Intermediate corrosion risk
>-125	>-200	Low(10% risk of corrosion)

4.6.1 Control Mix and Commercial Grouts

Figure 4.25 shows the variation of potential with exposure time of the control mix and the two commercial grouts. From the graph, the control mix had almost similar potentials to those of the commercial grouts. After above 250 days of exposure, the corrosion potentials of steel in these three mixes were less than the threshold potential indicating that the reinforcement were in a passive condition.

4.6.2 Mixes Containing SF

Figure 4.26 shows the variation of potential with exposure time of HPNSG specimens representing the mixes containing SF. From the data in this figure, it is clear that none of these mixtures had the embedded steel in the active state of corrosion within the 250 days of exposure. Also, the potentials are not in an uptrend, which is an indication that the time to initiation of corrosion may be very long. This high durability

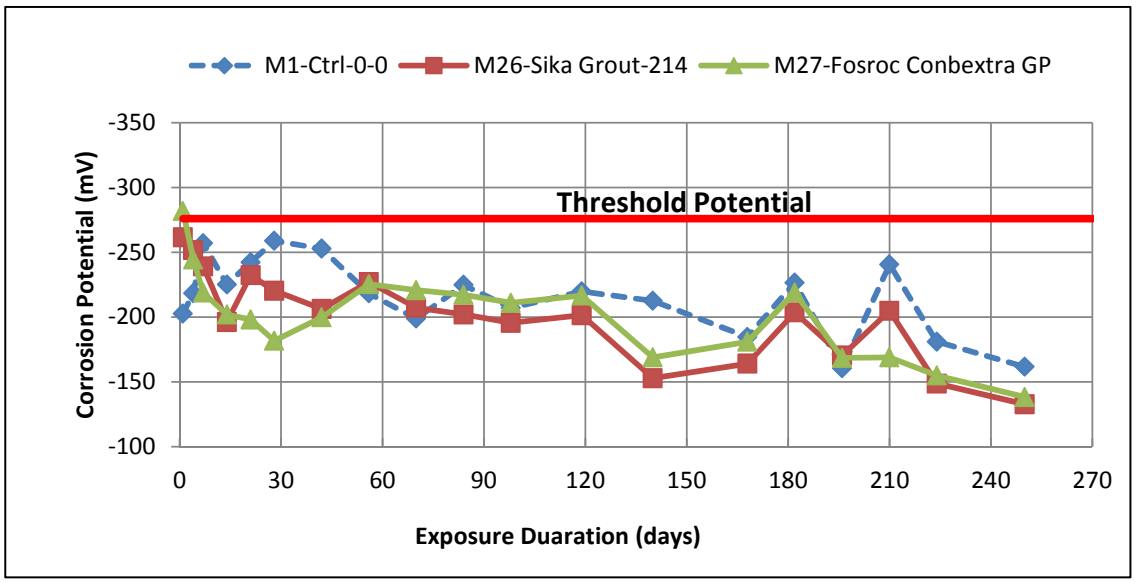

Figure 4.25: Variation of potential with exposure time for Control mix and commercial grouts.

quality is attributable to the excellent filling effect of SF [144, 145] thereby making the microstructure of these specimens very dense and impermeable.

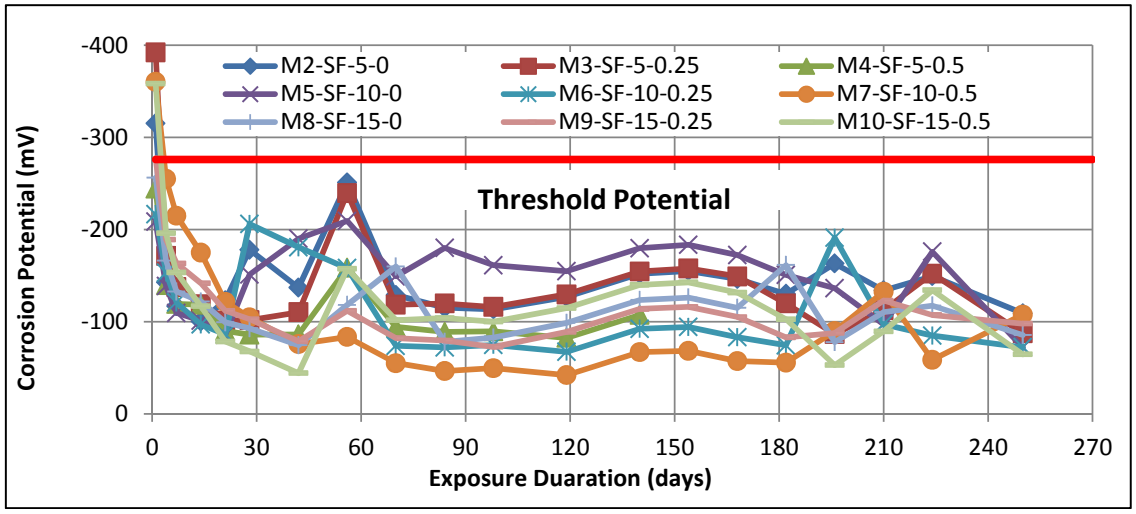

Figure 4.26: Variation of potential with exposure time for SF mixes.

4.6.3 Mixes Containing LSP

Figure 4.27 shows the variation of potential with exposure time of HPNSG specimens representing the mixes containing LSP. The data in this figure indicate that the trend is declining with time (The potential values after 200 days was lower than that of 28 days). None of the mixes reached the threshold line, indicating the good durability characteristics of these mixes. Limestone powder improves the durability features of concretes by providing more compact structure through its pore-filling effect [146–148].

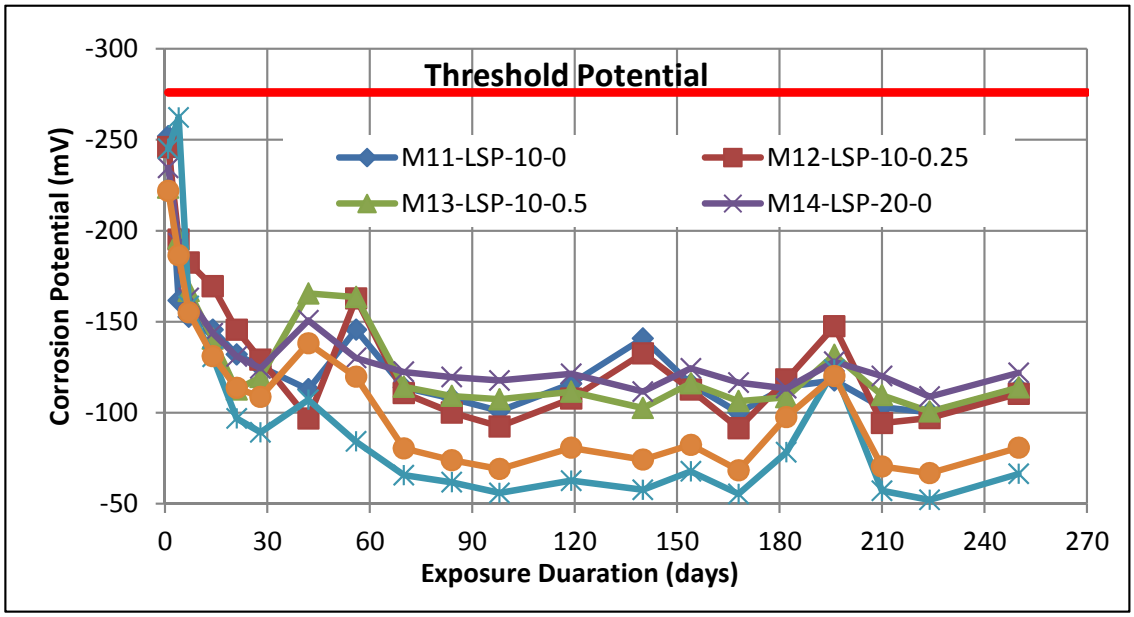

Figure 4.27: Variation of potential with exposure time for LSP mixes.

4.6.4 Mixes Containing NP

Figure 4.28 shows the variation of potential with exposure time of HPNSG specimens representing the mixes containing NP. From the data in this figure, it is clear that all the three mixes had low potential to corrosion.

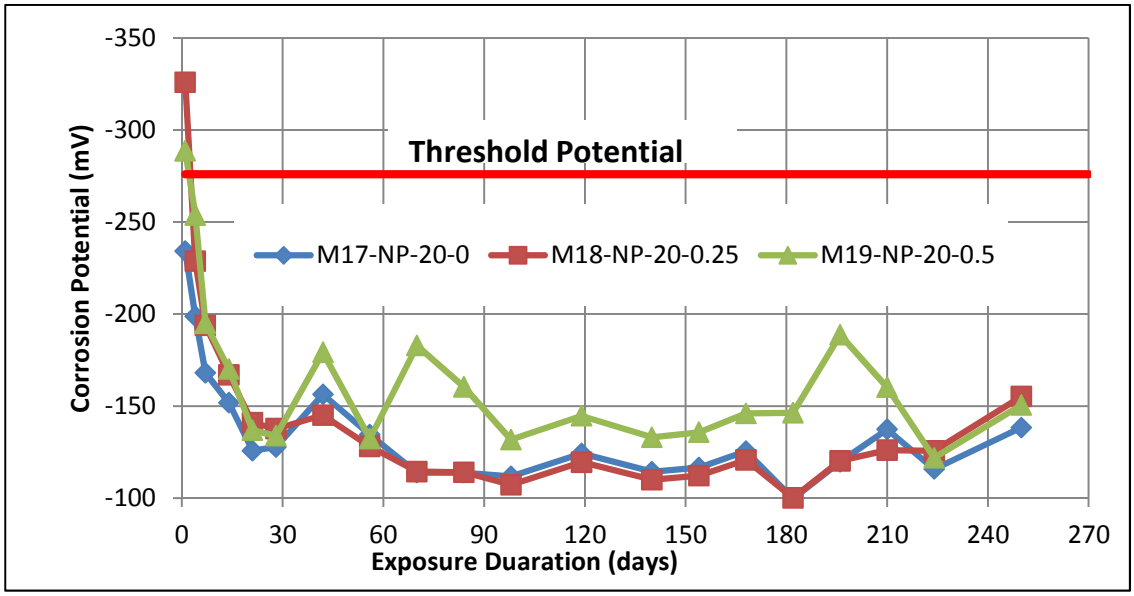

Figure 4.28: Variation of potential with exposure time for NP mixes.

4.6.5 Mixes Containing MK

Figure 4.29 shows the variation of potential with exposure time of HPNSG specimens representing the mixes containing MK. As it is clear from the figure, the potential reached the threshold only at very early ages, then declined with time. It was reported by several researchers that using MK as replacement of cement makes durable structures [130, 131, 149].

4.7 CORROSION CURRENT DENSITY

Figures 4.30 through 4.34 show the variation of corrosion current density, I_{corr}, with exposure time to the 5% NaCl solution for each group of HPNSG specimens. As expected, the value of I_{corr} tended to increase with the exposure time.

The criteria for corrosion initiation have been reported from both field and laboratory investigations [150–152] and presented in Table 4.27.

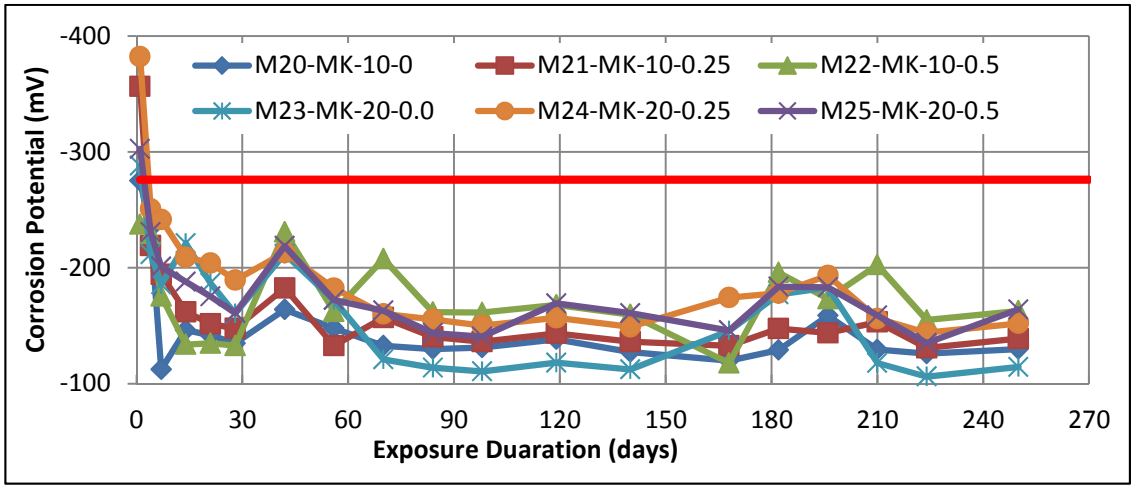

Figure 4.29: Variation of potential with exposure time for MK mixes.

Table 4.27: Corrosion current vs. condition of the rebar.

Corrosion current (I_{corr})	**Rebar Condition**
$I_{corr} < 0.1\ \mu A/cm^2$	Passive condition
$I_{corr}\ 0.1 - 0.5\ \mu A/cm^2$	Low to moderate corrosion
$I_{corr}\ 0.5 - 1.0\ \mu A/cm^2$	Moderate to high corrosion
$I_{corr} > 1.0\ \mu A/cm^2$	High corrosion rate

4.7.1 Control Mix and Commercial Grouts

Figure 4.30 shows the variation of corrosion current density of the control mix and the two commercial grouts used in this study. From the data in this graph, no any sign of corrosion initiation was noticed.

4.7.2 Mixes Containing SF

Figure 4.31 shows the variation of I_{corr} of HPNSG specimens for the mixes containing SF. From the data in this figure, all the mixes containing SF fell in the zone of passive condition ($I_{corr} < 0.1\ \mu A/cm^2$), hence, no corrosion was expected.

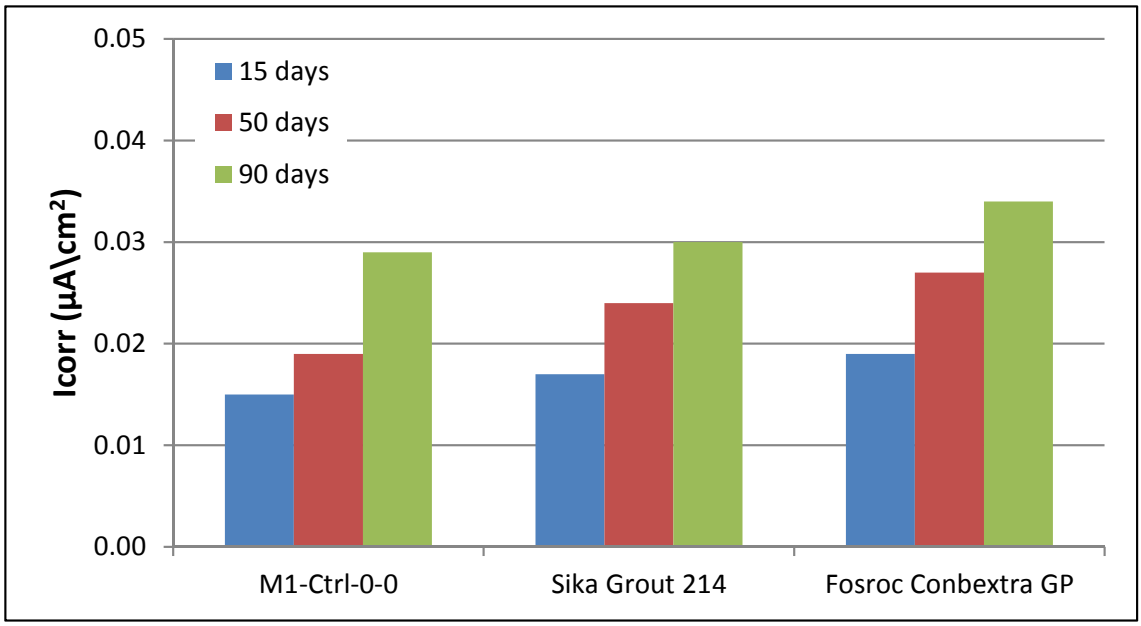

Figure 4.30: Variation of corrosion current density with exposure time for the control and commercial grouts mixes.

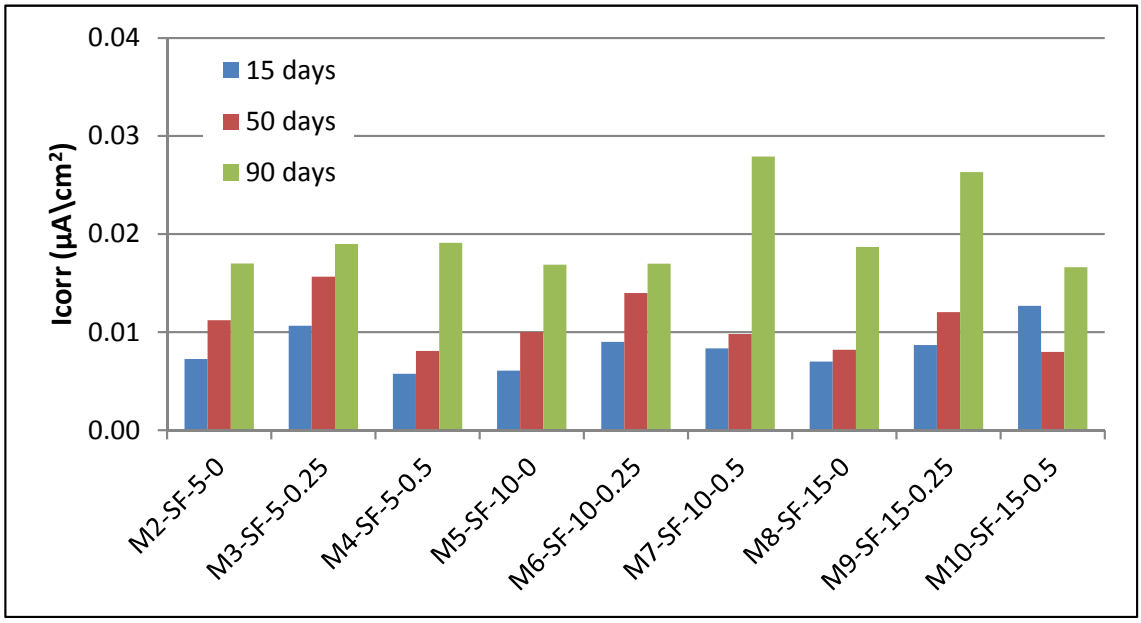

Figure 4.31: Variation of corrosion current density with exposure time SF mixes.

4.7.3 Mixes Containing LSP

Figure 4.32 shows the variation of corrosion current density of HPNSG specimens for the mixes containing LSP. As shown in this figure, LSP has high resistant to corrosion as mentioned in the section of potential.

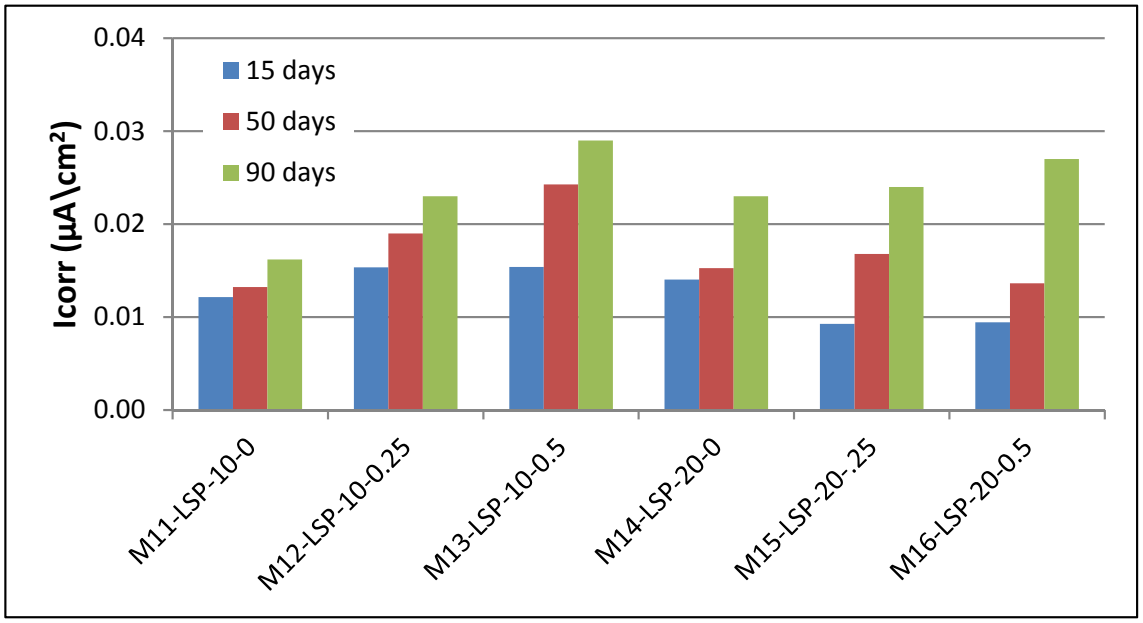

Figure 4.32: Variation of corrosion current density with exposure time LSP mixes.

4.7.4 Mixes Containing NP

Figure 4.33 shows the variation of corrosion current density of HPNSG specimens for mixes containing NP. All the mixes exhibited I_{corr} value below the threshold value of 0.1 $\mu A/cm^2$.

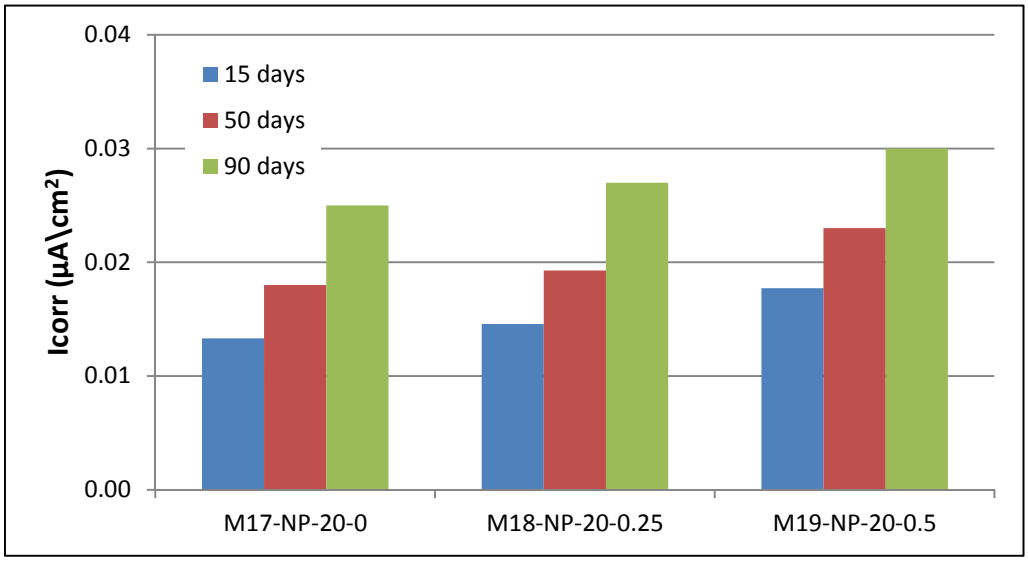

Figure 4.33: Variation of corrosion current density with exposure time NP mixes.

4.7.5 Mixes Containing MK

Figure 4.34 shows the variation of corrosion current density of HPNSG specimens for mixes containing MK. From the graph, no any sign of corrosion initiation was noticed.

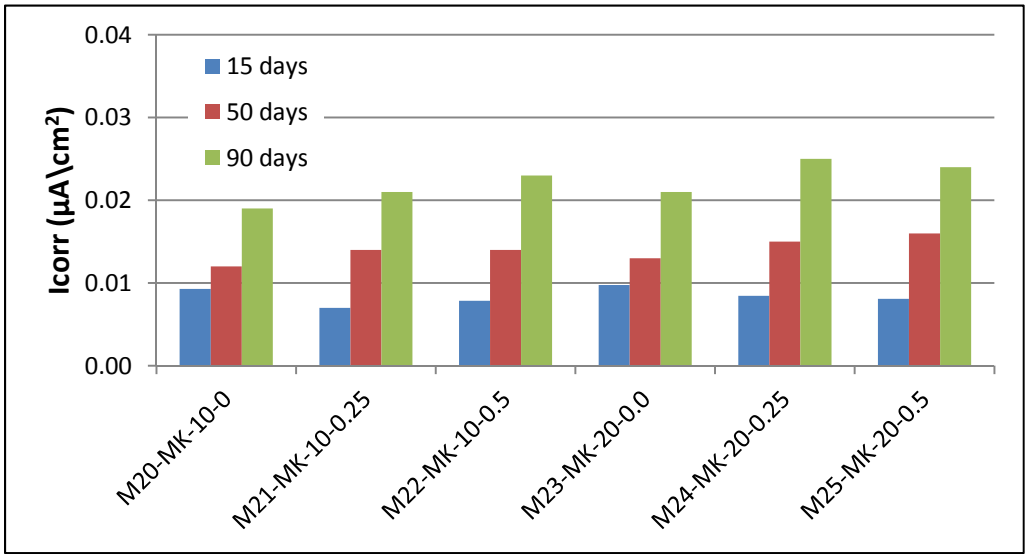

Figure 4.34: Variation of corrosion current density with exposure time MK mixes.

4.7.6 Summary of Corrosion Current Density for all Mixes

Table 4.28 summarizes the corrosion current density of all mixes in this study. It is clear from the data in this table at 90 days, the maximum I_corr was 0.034 $\mu A/cm^2$, which is far away from the threshold 0.1 $\mu A/cm^2$ which indicates that none of any reinforcement had started corroding yet. This could be attributed to the short term exposure.

Table 4.28: corrosion current density of all Mixes in this study.

Mix ID	Corrosion Current Density ($\mu A/cm^2$)		
	15 days	**50 days**	**90 days**
M1-Ctrl-0-0	0.015	0.019	0.029
M2-SF-5-0	0.007	0.011	0.017
M3-SF-5-0.25	0.011	0.016	0.019
M4-SF-5-0.5	0.006	0.008	0.019
M5-SF-10-0	0.006	0.010	0.017
M6-SF-10-0.25	0.009	0.014	0.017
M7-SF-10-0.5	0.008	0.010	0.028
M8-SF-15-0	0.007	0.008	0.019
M9-SF-15-0.25	0.009	0.012	0.026
M10-SF-15-0.5	0.013	0.008	0.017
M11-LSP-10-0	0.012	0.013	0.016
M12-LSP-10-0.25	0.015	0.019	0.023
M13-LSP-10-0.5	0.015	0.024	0.029
M14-LSP-20-0	0.014	0.015	0.023
M15-LSP-20-.25	0.009	0.017	0.024
M16-LSP-20-0.5	0.009	0.014	0.027
M17-NP-20-0	0.013	0.018	0.025
M18-NP-20-0.25	0.015	0.019	0.027
M19-NP-20-0.5	0.018	0.023	0.030
M20-MK-10-0	0.009	0.012	0.019
M21-MK-10-0.25	0.007	0.014	0.021
M22-MK-10-0.5	0.008	0.014	0.023
M23-MK-15-0	0.010	0.013	0.021
M24-MK-15-0.25	0.008	0.015	0.025
M25-MK-15-0.5	0.008	0.016	0.024
M26-Sika grout-214	0.017	0.024	0.030
M27-Fosroc Conbextra GP	0.019	0.027	0.034

4.8 CHLORIDE DIFFUSION

The chloride profiles for free chloride concentrations are shown in Figures 4.35 through 4.59. Only selected mixes were presented for clarification. The chloride-ion contents were given as percentage by weight of grout.

The values of surface concentration and apparent chloride diffusion coefficient were determined by fitting Equation 2.4 to the measured chloride-ion contents by means of a non-linear regression analysis using the method of least squares [153].

4.8.1 Control Mix and Commercial Grouts

Figures 4.35 to 4.37 show the free chloride profile for the control mix, Sika® 214, and Fosroc® Conbextra GP, respectively.

Table 4.29 shows the apparent chloride diffusion coefficient (D_a) for the control mix and commercial grouts and the ratio of D_a to the control mix value. From the data in this table; the chloride diffusion coefficient for the control mix was less than that of both commercial grouts used in this study. The Sika® grout-214 was greater than the control mix by only 2%, while the Fosroc® grout was higher by 17%.

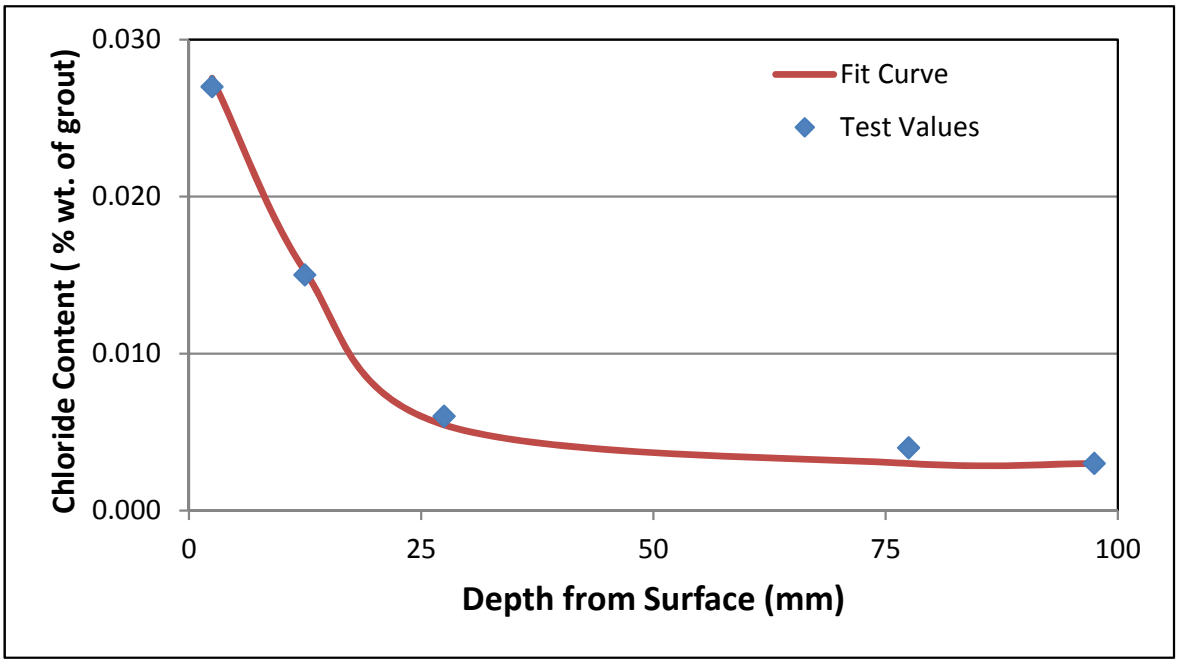

Figure 4.35: Free chloride profile for the control mix.

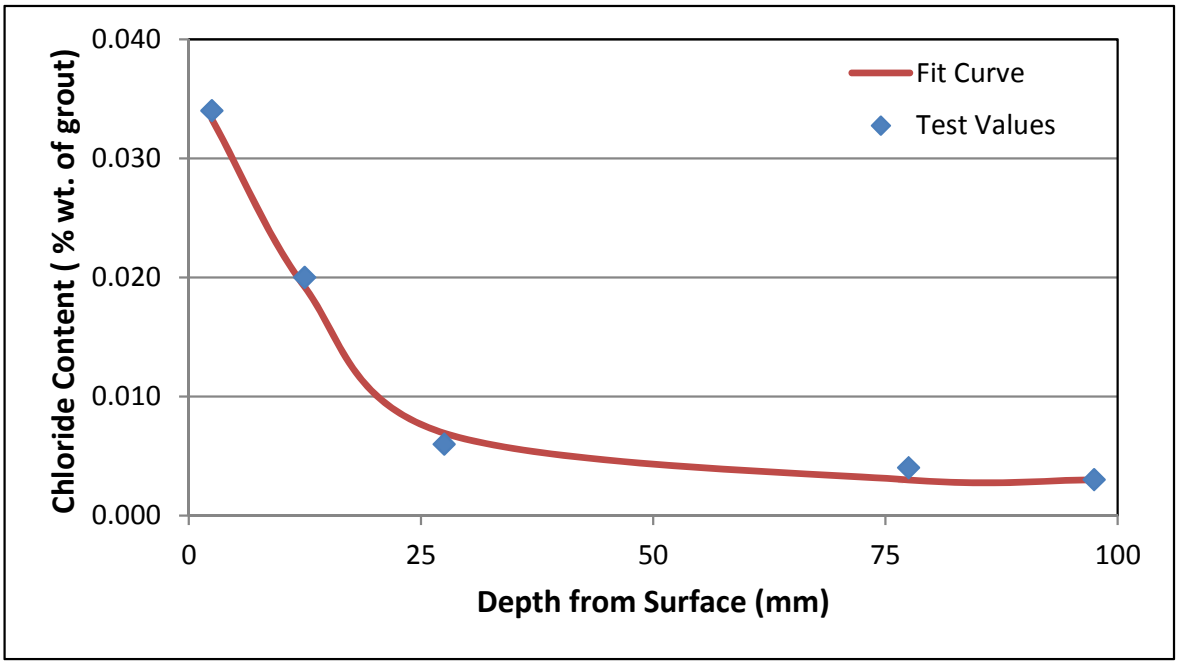

Figure 4.36: Free chloride profile for M26-Sika®-214.

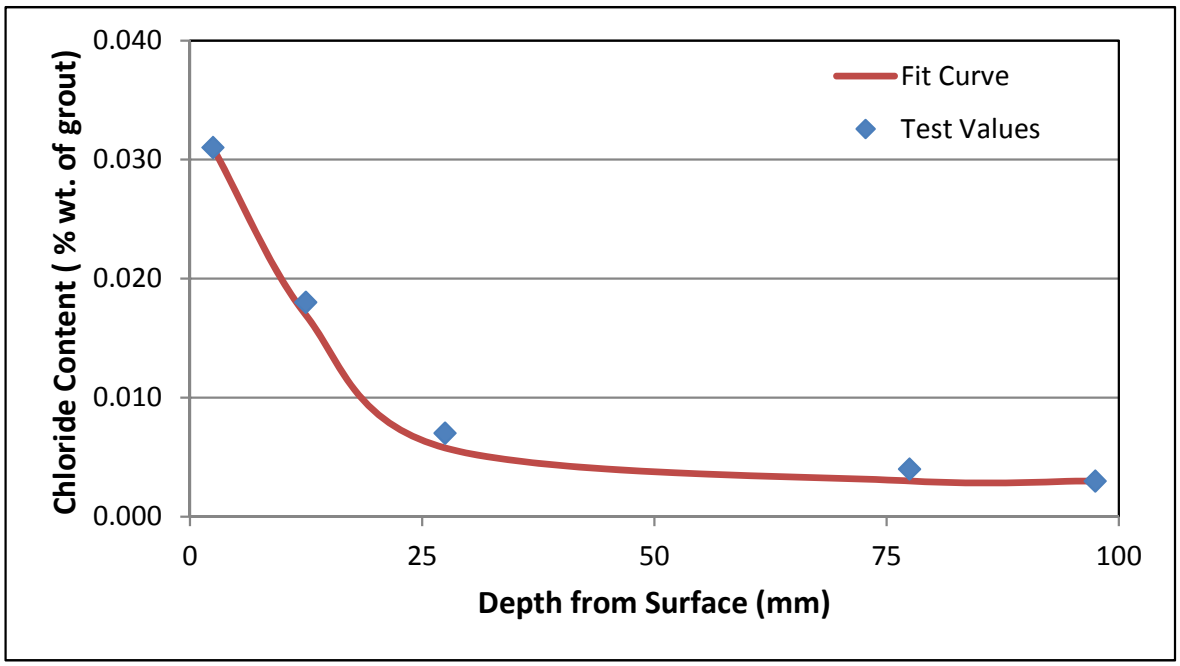

Figure 4.37: Free chloride profile for M27-Fosroc® Conbextra GP.

Table 4.29: Diffusion coefficient for the control mix and commercial grouts.

Mix ID	D_a ($\times$ 10^{-12} m^2/s)	**Ratio in terms of the control**
M1-Ctrl-0-0	9.81	1.00
M26-Sika® grout 214	11.5	1.17
M27-Fosroc® Conbextra GP	9.98	1.02

4.8.2 Mixes Containing SF

Figures 4.38 to 4.46 show the free chloride profile for silica fume mixes, while Table 4.30 summarizes the apparent chloride diffusion coefficient (D_a) for the mixes containing SF.

It's clear from the data in Table 4.30 that all SF mixes had lower diffusion coefficient than the control mix. These results coincide with previous research [154–158]. The ratio of diffusion coefficient between the mixes containing SF as replacement to that of the control mix varied between 25% to 81%. This is because silica fume improves the mechanical and durability properties by enhancing the microstructure of concrete. Furthermore, the data in Table 4.30 indicate that with increasing the percentage of expansive agent, there was marginal increase in chloride diffusion.

SF increases the diffusion resistance of concrete in several ways. As a mineral admixture with extreme fineness and high pozzolanic reactivity, SF improves the diffusion resistance of concrete by refining the pore structure of interfacial transition zone of concrete [159] and by producing a greater solid volume of C-S-H gel [160], and also reducing the porosity for fixed degree of cement hydration [161]. Bentz et al. [156] observed that the pozzolanic gel produced from SF had about 25 times less diffusivity than the gel produced from normal cement hydration.

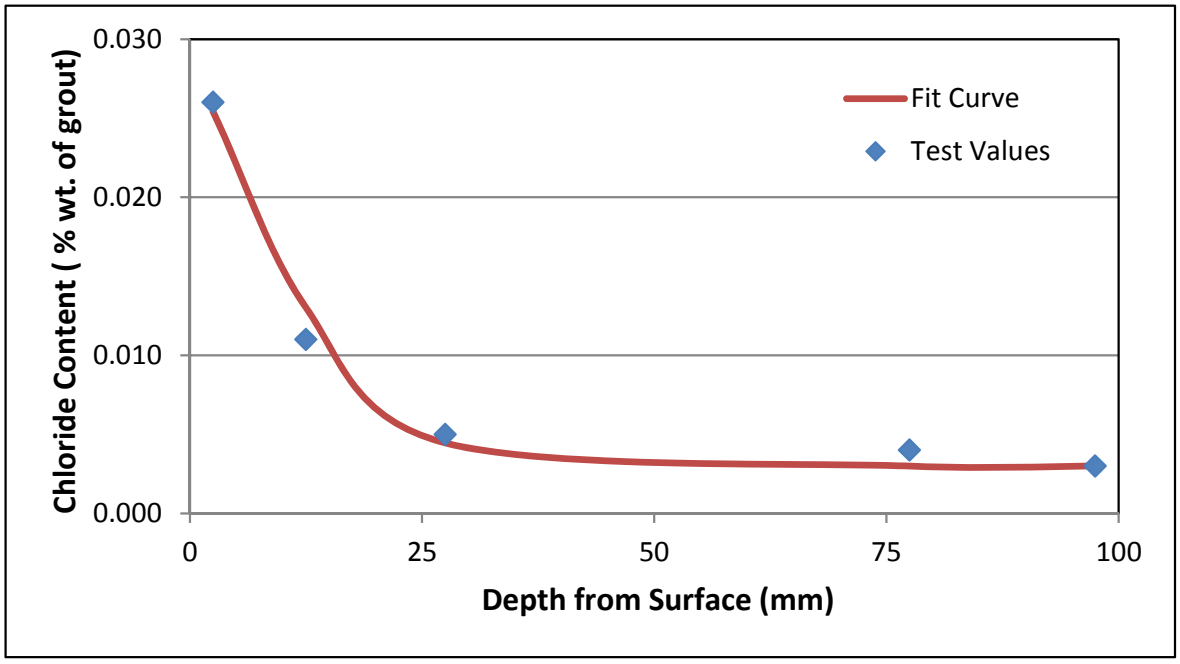

Figure 4.38: Free chloride profile for M2-SF-5-0.

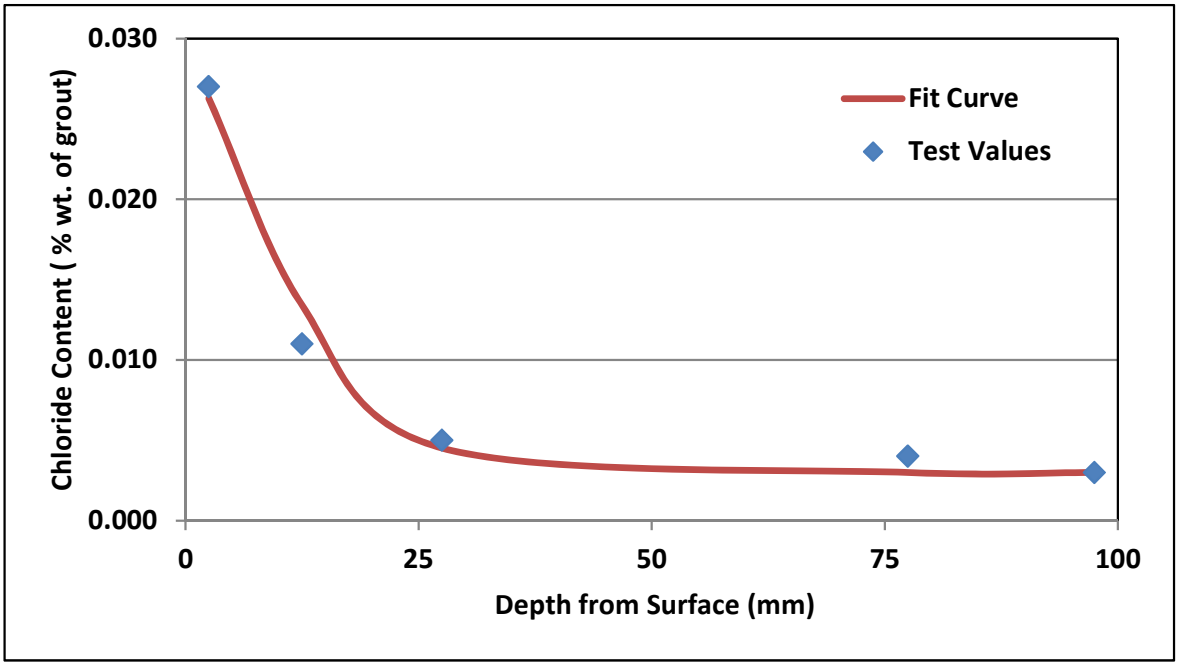

Figure 4.39: Free chloride profile for M3-SF-5-0.25.

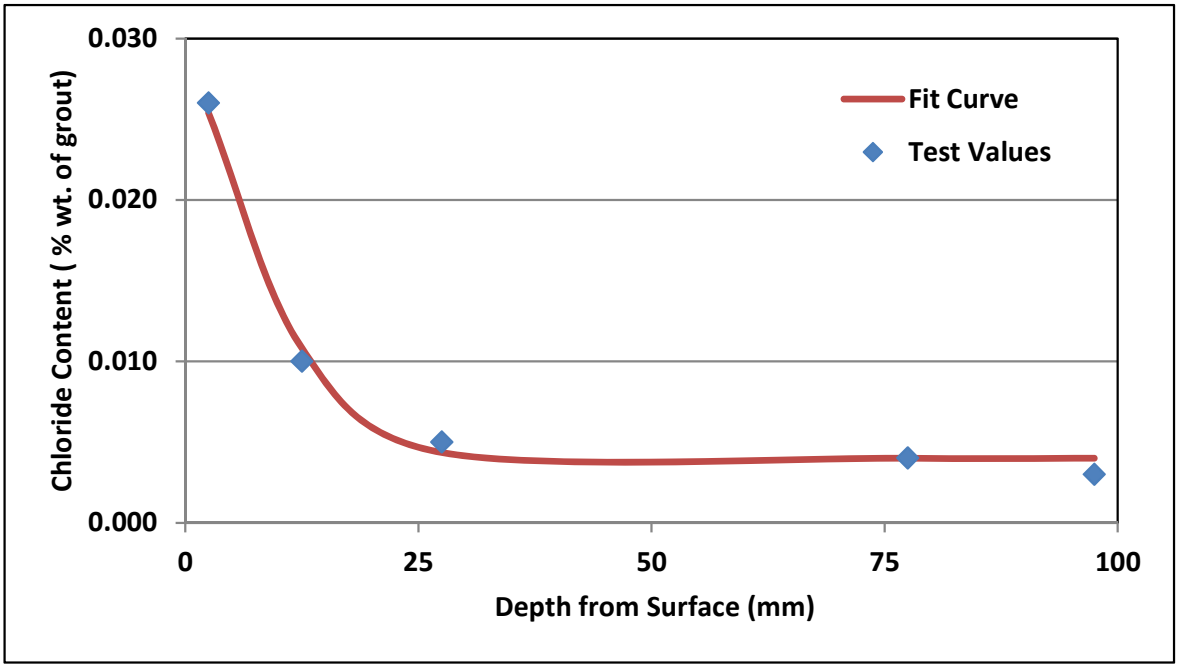

Figure 4.40: Free chloride profile for M4-SF-5-0.5.

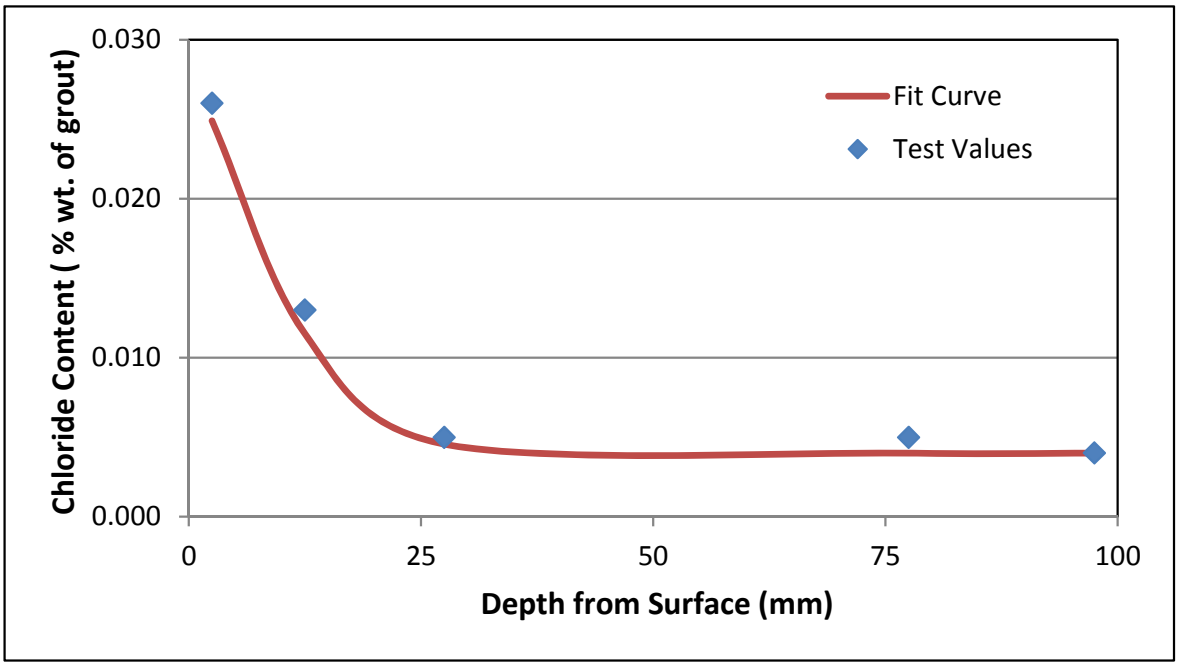

Figure 4.41: Free chloride profile for M5-SF-10-0.

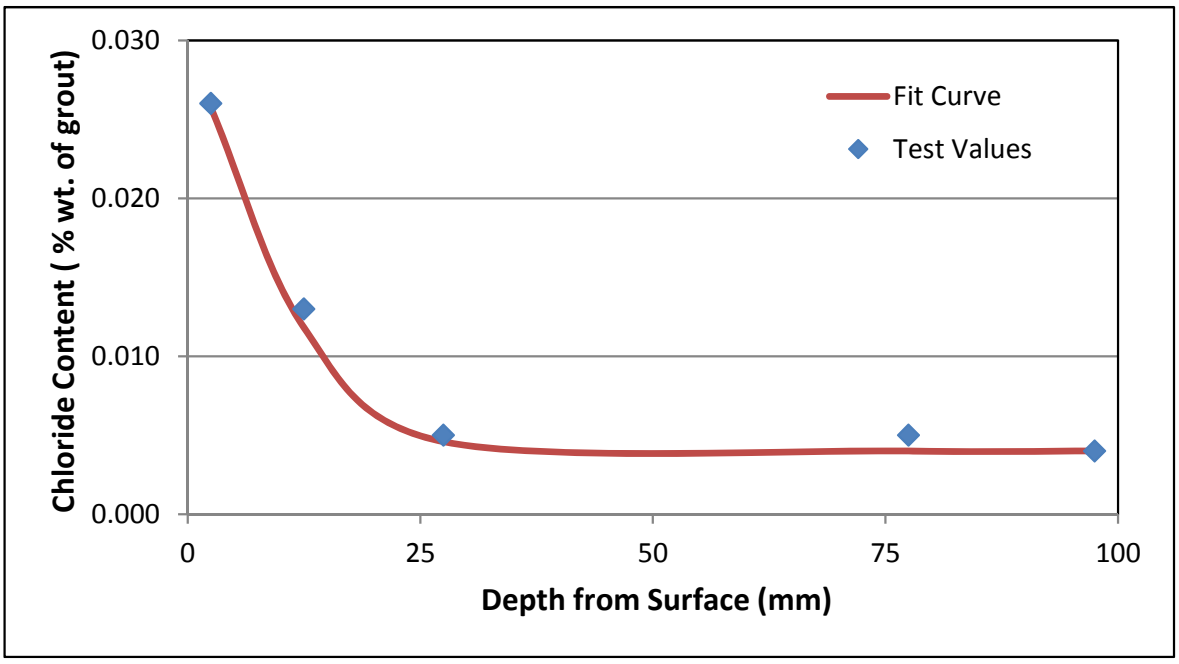

Figure 4.42: Free chloride profile for M6-SF-10-0.25.

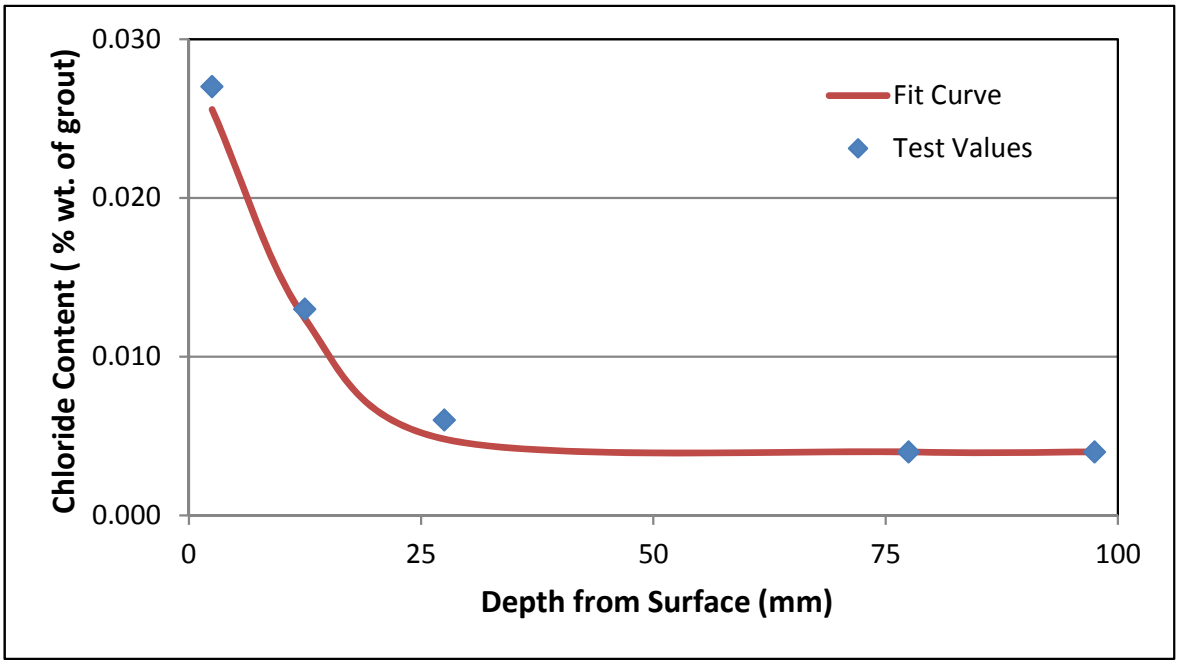

Figure 4.43: Free chloride profile for M7-SF-10-0.5.

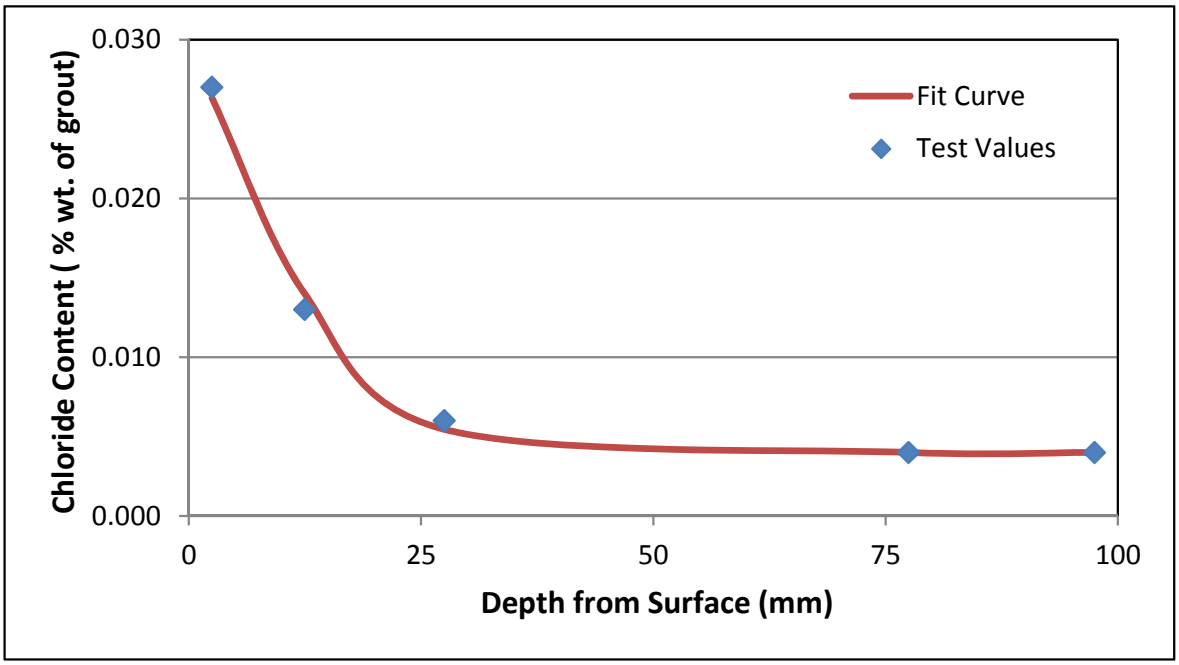

Figure 4.44: Free chloride profile for M8-SF-15-0.

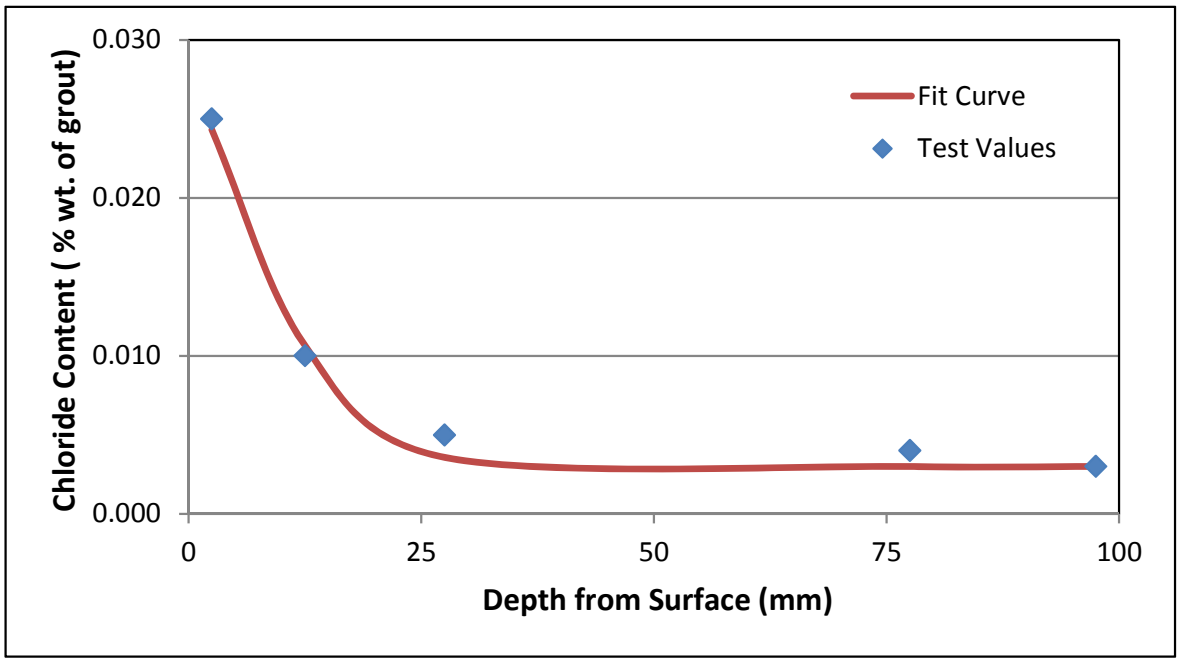

Figure 4.45: Free chloride profile for M9-SF-15-0.25.

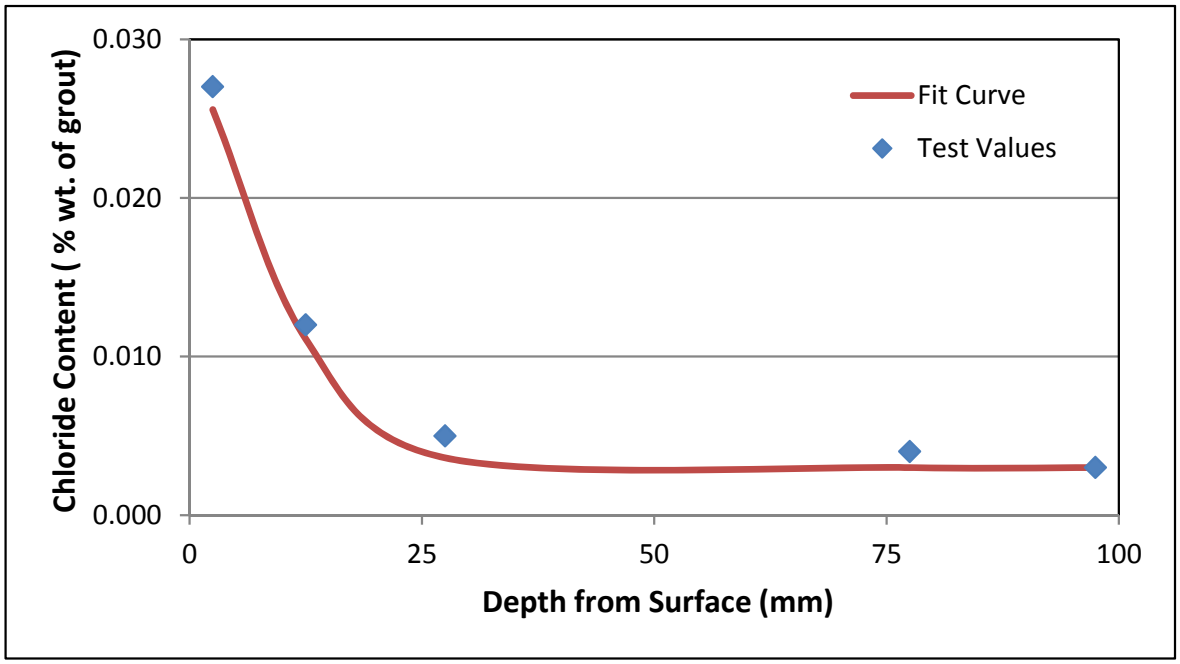

Figure 4.46: Free chloride profile for M10-SF-15-0.5.

Table 4.30: Diffusion coefficient for mixes contain SF.

Mix ID	D_a ($\times$ $\mathbf{10^{-12}}$ $\mathbf{m^2/s}$)	**Ratio in terms of the control**
M1-Ctrl-0-0	9.81	1.00
M2-SF-5-0	7.85	0.80
M3-SF-5-0.25	7.91	0.81
M4-SF-5-0.5	7.94	0.81
M5-SF-10-0	5.51	0.56
M6-SF-10-0.25	5.61	0.57
M7-SF-10-0.5	6.20	0.63
M8-SF-15-0	2.43	0.25
M9-SF-15-0.25	2.87	0.29
M10-SF-15-0.5	3.03	0.31

4.8.3 Mixes Containing LSP

Figures 4.47 to 4.52 show the free chloride profile for LSP mixes. The data in Table 4.31 summarizes the apparent chloride diffusion coefficient (D_a) for the mixes containing LSP.

Table 4.31 indicate that all the LSP mixes had lower diffusion coefficient than the control mix. The reduction is attributed to the filler effect on the tortuosity of the mixture [162]. Previous researches have similar findings [162–164]. However, there is slightly increase in the chloride diffusion with increasing the expansive agent. The ratio of diffusion coefficient between mixes contain LSP and the control mix was in the range of 56% to 66%.

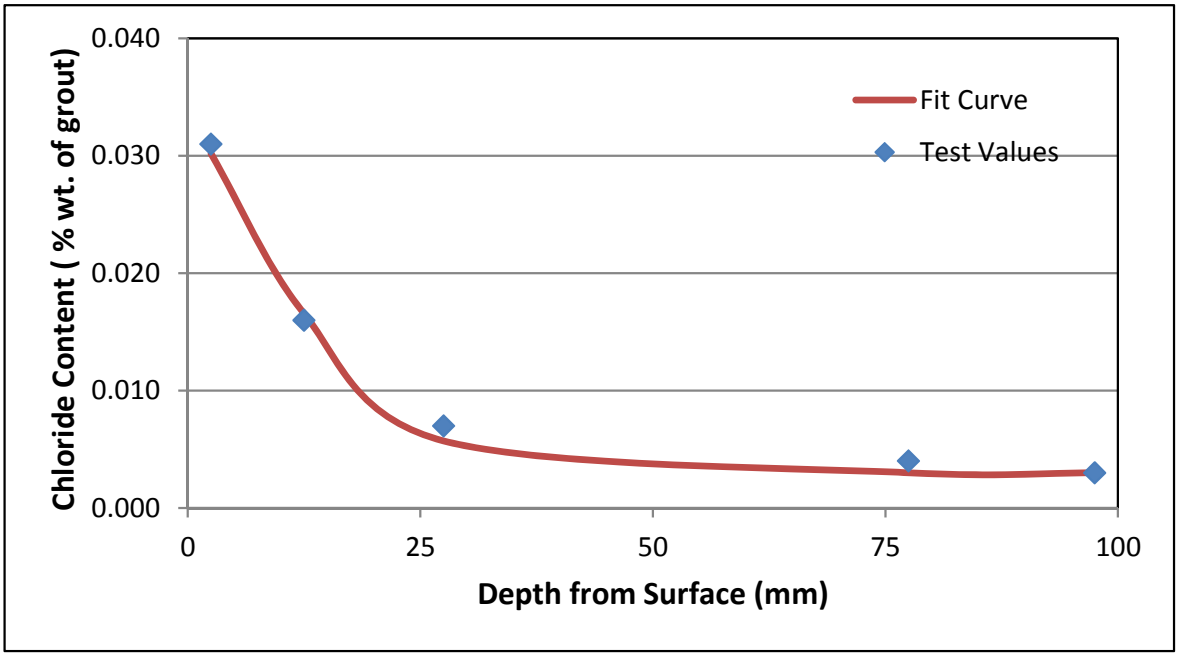

Figure 4.47: Free chloride profile for M11-LSP-10-0.

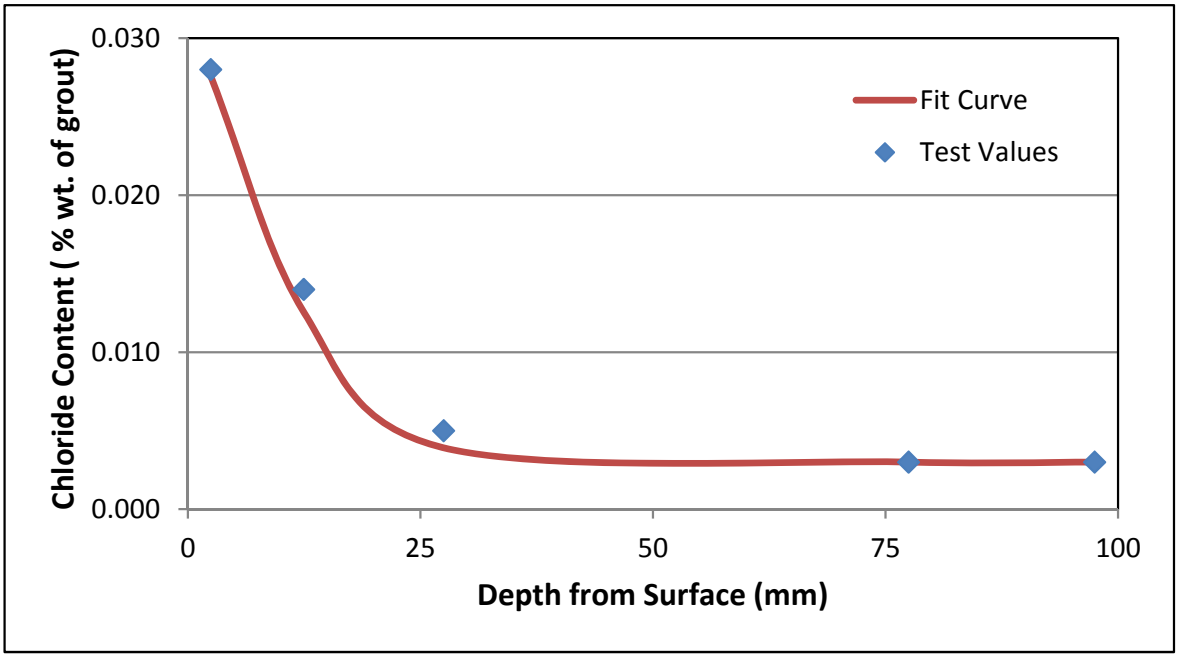

Figure 4.48: Free chloride profile for M12-LSP-10-0.25.

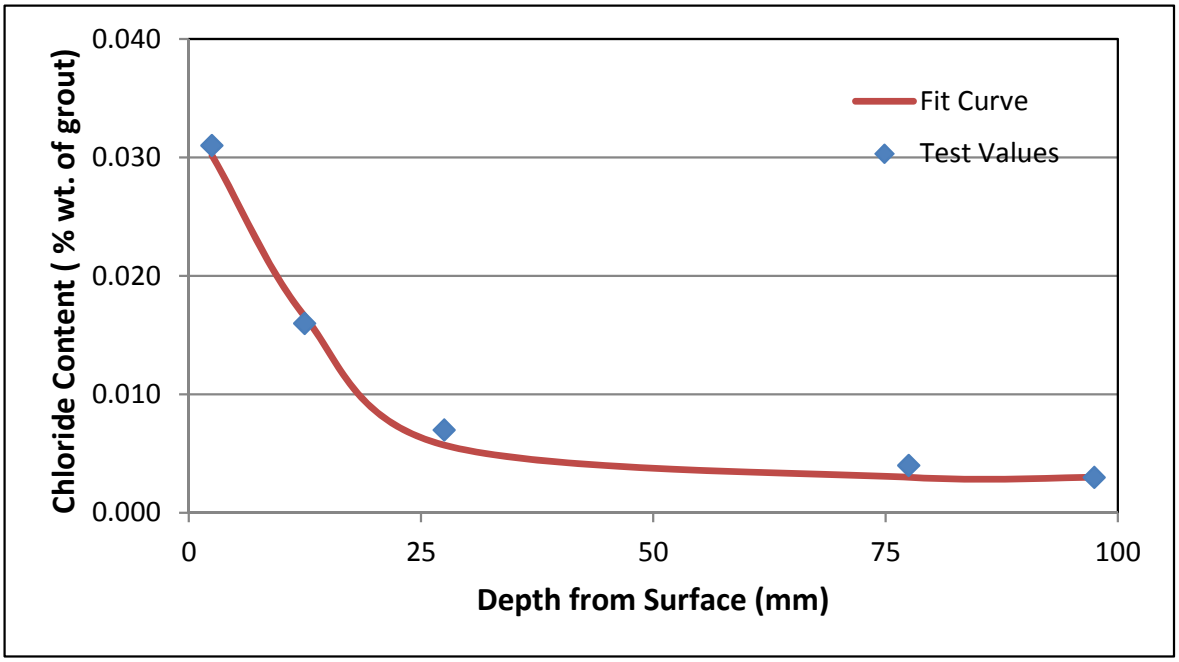

Figure 4.49: Free chloride profile for M13-LSP-10-0.5.

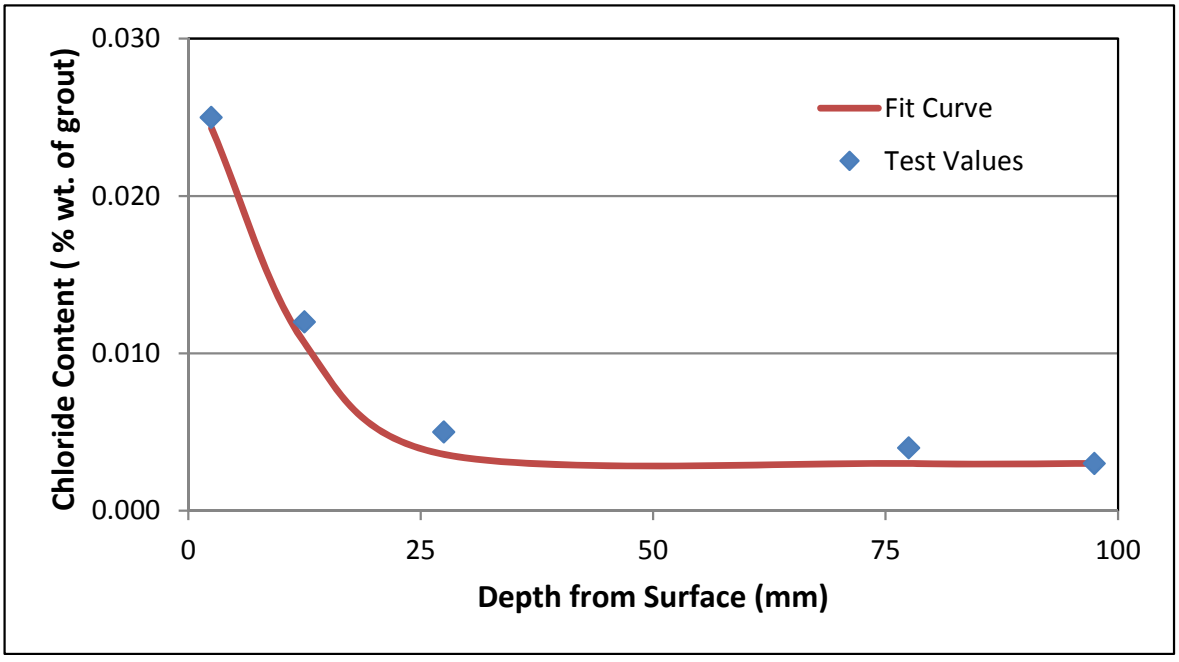

Figure 4.50: Free chloride profile for M14-LSP-20-0.

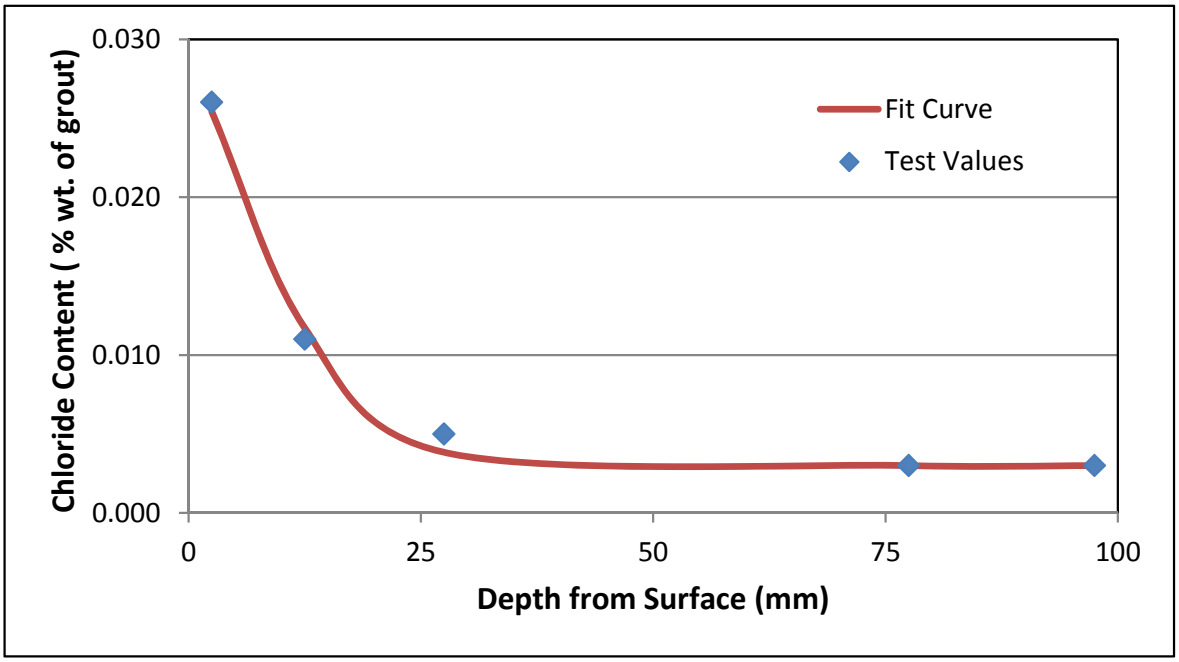

Figure 4.51: Free chloride profile for M15-LSP-20-0.25.

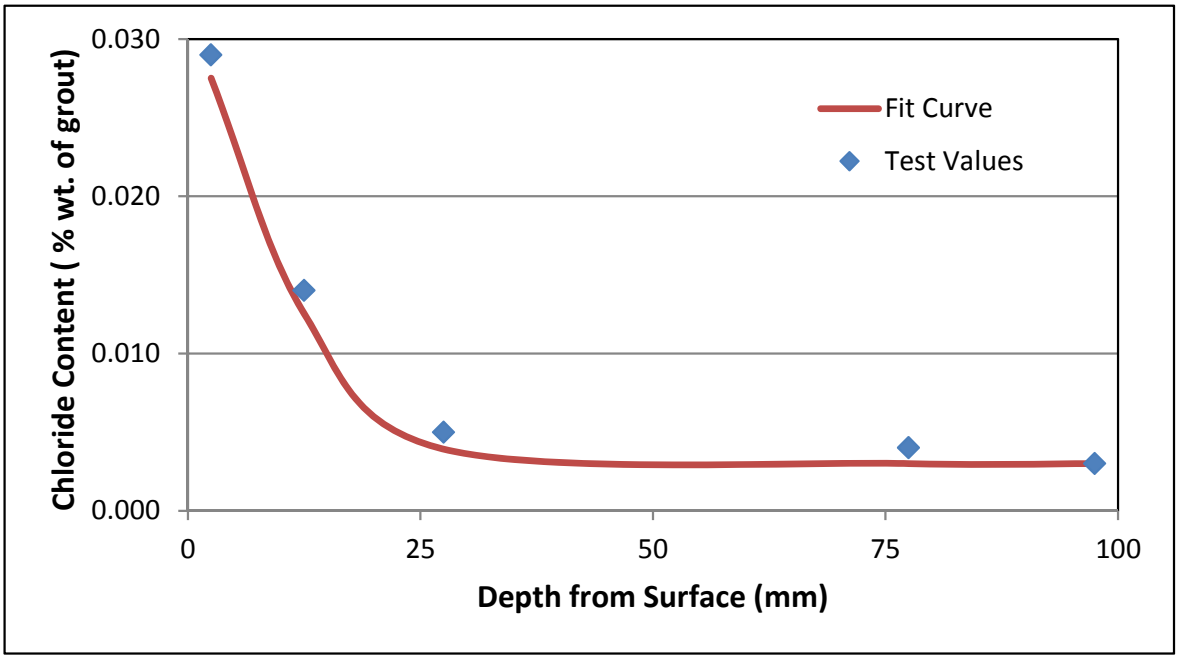

Figure 4.52: Free chloride profile for M16-LSP-20-0.5.

Table 4.31: Diffusion coefficient for mixes contain LSP.

Mix ID	D_a ($\times$ $\mathbf{10^{-12}}$ $\mathbf{m^2/s}$)	**Ratio in terms of the control**
M1-Ctrl-0-0	9.81	1.00
M11-LSP-10-0	6.18	0.63
M12-LSP-10-0.25	6.23	0.64
M13-LSP-10-0.5	6.45	0.66
M14-LSP-20-0	5.51	0.56
M15-LSP-20-0.25	5.97	0.61
M16-LSP-20-0.5	6.02	0.61

4.8.4 Mixes Containing NP

Figures 4.53 to 4.55 show the free chloride profile for NP mixes, while Table 4.32 summarizes the apparent chloride diffusion coefficient (D_a) for the mixes containing NP.

It is clear from the data in Table 4.32 that all NP mixes had lower diffusion coefficients than the control mix. However, with increasing the percentage of expansive agent, there was marginal increase in the chloride diffusion coefficient. Previous researches had shown the same conclusion [165, 166]. The ratio of chloride diffusion coefficient of mixes containing NP as replacement to that of the control mix was 49%, 56% and 70% for M17, M18 and, M19, respectively.

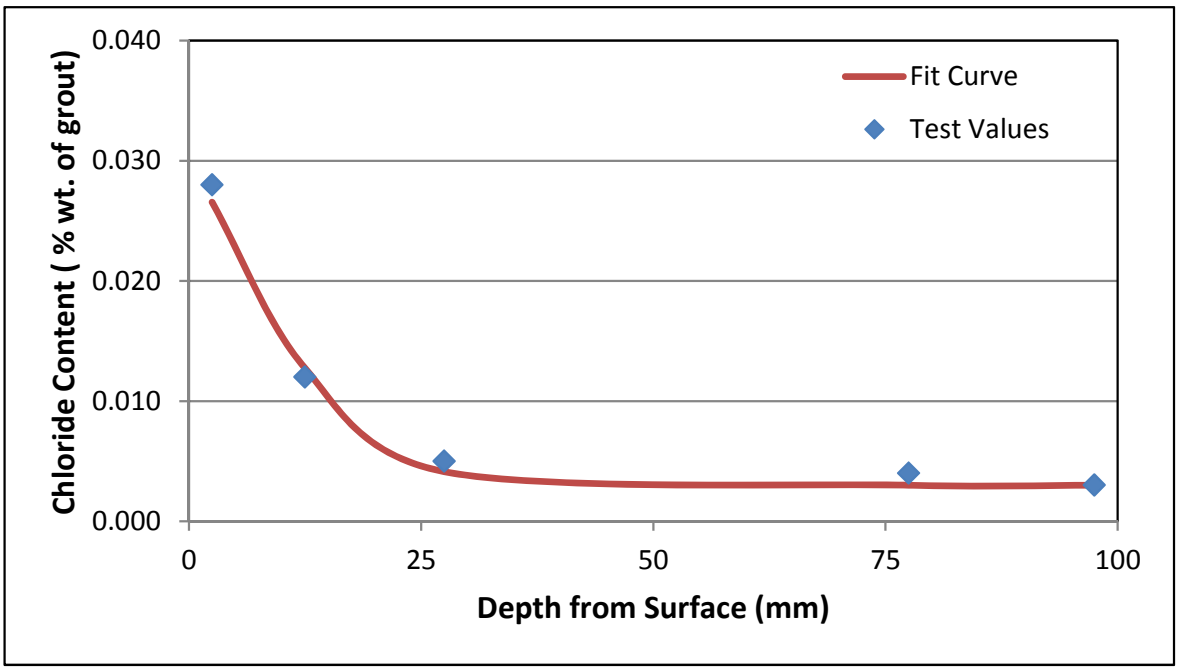

Figure 4.53: Free chloride profile for M17-NP-20-0.

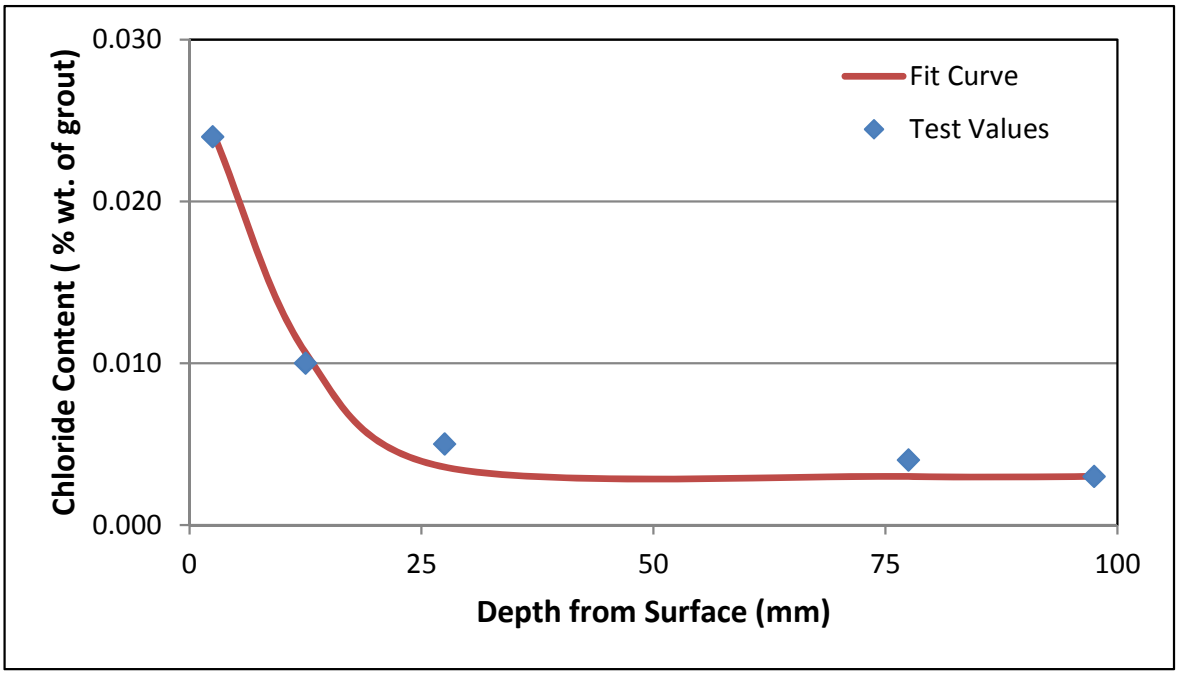

Figure 4.54: Free chloride profile for M18-NP-20-0.25.

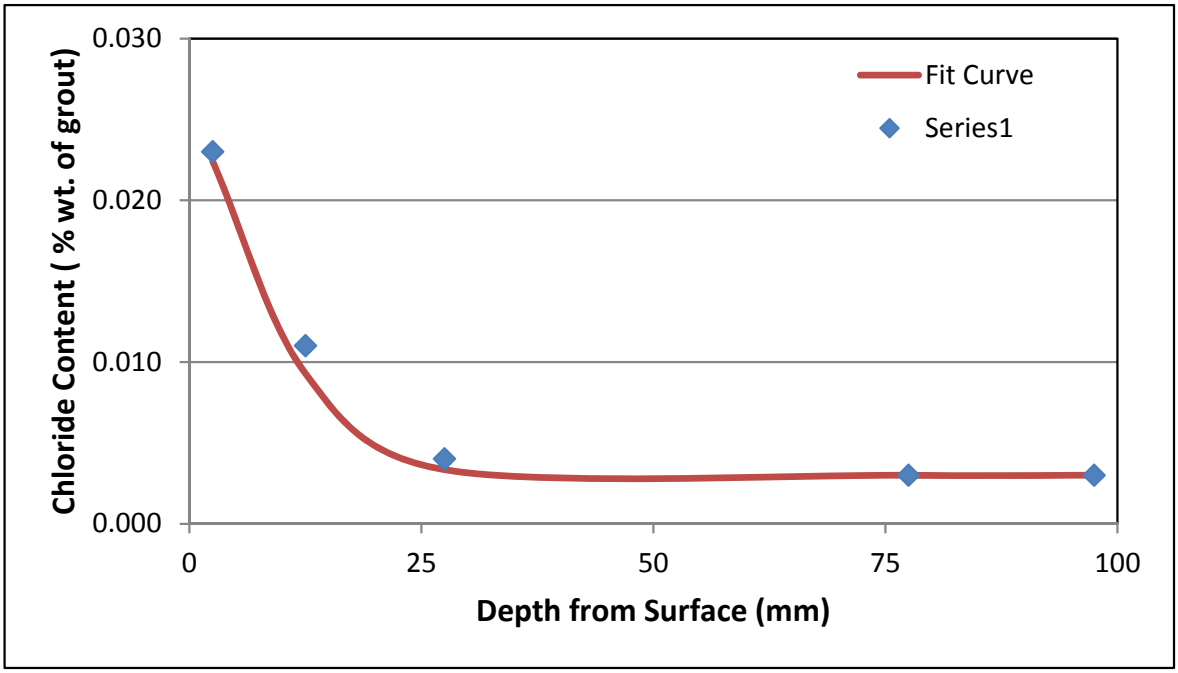

Figure 4.55: Free chloride profile for M19-NP-20-0.5.

Table 4.32: Diffusion coefficient for mixes contain NP.

Mix ID	D_a ($\times$ $\mathbf{10^{-12}}$ $\mathbf{m^2/s}$)	**Ratio in terms of the control**
M1-Ctrl-0-0	9.81	1.00
M17-NP-20-0	4.81	0.49
M18-NP-20-0.25	5.51	0.56
M19-NP-20-0.5	6.85	0.70

4.8.5 Mixes Containing MK

Figure 4.56 to 4.61 show the free chloride profile for MK mixes, while Table 4.33 shows the apparent chloride diffusion coefficient (D_a) for the mix containing MK.

It is clear from the data in Table 4.33 that all MK mixes had lower diffusion coefficient than the control mix. Further, with increasing the percentage of expansive agent, the chloride diffusion coefficient went slightly up. Previous researches reported the same conclusion [167, 168]. The ratio of diffusion coefficient between the mixes containing MK as replacement to that of the control mix, varied between 19% to 50%.

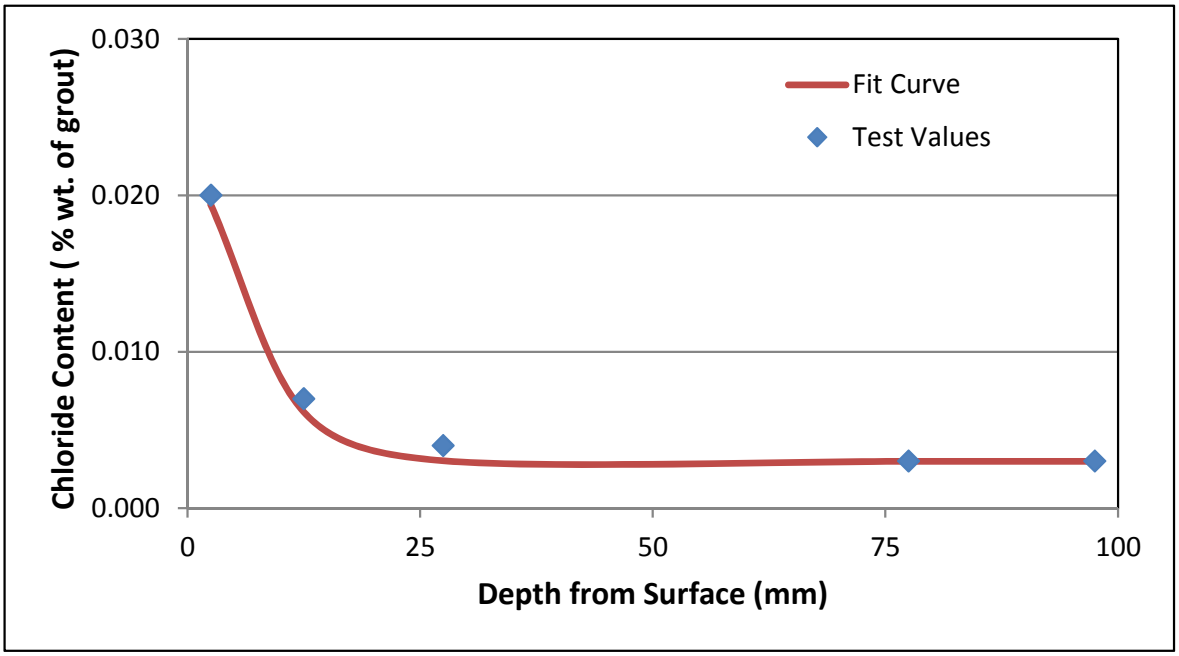

Figure 4.56: Free chloride profile for M20-MK-10-0.

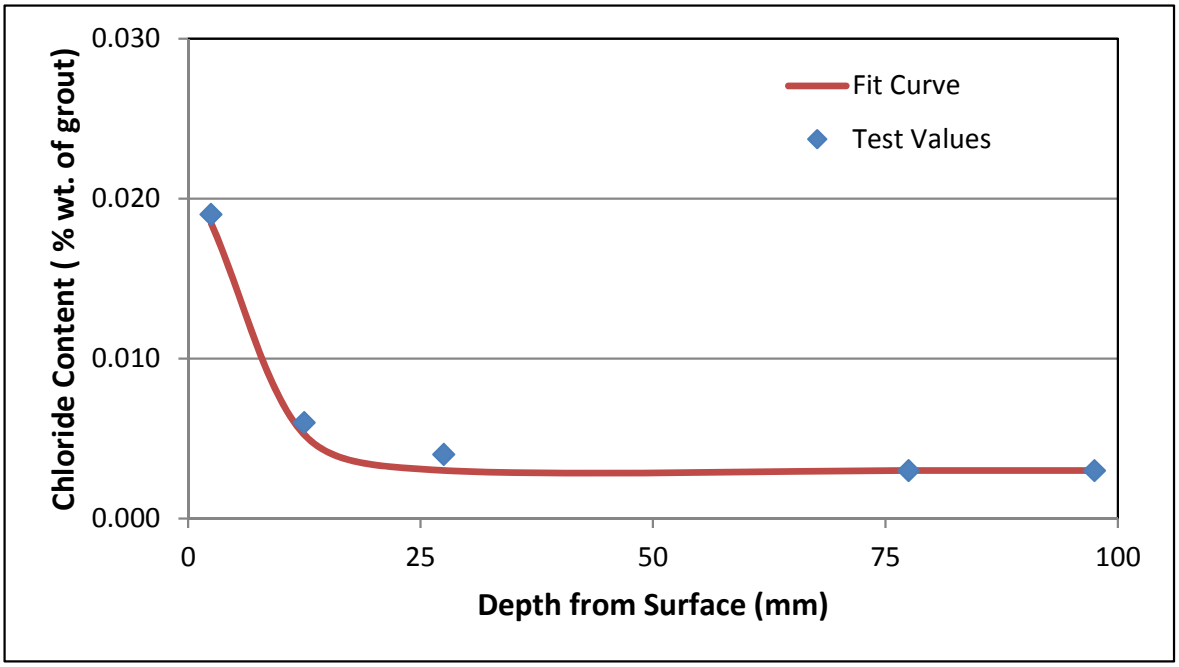

Figure 4.57: Free chloride profile for M21-MK-10-0.25.

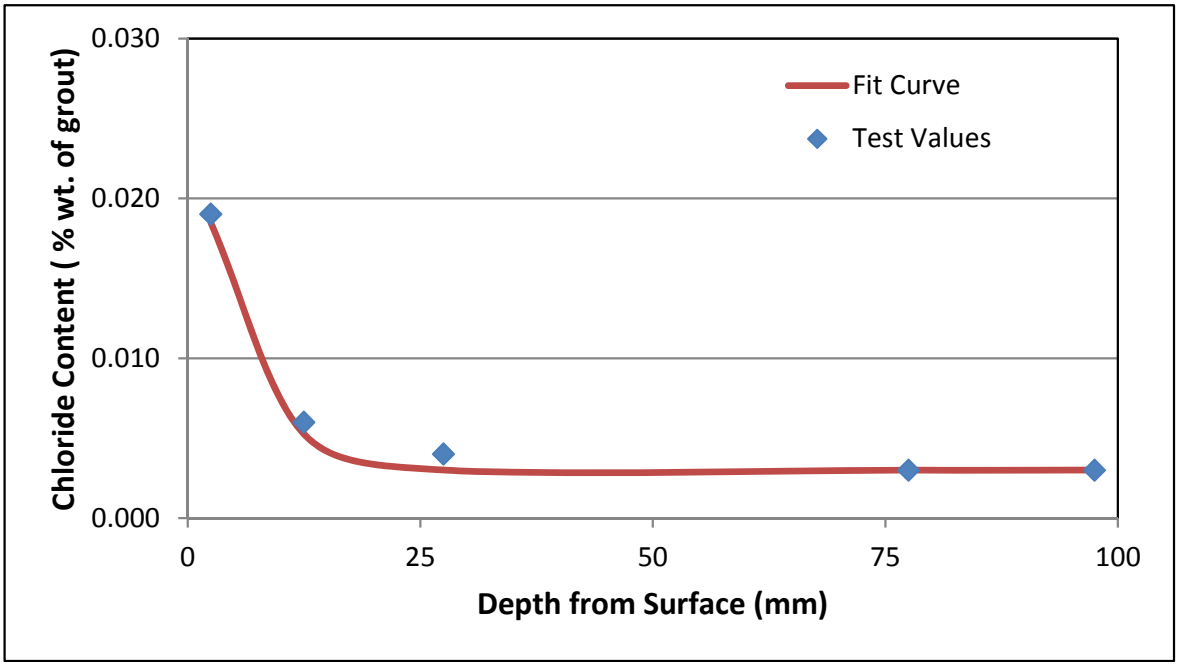

Figure 4.58: Free chloride profile for M22-MK-10-0.5.

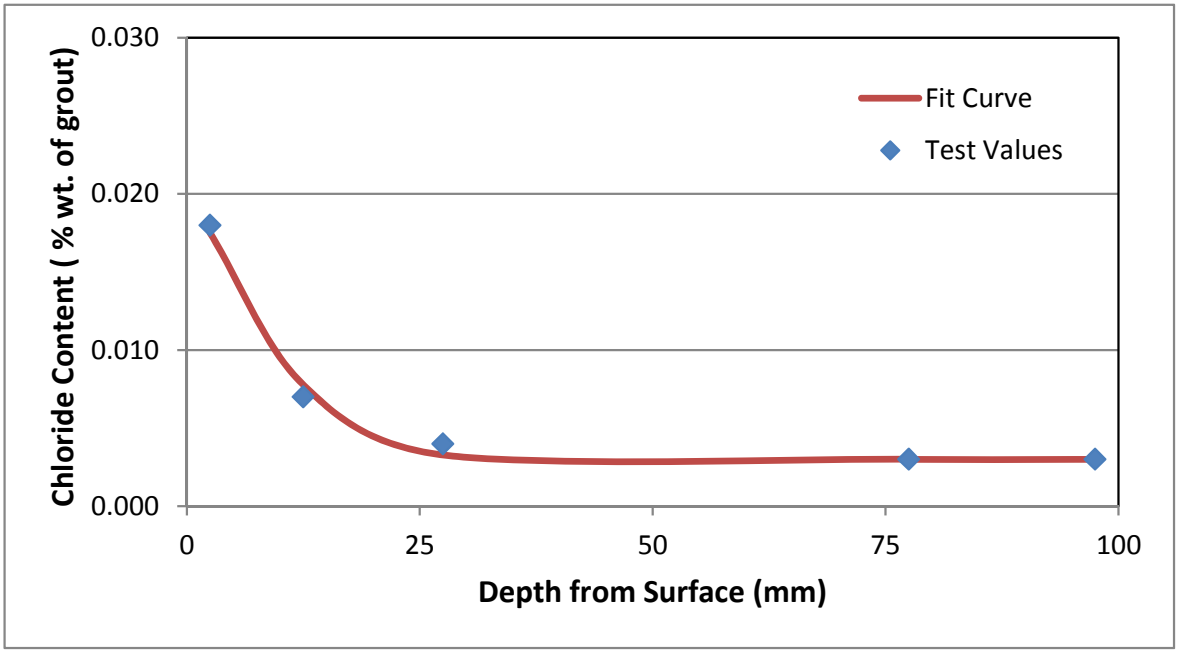

Figure 4.59: Free chloride profile for M23-MK-15-0.

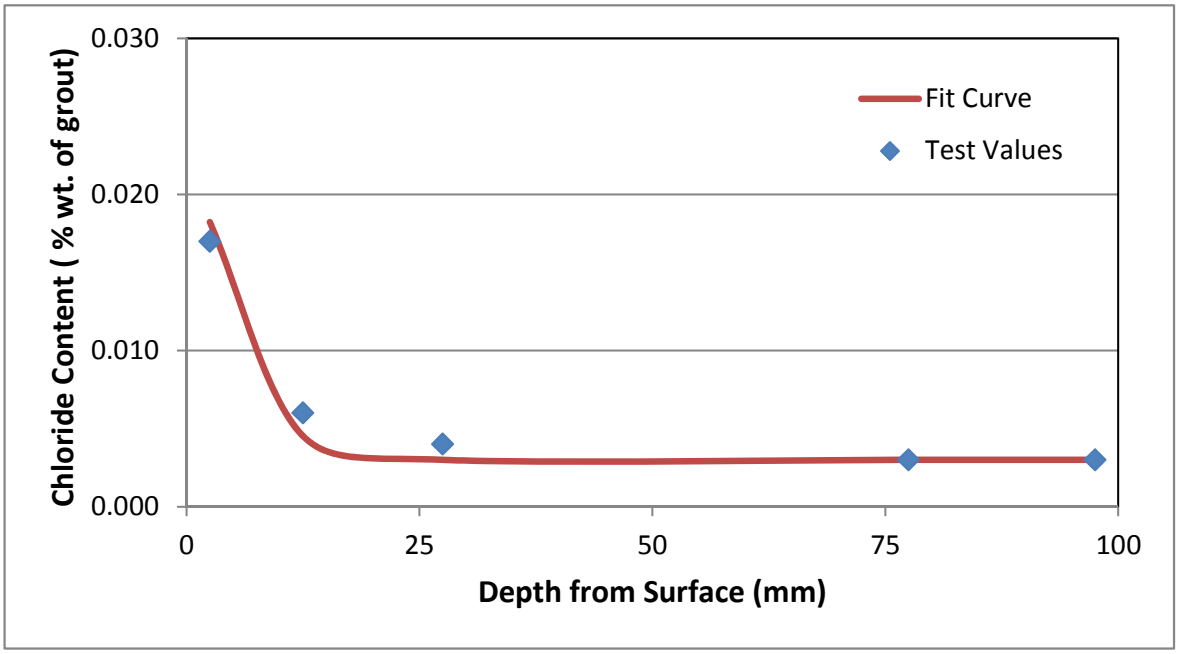

Figure 4.60: Free chloride profile for M24-MK-15-0.25.

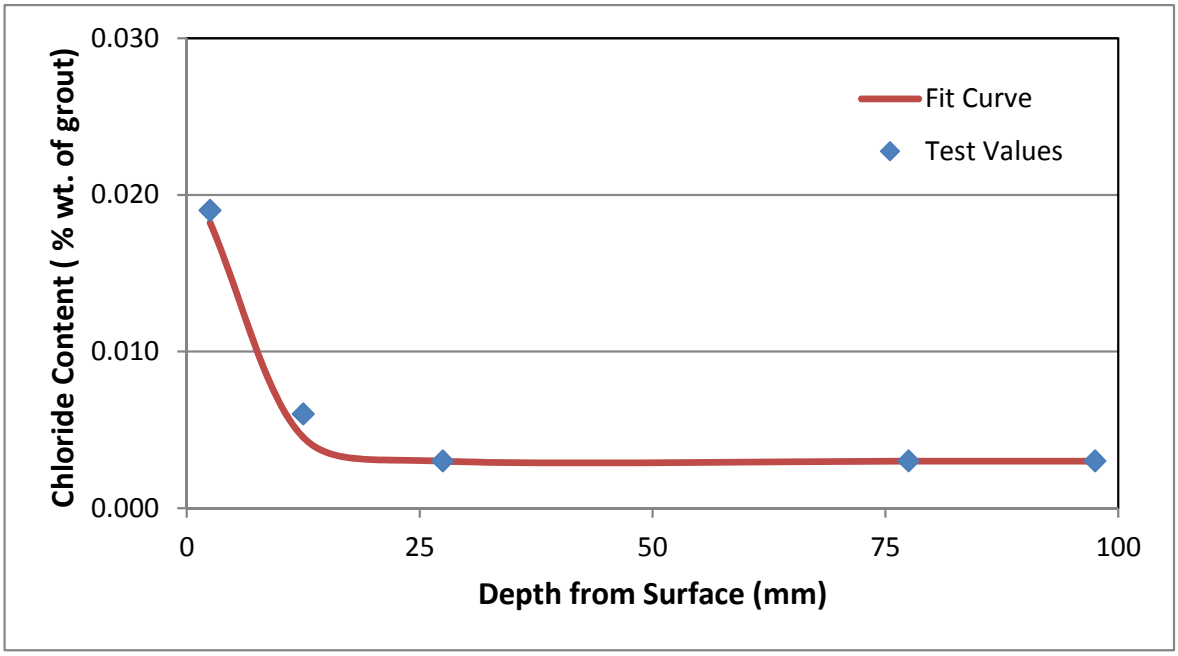

Figure 4.61: Free chloride profile for M25-MK-15-0.5.

Table 4.33: Diffusion coefficient, surface and initial concentration for mixes contain MK.

Mix ID	D_a ($\times$ 10^{-12} m^2/s)	**Ratio in terms of the control**
M1-Ctrl-0-0	9.81	1.00
M20-MK-10-0	2.86	0.29
M21-MK-10-0.25	3.10	0.32
M22-MK-10-0.5	4.90	0.50
M23-MK-15-0	1.82	0.19
M24-MK-15-0.25	2.94	0.30
M25-MK-15-0.5	3.54	0.36

4.8.6 Summary of Chloride Diffusion Coefficient for all Mixes

Table 4.34 summarizes the results of chloride diffusion coefficient for all mixes in this study. The data in this table indicate that the two commercial grouts and the control mix had the highest chloride diffusion coefficient, while the lowest values were attained by SF and MK mixes, specially at their high dosages. Furthermore, it can be easily noted that the chloride diffusion coefficient tended to increase marginally with the increase in the dosage of the expansive agent.

4.9 EXPECTED SERVICE LIFE

The service life of the different mixtures was estimated based on the following assumptions:

1. The diffusion rate is constant with depth into the specimen.
2. The cover to reinforcing steel is 50 mm (2 inches) for all specimens.
3. A free chloride threshold level of 0.02% by the total mass of grout is sufficient to depassivate the reinforcement [169].

The expected service life (t) was found by substituting ($C_{(x,t)}$ = 0.02), (x =50 mm) and the values of (D_a, C_s, and C_i) for each mix in Equation 2.4. Table 4.35 summarizes the expected service life for both the developed and commercial grouts.

The expected service life for the control mix was estimated to be 20 years, which is longer than both types of the commercial grouts, which had values of 15 and 17 years for Sika® grout-214 and Fosroc® Conbextra GP, respectively. This better performance of the control mix may be ascribed to the high quality of this mix in terms of low water to binder ratio (w/b = 0.32), cement content, fine aggregates, etc.

Since all the 24 developed grouts (M2 to M24) were similar to the control mix (M1) in terms of the mix design parameters, it is rational to expect longer service

Table 4.34: Diffusion coefficient, surface and initial concentration for mixes contain MK.

Mix ID	D_a ($\times$ $\mathbf{10^{-12}}$ $\mathbf{m^2/s}$)	**Ratio in terms of the control**
M1-Ctrl-0-0	9.81	1.00
M2-SF-5-0	7.85	0.80
M3-SF-5-0.25	7.91	0.81
M4-SF-5-0.5	7.94	0.81
M5-SF-10-0	5.51	0.56
M6-SF-10-0.25	5.61	0.57
M7-SF-10-0.5	6.20	0.63
M8-SF-15-0	2.43	0.25
M9-SF-15-0.25	2.87	0.29
M10-SF-15-0.5	3.03	0.31
M11-LSP-10-0	6.18	0.63
M12-LSP-10-0.25	6.23	0.64
M13-LSP-10-0.5	6.45	0.66
M14-LSP-20-0	5.51	0.56
M15-LSP-20-0.25	5.97	0.61
M16-LSP-20-0.5	6.02	0.61
M17-NP-20-0	4.81	0.49
M18-NP-20-0.25	5.51	0.56
M19-NP-20-0.5	6.85	0.70
M20-MK-10-0	2.86	0.29
M21-MK-10-0.25	3.10	0.32
M22-MK-10-0.5	4.90	0.50
M23-MK-15-0	1.82	0.19
M24-MK-15-0.25	2.94	0.30
M25-MK-15-0.5	3.54	0.36
M26-Sika® grout 214	11.5	1.17
M27-Fosroc® Conbextra GP	9.98	1.02

life for these grouts because part of the cement was exchanged with active/reactive material (i.e., SF, NP, LSP, MK).

As shown in Table 4.35, all the developed grouts had longer service life than the control mix. Their service life was in the range of 25 to 70 years for silica fume mixes, 26 to 31 years for limestone powder, 25 to 35 years for natural pozzolan, and 35 to 94 years for metakaolin mixes. Among all the developed mixes, the MK mixes had the longest expected service life followed by SF mixes.

Table 4.35: Predicted life for developed and commercial grouts

MIX ID	**Expected Life (years)**
M1-Ctrl-0-0	20
M2-SF-5-0	25
M3-SF-5-0.25	25
M4-SF-5-0.5	25
M5-SF-10-0	42
M6-SF-10-0.25	42
M7-SF-10-0.5	38
M8-SF-15-0	70
M9-SF-15-0.25	69
M10-SF-15-0.5	65
M11-LSP-10-0	28
M12-LSP-10-0.25	27
M13-LSP-10-0.5	26
M14-LSP-20-0	31
M15-LSP-20-.25	29
M16-LSP-20-0.5	28
M17-NP-20-0	35
M18-NP-20-0.25	31
M19-NP-20-0.5	25
M20-MK-10-0	60
M21-MK-10-0.25	55
M22-MK-10-0.5	35
M23-MK-15-0	94
M24-MK-15-0.25	58
M25-MK-15-0.5	48
M26-Sika® grout-214	15
M27-Fosroc® Conbextra GP	17

4.10 COST ANALYSIS

In order to compare the cost of the 25 investigated HPNSGs, the local unit costs of materials were collected from the manufacturers and quarries and presented in Table 4.37 through 4.41. It should be noted that the overall cost of grout production excludes the costs of transportation, handling, placement and quality control. A summary of the cost in Saudi Riyals per cubic meter is presented in Table 4.36 for the sake of relative comparison.

It is clear from the data in Table 4.36 that the cheapest mixes were the ones containing metakaolin as replacement, followed by limestone powder, natural pozzolan, while the most expensive ones were those containing silica fume as replacement. Furthermore, it could be noted that with increasing the percentage of expansive agent, the cost went up. Also, it is obvious that the cost of developed grouts was much less than that of both the commercial grouts used in this study. Hence, the principal objective of this research investigation has been fulfilled.

Table 4.36: Cost analysis for all mixes in this study.

Mix ID	**Cost SR/m^3**
M1-Ctrl-0-0	408
M2-SF-5-0	443
M3-SF-5-0.25	539
M4-SF-5-0.5	586
M5-SF-10-0	530
M6-SF-10-0.25	578
M7-SF-10-0.5	625
M8-SF-15-0	571
M9-SF-15-0.25	619
M10-SF-15-0.5	666
M11-LSP-10-0	340
M12-LSP-10-0.25	426
M13-LSP-10-0.5	465
M14-LSP-20-0	366
M15-LSP-20-.25	404
M16-LSP-20-0.5	443
M17-NP-20-0	448
M18-NP-20-0.25	535
M19-NP-20-0.5	574
M20-MK-10-0	355
M21-MK-10-0.25	441
M22-MK-10-0.5	479
M23-MK-15-0	398
M24-MK-15-0.25	436
M25-MK-15-0.5	475
M26-Sika grout-214	3080
M27-Fosroc Conbextra GP	3472

Table 4.37: Cost analysis for commercial grouts used in this study.

Type	**Density**	**Rate, SR/ton**	**Cost, SR/m^3**
M26-Sika® Grout-214	2200	1400	**3080**
M27-Fosroc® Conbextra GP	2170	1600	**3472**

Table 4.38: Cost analysis for SF HPNSG mixes used in this study.

MIX ID	Constituent	Cem. (kg)	SF (kg)	Wat. (L)	Sand (kg)	Agg. (kg)	SP (kg)	EXP. (kg)	Total
	Rate, SR\ton (Lit)	300	1200	0.2	40	75	5000	25000	
M1-Ctrl-0-0	Quantity kg/m^3	758.7	0.0	242.8	531.1	796.7	10.2	0.0	**408**
	Cost, SR/m^3	228	0	49	21	60	51	0	
M2-SF-5-0	Quantity kg/m^3	720.8	37.9	242.8	526.2	789.2	20.2	0.0	**443**
	Cost, SR/m^3	216	46	0	21	59	101	0	
M3-SF-5-0.25	Quantity kg/m^3	720.8	37.9	242.8	526.2	789.2	20.2	1.9	**539**
	Cost, SR/m^3	216	46	49	21	59	101	47	
M4-SF-5-0.5	Quantity kg/m^3	720.8	37.9	242.8	526.2	789.2	20.2	3.8	**586**
	Cost, SR/m^3	216	46	49	21	59	101	95	
M5-SF-10-0	Quantity kg/m^3	682.9	75.9	242.8	521.2	781.8	21.2	0.0	**530**
	Cost, SR/m^3	205	91	49	21	59	106	0	
M6-SF-10-0.25	Quantity kg/m^3	682.9	75.9	242.8	521.2	781.8	21.2	1.9	**578**
	Cost, SR/m^3	205	91	49	21	59	106	47	
M7-SF-10-0.5	Quantity kg/m^3	682.9	75.9	242.8	521.2	781.8	21.2	3.8	**625**
	Cost, SR/m^3	205	91	49	21	59	106	95	
M8-SF-15-0	Quantity kg/m^3	644.9	113.8	242.8	516.2	774.4	22.8	0.0	**571**
	Cost, SR/m^3	193	137	49	21	58	114	0	
M9-SF-15-0.25	Quantity kg/m^3	644.9	113.8	242.8	516.2	774.4	22.8	1.9	**619**
	Cost, SR/m^3	193	137	49	21	58	114	47	
M10-SF-15-0.5	Quantity kg/m^3	644.9	113.8	242.8	516.2	774.4	22.8	3.8	**666**
	Cost, SR/m^3	193	137	49	21	58	114	95	

Table 4.39: Cost analysis for LSP HPNSG mixes used in this study.

MIX ID	Constituent	Cem. (kg)	LSP (kg)	Wat. (L)	Sand (kg)	Agg. (kg)	SP (kg)	EXP. (kg)	Total
	Rate, SR\ton (Lit)	300	50	0.2	40	75	5000	25000	
M11-LSP-10-0	Quantity kg/m^3	682.9	75.8	242.8	507.1	760.7	10.7	0.0	**340**
	Cost, SR/m^3	204.9	3.8	0.0	20.3	57.1	53.7	0.0	
M12-LSP-10-0.25	Quantity kg/m^3	682.9	75.8	242.8	507.1	760.7	8.9	1.9	**426**
	Cost, SR/m^3	204.9	3.8	48.6	20.3	57.1	44.4	47.4	
M13-LSP-10-0.5	Quantity kg/m^3	682.9	75.8	242.8	507.1	760.7	7.2	3.8	**465**
	Cost, SR/m^3	204.9	3.8	48.6	20.3	57.1	35.8	94.8	
M14-LSP-20-0	Quantity kg/m^3	607.0	151.7	242.8	483.1	724.7	10.7	0.0	**366**
	Cost, SR/m^3	182.1	7.6	48.6	19.3	54.3	53.7	0.0	
M15-LSP-20-0.25	Quantity kg/m^3	607.0	151.7	242.8	483.1	724.7	8.9	1.9	**404**
	Cost, SR/m^3	182.1	7.6	48.6	19.3	54.3	44.4	47.4	
M16-LSP-20-0.5	Quantity kg/m^3	607.0	151.7	242.8	483.1	724.7	7.2	3.8	**443**
	Cost, SR/m^3	182.1	7.6	48.6	19.3	54.3	35.8	94.8	

Table 4.40: Cost analysis for NP HPNSG mixes used in this study.

MIX ID	Constituent	Cem. (kg)	NP (kg)	Wat. (L)	Sand (kg)	Agg. (kg)	SP (kg)	EXP. (kg)	Total
	Rate, SR\ton (Lit)	300	750.0	0.2	40	75	5000	25000	
M17-NP -20-0	Quantity kg/m^3	607.0	151.7	242.8	528.6	793.0	14.3	0.0	448
	Cost, SR/m^3	182.1	113.8	0.0	21.1	59.5	71.6	0.0	
M18-NP -20-0.25	Quantity kg/m^3	607.0	151.7	242.8	528.6	793.0	12.5	1.9	535
	Cost, SR/m^3	182.1	113.8	48.6	21.1	59.5	62.3	47.4	
M19-NP -20-0.5	Quantity kg/m^3	607.0	151.7	242.8	528.6	793.0	10.7	3.8	574
	Cost, SR/m^3	182.1	113.8	48.6	21.1	59.5	53.7	94.8	

Table 4.41: Cost analysis for MK HPNSG mixes used in this study.

MIX ID	Constituent	Cem. (kg)	MK (kg)	Wat. (L)	Sand (kg)	Agg. (kg)	SP (kg)	EXP. (kg)	Total
	Rate, SR\ton (Lit)	300	200	0.2	40	75	5000	25000	
M20-MK-10-0	Quantity kg/m^3	682.9	75.8	242.8	516.9	775.3	11.2	0.0	**355**
	Cost, SR/m^3	204.9	15.2	0.0	20.7	58.1	55.8	0.0	
M21-MK-10-0.25	Quantity kg/m^3	682.9	75.8	242.8	516.9	775.3	9.3	1.9	**441**
	Cost, SR/m^3	204.9	15.2	48.6	20.7	58.1	46.5	47.4	
M22-MK-10-0.5	Quantity kg/m^3	682.9	75.8	242.8	516.9	775.3	7.4	3.8	**479**
	Cost, SR/m^3	204.9	15.2	48.6	20.7	58.1	37.2	94.8	
M23-MK-15-0	Quantity kg/m^3	644.9	113.8	242.8	509.7	764.6	11.2	0.0	**398**
	Cost, SR/m^3	193.5	22.8	48.6	20.4	57.3	55.8	0.0	
M24-MK-15-0.25	Quantity kg/m^3	644.9	113.8	242.8	509.7	764.6	9.3	1.9	**436**
	Cost, SR/m^3	193.5	22.8	48.6	20.4	57.3	46.5	47.4	
M25-MK-15-0.5	Quantity kg/m^3	644.9	113.8	242.8	509.7	764.6	7.4	3.8	**475**
	Cost, SR/m^3	193.5	22.8	48.6	20.4	57.3	37.2	94.8	

CHAPTER 5

CONCLUSIONS, RECOMMENDATIONS AND FUTURE WORK

5.1 CONCLUSIONS

This research investigation was conducted to produce high performance non-shrinking grout utilizing the locally available materials, such as limestone powder, natural pozzolan, metakoline and silica fume. Several tests were conducted to assess the mechanical properties and durability characteristic of these grouts. Furthermore, cost analysis was conducted. Based on the experimental data obtained in this study, the following conclusions could be drawn:

5.1.1 Control Mix and Commercial Grouts

1. The compressive strength at 28 days for the control mix was 54.6 MPa, while it was 60.1 MPa for Sika®grout-214 and 63.1 MPa for Fosroc® grout Conbextra GP. The values of splitting tensile strength for these mixes at 28 days were 3.7, 4.1 and, 3.9 MPa, while at 28 days the modulus of elasticity was 28.4, 21.8 and,

32.9 GPa for the control mix, Sika®grout-214 and, Fosroc® grout Conbextra GP, respectively.

2. The drying shrinkage after 7 days for the control mix, Sika®-214 grout and Fosroc® Conbextra GP grout was: 240, 303 and 174 microns, respectively, as compared with 463, 588 and 632 microns after 259 days.

3. The ontrol mix and both commercial grouts were not active in corrosion after 250 days of exposure to the 5% chloride solution. All the three mixes were in intermediate corrosion risk zone. Further, the I_{corr} results indicted that all the rebars were in a passive condition after 90 days of exposure. The apparent chloride diffusion coefficient for the control mix, Sika® 214 grout, and Fosroc® Conbextra GP grout were: 9.80, 11.5, and 9.76 $\times$ 10^{-12} m^2/sec, respectively.

4. The expected service life was 20, 15 and, 17 years for the control mix, Sika® 214 grout, and Fosroc® Conbextra GP, with initial cost of 408, 3080 and 3472 SR/m^3 in the same order.

5.1.2 Mixes Containing Silica Fume

1. The HPNSG mixes containing silica fume exhibited high compressive strength. All the mixes had a compressive strength above 45.0 MPa, with an average 28-day strength of about 56.4 MPa, 57.0 MPa and 61.2 MPa for SF replaced by 5%, 10% and 15%, respectively, compared to 54.6 MPa to the control mix. The highest strength was 64.5 MPa, while the lowest one was 53.7 MPa. The splitting tensile strength had values between 3.5 to 4.1 MPa compared to 3.7 MPa to the control mix, and the modulus of elasticity was in the range of 28.4 to 32.9 GPa compared to 28.4 GPa for the control mix.

2. The drying shrinkage for SF mixes was in ranges 82 to 336 microns after 7 days, while it was 315 to 560 microns after 259 days. The influence of expansive

material on drying shrinkage of SF mixes indicated that the drying shrinkage was declined with increasing the dosage of expansive agent.

3. All SF blends had not been active in corrosion after 250 days of exposure to the 5% chloride solution. Most of the mixes were in the zone of low corrosion (less than 10% corrosion probability), while part of the mixes were in the intermediate corrosion risk zone. These results were backed up by the I_{corr} values which indicated that all the rebars were in a passive condition after 90 days of measurement. The apparent chloride diffusion coefficient for SF mixes was in the range of 2.90 to 7.85 $\times$ 10^{-12} m^2/sec.

4. The expected service life was in the range of 25 to 70 years with an initial cost between 443 to 666 SR/m^3.

5.1.3 Mixes Containing Limestone Powder

1. All the HPNSG mixes containing limestone powder had a strength exceeding 45.0 MPa. The average strength at 28 days was 51.7 MPa and 50.0 MPa with 10% and 20% of LSP replaced, respectively. Among all the six mixes, the lowest compressive strength at 28 days was 48.3 MPa and the highest one was 51.7 MPa. The splitting tensile strength values were between 3.4 to 3.7 MPa, and the modulus of elasticity was in the range of 26.6 to 28.5 GPa.

2. The drying shrinkage for LSP's mixes was in the ranges 158 to 215 microns, after 7 days, while it was 341 to 506 microns after 259 days.

3. All LSP blends were not active in corrosion after 250 days of exposure to the 5% chloride solution. Though all the mixes were in the low risk zone (less than 10% corrosion probability) at early age, part of the mixes were in the intermediate corrosion risk zone. Similar results were noted from the I_{corr} values that indicated

all the rebars were still in the passive condition after 90 days of exposure. The apparent chloride diffusion coefficient for LSP mixes was in the range 3.18 to 6.17 $\times$ 10^{-12} m^2/sec.

4. The expected service life was in the range of 26 to 31 years with an initial cost between 340 to 443 SR/m^3.

5.1.4 Mixes Containing Natural Pozzolan

1. All the three HPNSG mixes replaced by 20% natural pozzolan had strength greater than 45 MPa. The compressive strength at 28 days was in the range between 54.0 MPa and 59.4 MPa with an average of 57.0 MPa. The splitting tensile strength values were between 3.6 to 4.3 MPa, and the modulus of elasticity was in the range of 27.5 to 30.6 GPa.

2. The drying shrinkage for NP's mixes was in the range of 157 to 258 microns after 7 days, while it was 333 to 396 microns after 259 days. The drying shrinkage de-escalated when the expansive material was increased.

3. All the NP blends were not active in corrosion after 250 days of exposure to the 5% chloride solution. It was fluctuating between low to intermediate risk zones, with a general trend to decline with time and entering the low risk zone. The I_{corr} values matched that conclusion, after 90 days of exposure, whereby all the rebars were in the passive condition. The apparent chloride diffusion coefficient for NP mixes was in the range of 4.81 and 6.65 $\times$ 10^{-12} m^2/sec.

4. The expected service life was in the range of 25 to 35 years with an initial cost between 448 to 574 SR/m^3.

5.1.5 Mixes Containing Metakaolin

1. The HPNSG mixes containing metakaolin had high compressive strength, All the mixes had compressive strength above 45.0 MPa, with an average 28-day strength of about 63.1 MPa and 67.0 MPa for MK replacements of 10% and 15%, respectively. The highest strength was 73.5 MPa, while the lowest one was 58.5 MPa. The splitting tensile strength had values between 3.9 to 4.4 MPa, and the modulus of elasticity was in the range of 28.7 to 33.9 GPa.

2. The drying shrinkage for MK mixes was in the range of 91 to 280 microns after 7 days, while it was 317 to 495 microns after 259 days.

3. All the MK blends were not active in corrosion after 250 days of exposure to the 5% chloride solution. In spite of the fact that most of the mixes were in the low risk zone (less than 10% corrosion probability), part of the mixes were in the intermediate corrosion risk zone. The I_{corr} values coincided with that conclusion. After 90 days of measurement, rebars were still in the passive condition. The apparent chloride diffusion coefficient for SF mixes was in the range of 1.82 to 4.91×10^{-12} m^2/sec.

4. The expected life was in the range of 35 to 94 years with an initial cost between 355 to 475 SR/m^3.

5.1.6 Models for Splitting Tensile Strength and Modulus of Elasticity

The relationship between splitting tensile strength (f_{st}, MPa) and compressive strength (f'_c, MPa) at 28 days for the developed grouts in this study can expressed as follows:

$$f_{st} = 0.145(f'_c)^{0.81} \tag{5.1}$$

While the the relationship between modulus of elasticity (E_c, GPa) and compressive strength (f'_c, MPa) at 28 days for the developed grout in this study can expressed as follows:

$$E_c = 1.75(f'_c)^{0.702} \tag{5.2}$$

5.1.7 Summary of Results

Table 5.1 summarizes the results for the tests carried out in the study.

Table 5.1: Summary of results for the tests conducted in study.

#	Rep. Mat.	% of Rep.	% of Exp. Mat.	28 days f'_c (MPa)	28 days f_{st} (MPa)	28 days E (GPa)	Drying Shrink. @259 days (microns)	D_a ($\times 10^{-12}$ m^2/s)	Exp. Life (years)	Cost SR/m^3
1	-	0	0	54.6	3.7	28.4	497	9.80	20	408
2	**SF**	5	0	59.1	3.9	31.1	503	7.85	25	443
3			0.25	56.4	3.7	29.9	323	2.90	80	539
4			0.5	53.7	3.5	28.4	315	4.71	36	586
5		10	0	60.4	3.9	31	554	5.51	36	530
6			0.25	56.5	3.7	30.1	390	5.61	35	578
7			0.5	54.1	3.6	29	380	6.20	38	625
8		15	0	64.5	4.1	32.9	560	7.85	22	571
9			0.25	60.5	4.0	32.5	399	5.51	42	619
10			0.5	58.7	3.9	31	392	3.03	56	666
11	**LSP**	10	0	53.7	3.7	28.5	506	6.18	28	340
12			0.25	51.5	3.5	27.8	418	6.17	28	426
13			0.5	49.8	3.4	26.8	353	3.18	54	465
14		20	0	51.3	3.5	27.6	454	5.51	31	366
15			0.25	50.4	3.5	27	345	6.2	27	404
16			0.5	49.9	3.4	26.6	341	4.49	38	443
17	**NP**	20	0	66.9	4.3	30.6	396	6.85	25	448
18			0.25	57.3	3.9	29.1	380	5.51	31	535
19			0.5	53.8	3.6	27.5	333	4.81	35	574
20	**MK**	10	0	67.5	4.4	32.7	495	2.86	60	355
21			0.25	63.2	4.3	31.5	472	2.30	74	441
22			0.5	58.5	3.9	29	391	4.90	35	479
23		15	0	73.5	4.8	33.9	480	4.91	35	398
24			0.25	67.9	4.3	32.1	371	1.82	94	436
25			0.5	59.5	4.0	28.7	317	3.54	48	475
26	**Sika® Grout 214**				4.1	21.8	596	11.5	15	3080
27	**Fosroc® Conbextra GP**				3.9	32.9	637	9.98	17	3472

5.2 RECOMMENDATIONS

Based on the experimental results of this research program, the following recommendations could be stated:

1. Grouts made with SF, LSP, NP and MK are recommended for use in high strength applications (structural purpose with required compressive strength greater than 45 MPa), even where reinforcement corrosion is critical.

2. Grout prepared with NP is recommended for use where small shrinkage is required.

3. Grout prepared with MK is recommended where chloride diffusion is an issue.

4. Limit the quantity of expansive material to 0.25% by weight of powder (cement+ replacement material) to minimize excessive expansive and cracking.

5.3 RECCOMMENDATIONS FOR FUTURE RESEARCH WORKS

1. Long-term study on durability of HPNSG, particularly with regard to assessment of rebar corrosion monitoring, in addition to other durability properties of concrete (i.e., sulfate attack), is highly recommended.

2. The performance of the developed grouts may be evaluated in the field.

3. The other durability parameters of HPNSG grouts produced with these waste materials are to be investigated (i.e., under heat-cool and wet-dry cycles, resistance to carbonation, etc.).

REFERENCES

[1] C. U. Grosse, *Advances in Construction Materials 2007*. Springer Berlin Heidelberg, 2007.

[2] M. Grantham, "Diagnosis, Inspection, Testing and Repair of Reinforced Concrete Structures," in: *Advanced Concrete Technology Set*, J. Newman and B. S. Choo, Eds. Butterworth Heinemann, 2003, ch. 6, pp. 1–54.

[3] L. G. Baltazar, F. M. Henriques, F. Jorne, and M. Cidade, "Combined Effect of Superplasticizer, Silica Fume and Temperature in the Performance of Natural Hydraulic Lime Grouts," *Construction and Building Materials*, vol. 50, pp. 584–597, Jan. 2014.

[4] C. Maltese, C. Pistolesi, A. Lolli, A. Bravo, T. Cerulli, and D. Salvioni, "Combined Effect of Expansive and Shrinkage Reducing Admixtures to Obtain Stable and Durable Mortars," *Cement and Concrete Research*, vol. 35, no. 12, pp. 2244–2251, Dec. 2005.

[5] S. Tarr, "Demystifying Concrete Shrinkage," *Concrete Construction*, vol. 59, no. 9, pp. 41–48, 2012.

[6] F. H. Wittmann and Z. P. Bazant, *Creep and Shrinkage in Concrete Structures*. New York: Wiley Chichester, 1982.

[7] D. M. Harrison, *The Grouting Handbook: A Step-by-step Guide to Heavy Equipment Grouting*. Gulf Professional Publishing, 2000.

[8] D. Eklund and H. k. Stille, "Penetrability Due to Filtration Tendency of Cement-Based Grouts," *Tunnelling and Underground Space Technology*, vol. 23, no. 4, pp. 389–398, Jul. 2008.

[9] R. Glossop, "The Invention and Development of Injection Processes, Part II: 1850- 1960," *Geotechnical Engineering*, vol. 11, no. 4, pp. 255–279, 1960.

[10] J. Warner, *Practical Handbook of Grouting: Soil, Rock, and Structures*. Hoboken, New Jersey: John Wiley & Sons, 2004.

[11] A. Fran, "Recommendations on Grouting for Underground Works," *Tunnelling and Underground Space Technology*, vol. 6, pp. 383–385, 1991.

[12] R. a. Silva, L. Schueremans, D. V. Oliveira, K. Dekoning, and T. Gyssels, "On the Development of Unmodified Mud Grouts for Rpairing Earth Constructions: Rheology, Strength and Adhesion," *Materials and Structures*, vol. 45, no. 10, pp. 1497–1512, Mar. 2012.

[13] D. M. Harrison, *The Grouting Handbook: A Step-by-step Guide to Heavy Equipment Grouting*. Houston, Texas: Gulf Professional Publishing, 2000.

[14] R. Gothäll and H. k. Stille, "Fracture–Fracture Interaction During Grouting," *Tunnelling and Underground Space Technology*, vol. 25, no. 3, pp. 199–204, May 2010.

[15] C. A. Anagnostopoulos, "Effect of Different Superplasticisers on the Physical and Mechanical Properties of Cement Grouts," *Construction and Building Materials*, vol. 50, no. 2014, pp. 162–168, Jan. 2014.

[16] H. Wong and H. Abdul Razak, "Efficiency of Calcined Kaolin and Silica Fume as Cement Replacement Material for Strength Performance," *Cement and Concrete Research*, vol. 35, no. 4, pp. 696–702, Apr. 2005.

[17] V.-H. Nguyen, S. Remond, and J.-L. Gallias, "Influence of Cement Grouts Composition on the Rheological Behaviour," *Cement and Concrete Research*, vol. 41, no. 3, pp. 292–300, Mar. 2011.

[18] R. Bowen, *Grouting in Engineering Practice*, 2nd ed. London: Apply Science, 1981.

[19] E. Nonveiller, *Grouting Theory and Practice*. Amsterdam: Elsevier BV, 1989.

[20] R. L. Rowan, "A History of the Development of Epoxy Grout," 2003. [Online]. Available: http://www.lmcc.com/concrete_news/0301/history_of_epoxy_grout.asp

[21] M. Chanqui, "How many Components in a Grout Mix?" *Geotechnical News*, vol. 24, no. 1, pp. 52–57, 2006.

[22] K. H. Khayat, A. Yahina, and P. Duffy, "High Performance Cement Grout for Post-Tensioning Applications," *ACI Materials Journal*, vol. 96, no. 4, pp. 471–477, 1999.

[23] A. J. Schokker, B. D. Koester, J. E. Breen, and M. E. Kreger, "Development of High Performance Grouts for Bonded Post-tensioned Structures," Center for Transportation Research, Bureau of Engineering Research, University of Texas at Austin, Texas, Tech. Rep. October, 1999.

[24] P. Domone and S. Jefferis, "Structural Grouts," P.L.J.Domone, Ed. Taylor & Francis, 1993.

[25] S. K. Lim, C. S. Tan, K. P. Chen, M. L. Lee, and W. P. Lee, "Effect of Different Sand Grading on Strength Properties of Cement Grout," *Construction and Building Materials*, vol. 38, pp. 348–355, Jan. 2013.

[26] A. Bras, F. M. Henriques, and M. Cidade, "Effect of Environmental Temperature and Fly Ash Addition in Hydraulic Lime Grout Behaviour," *Construction and Building Materials*, vol. 24, no. 8, pp. 1511–1517, Aug. 2010.

[27] A. Bras, R. Gião, V. Lúcio, and C. Chastre, "Development of an Injectable Grout for Concrete Repair and Strengthening," *Cement and Concrete Composites*, vol. 37, pp. 185–195, Mar. 2013.

[28] B. Felekoğlu, "Optimization of Self-Compacting Filling Grout Mixtures for Repair Purposes," *Construction and Building Materials*, vol. 22, no. 4, pp. 660–667, Apr. 2008.

[29] M. Axelsson, G. Gustafson, and A. Fransson, "Stop Mechanism for Cementitious Grouts at Different Water-to-Cement Ratios," *Tunnelling and Underground Space Technology*, vol. 24, no. 4, pp. 390–397, Jul. 2009.

[30] A. Miltiadou-Fezans and T. P. Tassios, "Penetrability of hydraulic grouts," *Materials and Structures*, vol. 46, no. 10, pp. 1653–1671, Jan. 2013.

[31] P. C. Hewlett and I. Odler, *Lea's Chemistry of Cement and Concrete*. Amsterdam, Netherlands: Elsevier, 2003.

[32] J. P. Guyer, F. Asce, and F. Aei, "An Introduction to Soil Grouting," New York, 2009.

[33] O. S. B. Al-Amoudi, M. Maslehuddin, M. Shameem, and M. Ibrahim, "Shrinkage of Plain and Silica Fume Cement Concrete Under Hot Weather," *Cement and Concrete Composites*, vol. 29, no. 9, pp. 690–699, Oct. 2007.

[34] V. Malhotra, "Fly Ash, Silca Fume, Slag and Natural Pozzolans in Concrete," in: *Proc., 2nd Int. Conf. Fly Ash, Silica Fume, Slag, and Natural Pozzolans in ConcreteI nternational Conference*. Detroit, MI (USA): American Concrete Institute, 1986, pp. 839–860.

[35] N. Barker, "Resistance of Microsilica Concrete to Steel Corrosion, Erosion and Chemical Attack," in: *Proc., 3rd Int. Conf. Fly Ash, Silica Fume, Slag, and Natural Pozzolans in Concrete*, V.M. Malhotra, Ed. Trondheim, Norway: American Concrete Institute, 1996, pp. 861–886.

[36] U. Diederichs and K. Schutt, "Silica Fume Modified Grouts for Corrosion Protection of Post- Tensioning Tendons," in: *Proc., 3rd Int. Conf. Fly Ash, Silica Fume, Slag, and Natural Pozzolans in Concrete*, V. Malhotra, Ed. Trondheim, Norway: American Concrete Institute, 1996, pp. 1173–1195.

[37] P. L. Domone and B. TankS, "Use of Condensed Silica Fume in Portland Cement Grouts." in: *Proc., 2nd Int. Conf. Fly Ash, Silica Fume, Slag, and Natural Pozzolans in Concrete*, V.M. Malhotra, Ed. Madrid, Spain: American Concrete Institute, 1986, pp. 1232–1260.

[38] P. Fidjestol, "Reinforcement Corrosion and the Use of CSF-Based Additives," in: *Concrete Durability: Katherine and Bryant Mather International Conference, ACI SP-100*, J. M. Scanlon, Ed., vol. 100, 1987, pp. 243–256.

[39] D. R. Lankard, M. M. Sprinkel, Y. P. Virmani, and N. Thompson, "Grouts for Bonded Post-Tensioned Concrete Construction: Protecting Prestressing Steel From Corrosion," *Materials Journal*, vol. 90, no. 5, pp. 406–414, 1993.

[40] E. Ranish, F. Rostasy, and F. Herschelmann, "Properties of Cement Grouts with Silica Fume Addition for the Injection of Post Tensioning Ducts." in: *Proc., 3rd Int. Conf. Fly Ash, Silica Fume, Slag, and Natural Pozzolans in Concrete*, V.M. Malhotra, Ed. Trondheim, Norway: American Concrete Institute, 1996, pp. 1159–1171.

[41] E.-H. Kadri, S. Aggoun, and G. De Schutter, "Interaction Between C_3A, Silica Fume and Naphthalene Sulphonate Superplasticiser in High Performance Concrete," *Construction and Building Materials*, vol. 23, no. 10, pp. 3124–3128, Oct. 2009.

[42] A. A. Almusallam, H. Beshr, M. Maslehuddin, and O. S. B. Al-Amoudi, "Effect of Silica Fume on the Mechanical Properties of Low Quality Coarse Aggregate Concrete," *Cement and Concrete Composites*, vol. 26, no. 7, pp. 891–900, Oct. 2004.

[43] K. O. Kjellsen, O. H. Wallevik, and M. Hallgren, "On the Compressive Strength Development of High Performance Concrete and Paste - Effect of Silica Fume," *Materials and Structures*, vol. 32, pp. 63–69, 1999.

[44] D. Whiting, *Silica Fume Concrete for Bridge Decks*, 4th ed. Washington D.C: Transportation Research Board, 1998.

[45] P. Aitcin, G. Ballivy, and R. Parizeau, "The Use of Condensed Silica Fume in Grouts," Detroit, pp. 1–18, 1984.

[46] O. S. Baghabra Al-Amoudi, M. Maslehuddin, and T. O. Abiola, "Effect of Type and Dosage of Silica Fume on Plastic Shrinkage in Concrete Exposed to Hot Weather," *Construction and Building Materials*, vol. 18, no. 10, pp. 737–743, Dec. 2004.

[47] S. Popovics, "Portland Cement-Fly Ash-Silica Fume Systems in Concrete," *Advanced Cement Based Materials*, vol. 1, no. 2, pp. 83–91, Dec. 1993.

[48] Wikipedia.org, "Limestone," 2014. [Online]. Available: http://en.wikipedia.org/wiki/Limestone

[49] B. Tsivilis, S., G. Chaniotakis, G. Grigoriadis, and D. Theodossis, "Properties and Behavior of Limestone Cement Concrete and Mortar," *Cement and Concrete Research*, vol. 30, pp. 1679–1683, 2000.

[50] A. Yahia, M. Tanimura, and A. Shimabukuro, "Effect of Limestone Powder on Rheological Behaviour of Highly Flowable Mortar," *Japan Concrete Institute*, vol. 21, no. 2, pp. 559–564, 1999.

[51] Y. Git and U. Urkel, "The Effect of Limestone Powder , Fly Ash and Silica Fume on The Properties of Self-Compacting Repair Mortars," *Sadhana*, vol. 34, no. April, pp. 331–343, 2009.

[52] H. Fujiwara, S. Nagataki, N. Otsuki, and H. Endo, "Study on Reducing Unit Powder Content on Highfluidity Concrete by Controlling Powder Particle Size Distribution," *Concrete Library International*, vol. 28, pp. 117–128, 1996.

[53] J. J. Domone P J, "Properties of Mortar for Self-Compacting Concrete," in: *1st Int. Rilem Symposium on Self-Compacting Concrete*. (SARL, Stockholm: RILEM Publications), 1999, pp. 109–120.

[54] I. Alp, H. Deveci, Y. H. Süngün, A. O. Yilmaz, A. kesi Mal, and E. Yilmaz, "Material for Use in Blended Cements," *Iranian Journal of Science and Technology, Transaction B, Engineering*, vol. 33, no. B4, pp. 291–300, 2009.

[55] J. Justs, G. Shakhmenko, D. Bajare, and T. Nikolajs, "Comparsion of Pozzolanic Additives for Normal and High Strength Concrete," in: *Proc., 8th Int. Scientific and Practical Conference*, vol. 2. Environment Technology Resources, 2011, pp. 79–84.

[56] M. Mouli and H. Khelafi, "Performance Characteristics of Lightweight Aggregate Concrete Containing Natural Pozzolan," *Building and Environment*, vol. 43, no. 1, pp. 31–36, 2008.

[57] E. Rodriguez-Camacho and R. Uribe-Afif, "Importance of Using the Natural Pozzolans on Concrete Durability," *Cement and Concrete Research*, vol. 32, pp. 1851–1858, 2002.

[58] F. Massazza, "Pozzolanic Cements," *Cement and Concrete Composites*, vol. 15, no. 4, pp. 185–214, 1993.

[59] N. Terzibaşıoğlu, "Usability of Andesite in Production of Trass Cements," in: *Proc., Industrial Minerals Symp.* Ontario: NRC Research Press, 1995, pp. 1–7.

[60] I. M. Khan and M. A. Alhozaimy, "Performance of Concrete Utilizing the Natural Pozzolanic Material Avilable in the Kindom of Saudi Arabia," King Saud University, College of Engineering, Research Center, Final Research Report No. 423 / 33, Tech. Rep. 423, 2005.

[61] R. S. Nicolas, M. Cyr, and G. Escadeillas, "Performance-based Approach to Durability of Concrete Containing Flash-Calcined Metakaolin as Cement Replacement," *Construction and Building Materials*, vol. 55, pp. 313–322, 2014.

[62] J. Ambroise, S. Maximilien, and J. Pera, "Properties of Metakaolin Blended Cements," *Advanced Cement Based Materials*, vol. 1, no. 4, pp. 161–168, 1994.

[63] S. Wild, J. M. Khatib, and A. Jones, "Relative Strength, Pozzolanic Activity and Cement Hydration in Superplasticised Metakaolin Concrete," *Cement and Concrete Research*, vol. 26, no. 10, pp. 1537–1544, 1996.

[64] CSA, *2004a. CAN/CSA S304.1-04 Design of Masonry Structures*. Mississauga, Ontario: Canadian Standards Association, 2014.

[65] B. Gerwick, *Construction of Prestressed Concrete Structures*. New York: John Wiley and Sons, Inc, 1993.

[66] P. Banfill, "Additivity Effects in the Rheology of Fresh Concrete Containing Water-Reducing Admixtures," *Construction and Building Materials*, vol. 25, no. 6, pp. 2955–2960, Jun. 2011.

[67] M. Collepardi, A. Borsoi, S. Collepardi, O. Olagot, J. Jacob, and R. Troli, "Effects of Shrinkage Reducing Admixture in Shrinkage Compensating Concrete Under Non-Wet Curing Conditions," *Cement and Concrete Composites*, vol. 27, no. 6, pp. 704–708, Jul. 2005.

[68] S. Chatterji and J. Jeffery, "The Volume Expansion of Hardened Cement Paste due to the Presence of 'Dead Burned' CaO," *Magazine of Concrete Research*, vol. 19, no. 55, pp. 65–68, 1966.

[69] S. Shh, M. Krguller, and M. Sarigaphuti, "Effects of Shrinkage-reducing Admixtures on Restrained Shrinkage Cracking of Concrete," *ACI Materials Journal*, vol. 89, no. 3, pp. 232–245, 1992.

[70] F. Rajabipour, G. Sant, and J. Weiss, "Interactions between shrinkage reducing admixtures (SRA) and cement paste's pore solution," *Cement and Concrete Research*, vol. 38, no. 5, pp. 606–615, 2008.

[71] L. Zongjin, *Advanced Concrete Technology*. Hoboken, New Jersey: John Wiley \& Sons, 2011.

[72] J. F. Lamond and J. H. Pielert, *Significance of tests and properties of concrete and concrete-making materials*. ASTM International, 2006, vol. 169.

[73] H. S. Steinour, "Concrete Mix Water - How Impure Can It Be?" Tech. Rep. 3, 1960.

[74] M. Eriksson, M. Friedrich, and C. Vorschulze, "Variations in The Rheology and Penetrability of Cement-Based Grouts—an Experimental Study," *Cement and Concrete Research*, vol. 34, no. 7, pp. 1111–1119, Jul. 2004.

[75] L. Maia, H. Figueiras, S. Nunes, M. Azenha, and J. Figueiras, "Influence of Shrinkage Reducing Admixtures on Distinct SCC mix Compositions," *Construction and Building Materials*, vol. 35, pp. 304–312, Oct. 2012.

[76] P. Klieger, "Effect of Mixing and Curing Temperature on Concrete Strength," *ACI Journal Proceedings*, vol. 54, no. 6, pp. 1063–1081, 1958.

[77] P. C. Aïtcin, *High Performance Concrete*. CRC Press, 2011.

[78] E. G. Nawy, *Concrete Construction Engineering Handbook*, 2nd ed. Florida: CRC press, 2008.

[79] A. M. Neville, *Properties of Concrete*, 4th ed. New York: Wiley, 1997.

[80] R. G. Harwood and I. E. Tebbett, "The Assessment of Grout Compressive Strength by Destructive Testing," The Strength of Grouted Pile Sleeve Connections. Phase IV. Dept of Energy Report No. ST97/81A, London, Tech. Rep., 1981.

[81] R. A. Helmuth and D. M. Turk, "The Reversible and Irreversible Drying Shrinkage of Hardened PPortland Cement and Tricalcium Silicate Paste," *Portland Cement Association Journal Research and Development Laboratories*, vol. 9, 1967.

[82] P. Bamforth and D. Pocock, "Minimising the risk of chloride induced corrosion by selection of concreting materials," *Corrosion of Reinforcement in Concrete*, pp. 119–131, 1990.

[83] S. J. Thomas, M D A Pantazopoulou and B. Martin-Perez, "Service Life Modelling of Reinforced Concrete Structures Exposed to Chlorides - A Literature Review," Ministry of Transportation, Ontario, Ontario, Tech. Rep., 1995.

[84] S. Mindess, J. Young, and D. Darwin, *Concret*. New York: Pearson Education, Inc, 2003.

[85] W. H. Beyer, *CRC Handbook of Mathematical Sciences*, 5th ed. Florida: CRC Press, 1978.

[86] C. L. Page, N. R. Shert, and A. El Tarras, "Diffusion of Chloride Ions in Hardened Cement Paste," *Cement and Concrete Research*, vol. 11, no. 3, pp. 198–202, 1981.

[87] P. H. Emmons and A. M. Vaysburd, "Performance Criteria for Concrete Repair Materials, Phase I," Technical Report REMR-CS-47, Structural Preservation Systems, Inc., Baltimore,, Tech. Rep., 1995.

[88] R. W. Carlson, "Drying Shrinkage of Concrete as Affected by Many Factors," *American Society of Testing Materialsiety*, 1938.

[89] E. E. Holt, *Early Age Autogenous Shrinkage of Concrete*, 4th ed. Espoo: Technical Research Centre of Finland, 2001.

[90] D. Ravina and R. Shalon, "Tensile Stress and Strength of Fresh Mortar Subjected to Evaporation." in: *Proc., RILEM Int. Symp. on Concrete and Reinforced Concrete in Hot Countries.* Haifa: Israel Institute of Technology, 1971, pp. 275–296.

[91] I. Soroka, *Portland Cement Paste and Concrete.*New York: Chemical Publishing Co., Inc., 1980.

[92] M. M. Smadi, F. O. Slate, and A. H. Nilson, "Shrinkage and Creep of High-, Medium-, and Low-Strength Concretes, Including Overloads," *ACI Materials Journal*, vol. 84, no. 3, pp. 224–234, 1987.

[93] T. C. Powers, "Causes and Control of Volume Change," *Journal PCA Research Laboratories*, vol. 1, no. 1, pp. 29–39, 1959.

[94] O. Ishai, "The Time Dependent Deformation Behavior of Concrete Paste, Mortar and Concrete." in: *Proc., Int. Conf. on the Structure of Concrete and Its Behavior Under Load.* London: Cement and Concrete Association, 1965, pp. 345–364.

[95] R. L. Blaine, "A Statistical Study of the Shrinkage of Neat Cement Paste and Concretes," in: *Proc., Int. Colloq. on Shrinkage of Hydraulic Concretes*, RILEM/Cembureau, Ed., Madrid, 1968.

[96] R. G. L'Hermite, "Le Retrait des Ciments et Betons," *Inst. Technique du Batiment et des Travaux Publics*, 1947. [Online]. Available: http://trid.trb.org/view.aspx?id=1068617

[97] R. Dutron, ""Le retrait des ciments et betons," *Ann. Trav. Publ. de Belgique.*, 1934. [Online]. Available: https://tel.archives-ouvertes.fr/tel-00523299/

[98] O. Graf, *Versuche über Das Schwinden.* Berlin: Ernst, 1933. [Online]. Available: http://trid.trb.org/view.aspx?id=1034156

[99] P. Haller, *Schwinder und Kriechen von Mörtels und Beton*, Zurich, Discussionsbericht, 1940. [Online]. Available: link.springer.com/content/pdf/10.1007/978-3-662-30424-2_24.pdf

[100] H. Roper, J. E. Cox, and B. Erlin, "Petrographic Studies on Concrete Containing Shrinking Aggregate," *Journal of PCA, Research and Development Laboratories*, vol. 6, no. 3, pp. 43–56, 1964.

[101] B. Tremper and D. L. Spellman, "Shrinkage of Concrete-Comparison of Laboratory and Field Performance," *Highway Research Record*, vol. 3, 1963.

[102] R. C. Meininger, "Drying Shrinkage of Concrete," *Engineering Report No. RD3 (A Summary of Joint Research Laboratory Series J–135, J–145, and 173)*, vol. 143, 1966.

[103] P. Tattersall, Geoffrey Howarth Banfill, *The Rheology of Fresh Concrete*. Boston: Pitman Advanced Pub. Program, 1983.

[104] B. De Paoli, B. Bosco, R. Granata, and D. Bruce, "Fundamental Observations On Cement Based Grouts (1): Traditional Materials," *Grouting, Soil Improvement and Geosynthetics, ASCE, New Orleans*, pp. 474–485, 1992.

[105] L. G. Schwarz and R. J. Krizek, "Effects of Mixing on Rheological Properties of Microfine Cement Grout," in: *Proc., Grouting, Soil Improvement and Geosynthetics*. ASCE, 1992, pp. 512–525.

[106] K. Kong-Sio, "Properties Of Cement Based Permeation Grout Used In Ground Engineering," Ph.D. dissertation, 2006.

[107] J. Page, "The Effect of High Shear Mixing on The Heat Release of Cement Grouts," Queen Mary and Westfield College Internal Report, University of London, Tech. Rep., 1991.

[108] ASTM, "Standard Specification for Grout for Masonry," Philadelphia, pp. 1–10, 1999.

[109] "ASTM C 230, Standard Specification for Flow Table for Use in Tests of Hydraulic Cement," Philadelphia, pp. 1–7, 2013.

[110] ASTM, "Standard test method for compressive strength of hydraulic cement mortars (Using 2-in. or cube specimens)," Philadelphia, pp. 1–10, 2002.

[111] "ASTM C 157 Standard Test Method for Length Change of Hardened Hydraulic-Cement Mortar and Concrete," Philadelphia, pp. 1–7, 2008.

[112] "ASTM C 876 Standard Test Method for Half-cell Potentials of Uncoated Reinforcing Steel in Concrete," Philadelphia, 2005.

[113] M. Stern and A. L. Geary, "Electrochemical Polarization: A Theoretical Analysis of the Shape of Polarization Curves," *Journal of the Electrochemical Society*, vol. 104, no. 1, pp. 56–63, 1957.

[114] M. Raupach, B. Elsener, R. Polder, and J. Mietz, *Corrosion of Reinforcement in Concrete: Monitoring, Prevention and Rehabilitation Techniques*. Cambridge: Woodhead Publishing Limited, 2014.

[115] B. Elsener, S. Muller, M. Suter, and H. Bohnl, "Corrosion Monitoring of Steel in Concrete - Theory and Practice," *Corrosion of Reinforcement in Concrete*, pp. 348–357, 1990.

[116] A. Sagues and A. Alberto, "Corrosion Measurement Techniques for Steel in Concrete," in: *Proc., Corrosion National Association of Corrosion Engineers Annual Conference*. Florida: NACE, 1993, pp. 1–22.

[117] B. Uzal and L. Turanli, "Studies on Blended Cements Containing a High Volume of Natural Pozzolans," *Cement and Concrete Research*, vol. 33, no. 11, pp. 1777–1781, 2003.

[118] A. C. Andrade C., Castelo V., "Determination of the Corrosion Rate of Steel Embedded in Concrete," *STP 906, American Society for Testing and Materials, Philadelphia*, pp. 43–63, 1986.

[119] P. Lambert, C. L. Page, and P. R. W. Vassie, "Investigations of Reinforcement Corrosion. 2. Electrochemical Monitoring of Steel in Chloride-Contaminated Concrete," *Materials and Structures*, vol. 24, no. 5, pp. 351–358, 1991.

[120] O. S. B. Al-Amoudi, M. Maslehuddin, and M. Ibrahim, "Long-term Performance of Fusion-Bonded Epoxy-coated Steel Bars in Chloride-contaminated Concrete," *ACI Materials Journal*, vol. 101, no. 4, pp. 303–309, 2004.

[121] A. W. Saak, H. M. Jennings, and S. Shah, "New Methodology for Designing Self-Compacting Concrete," *ACI Materials Journal*, vol. 98, no. 6, pp. 429–439, 2001.

[122] J. Assaad, K. H. Khayat, and H. Mesbah, "Assessment of Thixotropy of Flowable and Self- Consolidating Concrete," *ACI Materials Journal*, vol. 100, no. 2, pp. 99–107, 2003.

[123] C. Meyer, "The Greening of the Concrete Industry," *Cement and Concrete Composites*, vol. 31, no. 8, pp. 601–605, 2009.

[124] O. Gencel, C. Ozel, W. Brostow, and G. Martínez-Barrera., "Mechanical Properties of Self-Compacting Concrete Reinforced with Polypropylene Fibres," *Materials Research Innovations*, vol. 15, no. 3, pp. 216–225, 2011.

[125] S. Liu and P. Yan, "Effect of Limestone Powder on Microstructure of Concrete," *Journal of Wuhan University of Technology, Materials Science Edition*, vol. 25, no. 2, pp. 328–331, 2010.

[126] V. Bosiljkov, "SCC Mixes with Poorly Graded Aggregate and High Volume of Limestone Filler," *Cement and Concrete Research*, vol. 33, no. 9, pp. 1279–1286, 2003.

[127] B. T. R. Naik, F. Canpolat, and A. Science, "Limestone Powder Use in Cement and Concrete," Department of Civil Engineering and Mechanics College of Engineering and Applied Science The University OF Wisconsin, Milwaukee, Tech. Rep. July, 2003.

[128] M. Shannag, "High Strength Concrete Containing Natural Pozzolan and Silica Fume," *Cement and Concrete Composites*, vol. 22, no. 6, pp. 399–406, Dec. 2000.

[129] M. J. Shannag and A. Yeginobali, "Properties of Pastes, Mortars and Concretes Containing Natural Pozzolan," *Cement and Concrete Research*, vol. 25, no. 3, pp. 647–657, 1995.

[130] B. Sabir, S. Wild, and J. Bai, "Metakaolin and Calcined Clays as Pozzolans for Concrete: A Review," *Cement and Concrete Composites*, vol. 23, no. 6, pp. 441–454, 2001.

[131] A. Ramezanianpour and H. Bahrami Jovein, "Influence of Metakaolin as Supplementary Cementing Material on Strength and Durability of Concretes," *Construction and Building Materials*, vol. 30, pp. 470–479, 2012.

[132] K. Melo and A. Carneiro, "Effect of Metakaolin's Finesses and Content in Self-Consolidating Concrete," *Construction and Building Materials*, vol. 24, no. 8, pp. 1529–1535, 2010.

[133] J. Khatib, "Performance of Self-Compacting Concrete Containing Fly Ash," *Construction and Building Materials*, vol. 22, no. 9, pp. 1963–1971, 2008.

[134] E. Güneyisi, M. Gesoğlu, and K. Mermerdaş, "Improving Strength, Drying Shrinkage, and Pore Structure of Concrete using Metakaolin," *Materials and Structures*, vol. 41, no. 5, pp. 937–949, 2008.

[135] A. 363R-92, "State of Art Report on High Strength Concrete (ACI Committee 363) (Reapproved 1997)," American Concrete Institute, Farmington Hills, MI, Tech. Rep., 1997.

[136] CEB-FIB, *CEB-FIB Model Code*. London: Thomas Telford, 1990.

[137] ACI-318, *Building Code Requirements for Reinforced Concrete*. Farmington Hills, MI: American Concrete Institute, 2008.

[138] G. Rao, "Long-term Drying Shrinkage of Mortar — influence of Silica Fume and size of Fine Aggregate," *Cement and Concrete Research*, vol. 31, no. 2, pp. 171–175, 2001.

[139] A. Itim, K. Ezziane, and E. H. Kadri, "Compressive Strength and Shrinkage of Mortar Containing Various Amounts of Mineral Additions," *Construction and Building Materials*, vol. 25, no. 8, pp. 3603–3609, 2011. [Online]. Available: http://dx.doi.org/10.1016/j.conbuildmat.2011.03.055

[140] D. P. Bentz, E. F. Irassar, B. E. Bucher, and W. J. Weiss, "Limestone Fillers Conserve Cement Part 2 : Durability Issues and the Effects of Limestone Fineness on Mixtures," *Concrete International*, no. December, pp. 35–39, 2009.

[141] T. C. Holland, "Silica Fume User's Manual," Tech. Rep., 2005.

[142] H.-W. Song and V. Saraswathy, "Corrosion Monitoring of Reinforced Concrete Structures," *Int. J. Electrochem. Sci*, vol. 2, pp. 1–28, 2007.

[143] S. Ahmad, "Reinforcement Corrosion in Concrete Structures, Its Monitoring and Service Life Prediction—a Review," *Cement and Concrete Composites*, vol. 25, no. 4-5, pp. 459–471, 2003.

[144] V. Thakur, D. Mandloi, D. Khare, and S. Gupta, "Significance of Silica Fume in Enhancing the Quality of Concrete," *International Journal of Innovative Technology and Exploring Engineering (IJITEE)*, vol. 96, no. 2, pp. 91–96, 2013.

[145] M. Panjehpour, A. Abdullah, A. Ali, R. Demirboga, and E. Faculty, "a Review for Characterization of Silica Fume and its Effects on Concrete Properties," *International Journal of Sustainable Construction Engineering & Technology*, vol. 2, no. 2, pp. 1–7, 2011.

[146] M. Gesoglu, E. Guneyisi, M. E. Kocabag, V. Bayram, and K. Mermerdaş, "Fresh and Hardened Characteristics of Self Compacting Concretes Made with Combined Use of Marble Powder, Limestone Filler, and Fly Ash," *Construction and Building Materials*, vol. 37, pp. 160–170, 2012.

[147] S. Agarwal and D. Gulati, "Utilization of Industrial Wastes and Unprocessed Microfillers for Making Cost Effective Mortars," *Construction and Building Materials*, vol. 20, pp. 999–1004, 2006.

[148] I. Elkhadiri, A. Diouri, A. Boukhari, J. Aride, and F. Puertas, "Mechanical Behaviour of Various Mortars Made by Combined Fly Ash and Limestone in Moroccan Portland Cement," *Cement and Concrete Research*, vol. 32, no. 1, pp. 597–603, 2002.

[149] J. Bai, S. Wild, and B. Sabir, "Chloride Ingress and Strength Loss in Concrete with Different PC–PFA–MK Binder Compositions Exposed to Synthetic Seawater," *Cement and Concrete Research*, vol. 33, no. 3, pp. 353–362, 2003.

[150] H. W. Song and V. Saraswathy, "Corrosion Monitoring of Reinforced Concrete Structures A Review," *International Journal of Electrochemical Science*, vol. 2, pp. 1–28, 2007.

[151] C. Andrade, M. C. Alonso, and J. A. Gonzalez, "An Initial Effort to Use the Corrosion Rate Measurements for Estimating Rebar Durability," pp. 29–37, 1990.

[152] J. Broomfield, J. Rodriguez, L. Ortega, and A. Garcia, "Corrosion Rate Measurement and Life Prediction for Reinforced Concrete Structures," in: *Proc., of the 5th Int. Conf. on Structural Faults and Repair held on June 29, 1993*, University of Edinburgh, 1993, pp. 155–163.

[153] ASTM C 1556, "Determining the Apparent Chloride Diffusion Coefficient of Cementitious Mixtures by Bulk Diffusion," Philadelphia.

[154] J. M. R. Dotto, a. G. De Abreu, D. C. C. Dal Molin, and I. L. Müller, "Influence of Silica Fume Addition on Concretes Physical Properties and on Corrosion Behaviour of Reinforcement Bars," *Cement and Concrete Composites*, vol. 26, no. 1, pp. 31–39, 2004.

[155] R. J. Detwiler, C. A. Fapohunda, and J. Natale, "Use of Supplementary Cementing Materials to Increase the Resistance to Chloride Ion Penetration of Concretes Cured at Elevated Temperatures," *ACI Materials Journal*, vol. 91, no. 1, pp. 63–66, 1994.

[156] D. P. Bentz, O. M. Jensen, a. M. Coats, and F. P. Glasser, "Influence of Silica Fume on Diffusivity in Cement-based Materials. Experimental and Computer Modeling Studies on Cement Pastes," *Cement and Concrete Research*, vol. 30, pp. 953–962, 2000.

[157] K. Byfors, "Influence of Silica Fume and Flyash on Chloride Diffusion and pH Values in Cement Paste," *Cement and Concrete Research*, vol. 17, no. 1, pp. 115–130, 1987.

[158] M. Mazloom, A. Ramezanianpour, and J. Brooks, "Effect of Silica Fume on Mechanical Properties of High-strength Concrete." *Cement and Concrete Research*, vol. 4, no. 347-357, 26.

[159] B. Hamad and M. Machaka, "Effect of Transverse Reinforcement on Bond Strength of Reinforcing Bars in Silica Fume Concrete," *Materials and Structures*, vol. 32, no. 6, pp. 468–476, 1999.

[160] D. Bentz and P. Stutzman, "Evolution of Porosity and Calcium Hydroxide in Laboratory Concretes Containing Silica Fume," *Cement and Concrete Composites*, vol. 24, no. 6, pp. 1044–1050, 1994.

[161] H. Song, J. Jang, V. Saraswathy, and K. Byun, "An Estimation of the Diffusivity of Silica Fume Concrete," *Building and Environment*, vol. 42, no. 3, pp. 1358–1367, 2007.

[162] H. Hornain, J. Marchand, V. Duhot, and M. Moranville-Regourd, "Diffusion of Chloride Ions in Limestone Filler Blended Cement Pastes and Mortars," *Cement and Concrete Research*, vol. 25, no. 8, pp. 1667–1678, 1995.

[163] S. Rebecca, "Influence of Limestone Powder Content and Size on Transport Properties of Self-Consolidating Concrete," Ph.D. dissertation, 2014.

[164] S. Supakit, "Chloride Diffusivity of Self-Compacting Concrete With Limestone Powder," Ph.D. dissertation, 2001.

[165] H. Siad, H. a. Mesbah, M. Mouli, G. Escadeillas, and H. Khelafi, "Influence of Mineral Admixtures on the Permeation Properties of Self-Compacting Concrete at Different Ages," *Arabian Journal for Science and Engineering*, vol. 39, no. 5, pp. 3641–3649, 2014.

[166] K. Celik, M. D. Jackson, M. Mancio, C. Meral, a. H. Emwas, P. K. Mehta, and P. J. M. Monteiro, "High-volume Natural Volcanic Pozzolan and Limestone Powder as Partial Replacements for Portland Cement in Self-compacting and Sustainable Concrete," *Cement and Concrete Composites*, vol. 45, pp. 136–147, 2014.

[167] P. Zbyšek, P. Milena, H. Benešová, J. Mihulka, Lukáš Fiala, and E. R., "Effect of Metakaolin Addition on the Moisture and Chloride Transport and Storage Properties of High Performance Concrete," *Modern Building Materials, Structures and Techniques. Vilnius: Technika*, pp. 239–244, 2010.

[168] M. Vujica, "Environmentally-friendly Self-compacting Concrete," *Gradevinar*, vol. 64, no. 9, pp. 905–913, 2012.

[169] U. Angst and Ø. Vennesland, "Critical chloride content in reinforced concrete–state of the art," *Networks-on-Chips: Theory and Practice*, p. 149, 2009.

VITAE

- **Personal Details:**
  - Name: Mohammed Abdelrahman
  - Nationality: Sudanese
  - Date of Birth: 23^{rd}, June, 1988
  - Email: *engineer.mas@hotmail.com / engmohammed@kfupm.edu.sa*
  - Permenant Address: House NO.123, Block NO.5, Emtidad-Nasir, East Khartoum, Khartoum, Sudan
  - Current Address: P.O. Box 8351, King Fahd University of of Petroleum & Minerals, Dhahran 31261, Saudi Arabia
  - Cell Phone: +966 5 46459797.

- **Educational Qualification::**
  - **MSc (Civil Engineering–Structures)**
    King Fahd University of Petroleum and Minerals, Dhahran, Saudi Arabia, excellent stand, 2015.

  - **BSc Civil Engineering**
    University of Khartoum, Khartoum, Sudan, first class, 2010.